Physical Limits of 13.56 MHz RFID Transponders with Loop Antennas at the Air Interface Described by Contactless System Properties

Master's Thesis

at

Graz University of Technology

submitted by

Markus Wobak

Institute of Microwave and Photonic Engineering
Graz University of Technology
8010 Graz, Austria

in cooperation with

NXP Semiconductors Austria GmbH
Mikronweg 1
8101 Gratkorn, Austria

Examiner: Prof. Dr. Erich Leitgeb
Supervisor: Dr. Michael Gebhart

March 28th, 2012

Abstract

Typical application scenarios for ISO/IEC 14443 compliant HF RFID transponders include the demand for decreasing the antenna size. Furthermore the chip and the antenna specifications have to be optimized for its intended operation field as early as possible in the pre-design phase to allow fast project development cycles. To analyse the physical limits of the reader-transponder coupling system, this thesis introduces a system level description of the transponder at its air interface, which allows a performance evaluation before actually implementing any hardware. By specifying the transponder's quality factor, its resonance frequency, the coupling coefficient and the transponder antenna inductance, a prediction of the load modulation amplitudes and the card loading effect according to ISO/IEC 10373-6 is made possible. The discussion includes an analytic derivation and a numerical simulation series with MATLAB and LTspice, which are both based on a network model of the measurement setup. An additional approach is to perform standard compliance measurements from a system level point-of-view. These results are to be used to verify the analytical and numerical considerations and to find an empirical system model. Finally, a lower antenna area bound required for ISO/IEC 14443-2 standard compliant load modulation amplitudes by means of passive load modulation is proposed. For verification all system level models are compared to product chip load modulation amplitudes measurements.

Kurzfassung

Bei vielen Anwendungsszenarien von ISO/IEC 14443 konformen HF RFID Transpondern ist die Verkleinerung der Antennengröße eine wichtiger Aspekt. Weiters sollen die Spezifikationen des integrierten Schaltkreises und der Antenne für das gewünschte Einsatzfeld so früh als möglich in der Entwicklungsphase berücksichtigt und optimiert werden, so dass die Projektdurchführung beschleunigt werden kann. Zur Analyse der physikalischen Grenzwerte eines Koppelsystems, bestehend aus einem Lesegerät und einem Transponder, wird im Rahmen dieser Arbeit eine Beschreibung des Transponders an seiner Luftschnittstelle auf Systemebene eingeführt. Dies erlaubt dessen Leistungsanalyse vor der Implementierung des Produkts. Durch die Spezifikation der Güte, der Resonanzfrequenz und der Antenneninduktivität des Transponders und des entsprechenden Koppelgrades ist eine Vorhersage der Lastmodulationsamplituden und des *Card Loading Effects* entsprechend ISO/IEC 10373-6 ermöglicht worden. Basierend auf einem Netzwerkmodell des Messaufbaus wurde eine analytische Ableitung und eine numerische Simulationsreihe mit MATLAB und LTspice durchgeführt. Ein weiterer Zugang wird durch die Durchführung von Standardkonformitätstests auf Systemebene erreicht. Diese Ergebnisse können zur Verifikation der analytischen und numerischen Betrachtungen herangezogen werden und dienen als Grundlage zur Spezifikation eines empirischen Systemmodells. Abschließend wird eine minimale Transponderantennengröße zur Erzeugung von ISO/IEC 14443-2 konformen Lastmodulationsamplituden durch passive Lastmodulation hergeleitet. Zur Verifikation werden die Ergebnisse auf Systemebene mit Ergebnissen eines gemessenen realen Produktschaltkreises verglichen.

Statutory Declaration

I declare that I have authored this thesis independently, that I have not used other than the declared sources/ resources, and that I have explicitly marked all material which has been quoted either literally or by content from the used sources.

Place	Date	Signature

Eidesstattliche Erklärung

Ich erkläre an Eides statt, dass ich die vorliegende Arbeit selbstständig verfasst, andere als die angegebenen Quellen/ Hilfsmittel nicht benutzt und die den benutzten Quellen wörtlich und inhaltlich entnommene Stellen als solche kenntlich gemacht habe.

Ort	Datum	Unterschrift

Contents

List of Figures

List of Tables

Chapter 1: Introduction

"The secret to creativity is knowing how to hide your sources."

[Albert Einstein]

1.1 Technological Overview

In the last two decades Radio Frequency Identification (RFID) in the high frequency (HF) range has become a mature and widely-used technology. Typical use-cases include logistics (item level tagging) and person-related applications like payment, automatic fare collection or ticketing.

Passive RFID transponders are cheap in mass production, are small and easy to use and can be operated contactlessly and without a battery. On the market RFID systems are established as a widely deployed alternative to bar code systems and contact based communications. The existing infrastructure and acceptance of RFID provided a basis for the emerging technology of Near Field Communications (NFC).

1.2 Basic RFID Communication

A schematic overview of a HF RFID communication link is illustrated in figure 1.1. An application is able to communicate with a RFID transponder by using a reader device which establishes a contactless connection to the mobile entity typically featuring a non-volatile memory. Batteryless, passive transponders can be supplied with energy and the clock signal over the H-field. This is only possible within the near field vicinity range of the reader device. The typical operational range is about ten centimetres (ISO/IEC 14443) up to about two meters (ISO/IEC 15693). The performance of 13.56 MHz RFID systems is hardly affected by water, but metallic objects degrade the operational range.

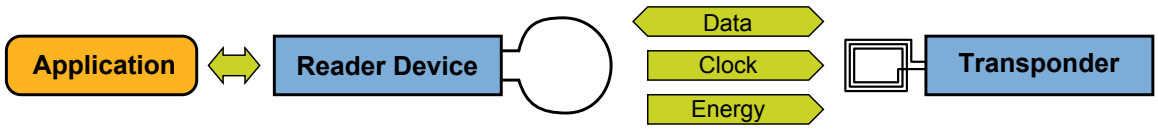

Figure 1.1: RFID block diagram

A good overview on various types of applications using RFID technology and the corresponding communication structure is given in [Fin10]. This thesis will concern ISO/IEC 14443-2 [IE10a] compliant transponders.

1.3 RFID System Performance

The usual approach when realizing RFID applications is to find an antenna that allows standard compliance with a specific RFID chip. While specifying and designing the integrated circuit (IC) no specific international standard related optimization criterion is available. In the chip development phase other internal IC parameters are used which result combined with a specific antenna in the complete transponder characteristics.

In fact, the performance of a transponder at its air interface is tested for standard compliance and should define the requirements of a transponder chip. By specifying system parameters of the transponder as early as possible in the product development cycle, application optimized results are to be expected.

Nowadays the market requires RFID *design-ins* to use as little space as possible at the cost of a reduced antenna size. This thesis will present a limit criterion for the antenna size compared to the system parameters, which allows to check the expected standard compliance of a specific IC and an antenna.

Chapter 2: Fundamentals of HF RFID Systems

"All theory, my friend, is grey."

[Goethe, "Faust I"]

2.1 A basic RFID Transponder

Before discussing a communicating transponder, it has to be defined. After a coarse discussion on transponder design the main building blocks relevant within this thesis will be discussed.

2.1.1 Transponder Design

A transponder or a (contactless) smart card is the mobile entity in a RFID application. In long range applications like logistics (item level tagging used for product tracking) the termini *tag* or *label* are used, whereas proximity range devices for person-related applications like mobile payment (credit cards, automatic fare collection) call it a *smart card* (obviously based on the possible additional cryptographic abilities of the integrated circuit). For simplicity this thesis names the mobile entity a transponder without loss of generality.

Although nowadays even a NFC enabled mobile phone can act as a transponder ("NFC Card Mode", [NFC12], [Fin10]), it has its main application in the mass market (e.g. labels, ticketing) and is accordingly realized with a minimum effort of hardware (e.g. payment using smart cards). The basic RFID transponder, which is discussed here, can be extended to a more sophisticated version that might reflect the reality in a better way or to even include further functional blocks like an antenna matching circuit used in NFC applications.

As RFID uses a wireless communication scheme, an antenna has to be used for transmitting and receiving data. In passive RFID this antenna is furthermore used to power an integrated circuit (IC) – the *RFID Chip* – by contactless energy transfer. This IC consists of an analogue frontend, a digital processing unit and a memory block (optional). These two units can be found in any transponder and are described in section 2.1.2 and 2.1.3 respectively. As the connection between these two blocks may not be perfect (e.g. a "zero-Ohm connection"), a coupling network should be modelled in many cases and is discussed in section 2.1.4. An additional capacitance is used sometimes to modify the resonance frequency of the transponder (see section 2.3.1). Figure 2.1 visualizes a typical transponder design as it will be discussed in detail in chapter 3.

2.1.2 Antenna of a Transponder

The commonly used antenna layout for 13.56 MHz RFID transponders is a planar spiral rectangular loop antenna with a small number of turns. Such an antenna can be seen as an inductor represented as a mixed series/ parallel equivalent circuit as shown in figure 2.1. Like any resonance circuit the behaviour of an antenna in frequency domain can be described using the quality factor Q_{ANT} and the self resonance frequency $f_{RES,ANT}$.

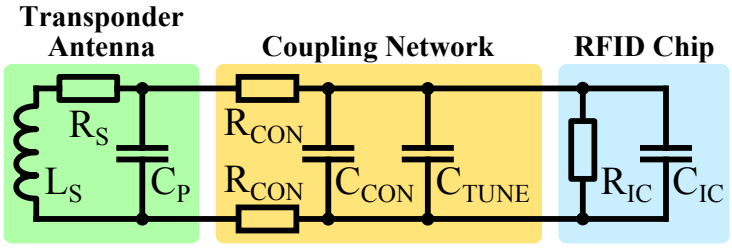

Figure 2.1: Basic RFID transponder

The outer dimensions for HF transponder antennas are defined by its application. The largest commonly used antenna fits in a ID 1 card defined by ISO/IEC 7810 [ISO03], which specifies an usable antenna size smaller than 81 x 49 mm. The embossing of a credit card reduces the available size for the antenna by a factor of two. Newer applications, for example watches, resulted in a demand of even smaller antenna sizes.

2.1.3 RFID Chip

In general a 13.56 MHz RFID transponder IC consists of an analogue RF interface or frontend, a digital control block and a non-volatile (re-)writeable memory, which are illustrated in figure 2.2.

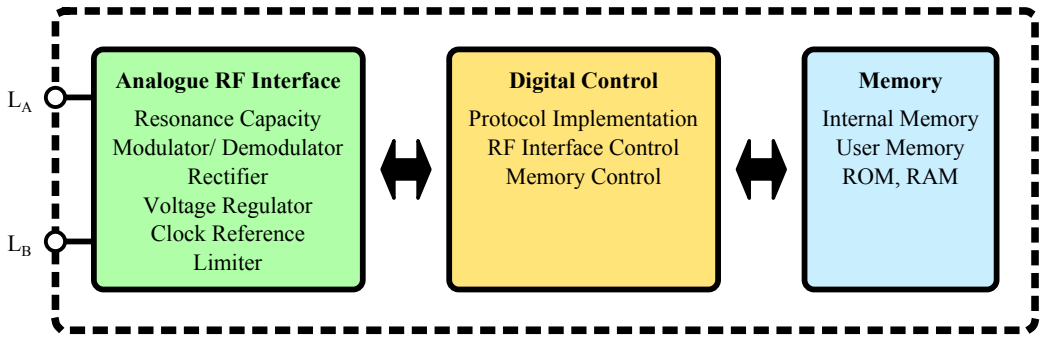

Figure 2.2: Functional blocks of a 13.56 MHz RFID transponder IC (simplified principle)

The input port of the IC consists of the pads L_A and L_B. As mentioned previously, the capacitance of the complete transponder is related to its resonance frequency. More precisely the relation of the coil inductance and the transponder capacitance has the main impact to f_{res}. As the value of the coil inductance is defined primarily by the antenna size and the number of turns, different application scenarios result in several options of necessary capacitances. This is the main reason why the same transponder IC is often offered with different input capacitance options(NC or "no cap", SC or "standard cap", HC or "high cap").

The demodulator shifts the information signal from the bandpass signal into baseband [Skl01], which is processed by the digital control block. A rectifier and voltage regulator block establishes a DC voltage supply for the internal circuitry. A clock reference signal is derived based on the carrier frequency to clock the digital part of the IC. A modulator is used for transponder to reader communications (described in section 2.2). A voltage limiter will take over the energy not needed by the chip, if the transponder is exposed to an H-field that supplies more energy than needed. The limiter has an impact on the resonant circuit system parameters and reduces the transponder quality factor as discussed in section 2.3.

The digital control block ensures the standard compliance of the IC in respect to protocol implementation, memory access and other aspects. A RFID chip may contain some non-volatile

memory (EEPROM or Flash) but this is not mandatory for each and every standard. For a reasonable utilisation of an IC, it should have at least some internal memory to store some kind of identifier and control bits. A memory can be split up into several memory regions like internal memory, protocol dependent memory and user memory.

Modelling the complex behaviour of the chip at system level can be done using its characteristics at the input port. The IC input impedance is mostly represented as a parallel network consisting of a resistance R_{IC} and capacitance C_{IC}, which both depend on chip input voltage U_{IC}. This dynamic behaviour challenges the system modelling as an operating point has to be found for each field strength.

2.1.4 Coupling between Antenna and IC

The chip is attached to the antenna by one out of four main process technologies (soldering, crimping, glueing or welding). In any real system this connection has a non-zero resistance and capacitance as modelled in figure 2.1. However, taking other parasitic elements and tolerances into account one may consider this non ideal behaviour as negligible.

In contrast to the small effect of the IC assembly some transponders use (external) parallel capacitors to tune the resonance frequency of the transponder to a desired value. The importance of this property is discussed in section 2.3.1.

A serial capacitor between the IC and the antenna may be used for small antennas which results in higher sideband amplitudes [GSM10]. A more sophisticated coupling network is used, for example, for NFC applications [NFC12].

2.2 Communication Links

In this section an overview on the communication links for RFID in the HF band is given. After a short overview on the commonly used communication standards the operational distances for communication are discussed.

2.2.1 Survey of commonly used RFID HF Communication Protocols

Table 2.1 lists some commonly used RFID standards in this frequency range. Note that different naming conventions are used for the system components. These standards are all defined for a passive wireless data transfer with *reader talks first* (the reader initiates the communication and the transponder is only allowed to send if he is asked to do so). The reader emits an H-field which is used to power the transponder IC by inductive proximity coupling (same principle as for power transformers) and to transmit data to the transponders. The carrier frequency f_C in this ISM band is 13.56 MHz.

Standard	Range	Reader	Transponder	Usage Examples
ISO/IEC 14443 [IE10a]	Proximity	PCD	PICC	AFC, Passports
ISO/IEC 15693 [IE06]	Long-range	VCD	VICC	Item level tagging
ISO/IEC 18000-3 [IE10b]	Long-range	Interrogator	Tag	Item level tagging
EMVCo 2.1 [EMV11]	Proximity	PCD	PICC	Contactless payment

Table 2.1: Listing of popular HF RFID standards and their naming conventions

2.2.2 Reader to Transponder

The operating volume of passive transponder ICs is limited by the required minimum power for chip operation. In the near field the magnetic field strength is inversely proportional to distance to the power of three. This limit criterion is specified by means of the *minimum field strength* (see section 2.4.1) up to the maximum distance to the reader antenna at which the IC has just enough energy for operation and defines the *energy distance*. The IC must be of course able to understand the modulation of the reader, but for systems with standard compliant communication this is not the limiting factor in this communication direction.

2.2.3 Transponder to Reader

Transponder to reader communication or the *"back link"* is realized with *load modulation*. A transponder within the energy distance is able to modulate its data sequence. This does not implicitly mean that the reader is able to understand this response. The maximum allowed distance between reader and transponder for two way communication is called *communication distance*, which is upper bounded by the energy distance per definition. This distinction is caused by the choice of the quality factors of the resonating circuits.

2.3 System Parameters

It is useful to define system properties rather than an equivalent circuit, which can describe the general behaviour of a system in order not to be limited to a specific realization of it. As HF RFID systems deal with coupled resonant circuits, it is reasonable to introduce the self resonance frequency f_{RES}, the quality factor Q, and the coupling coefficient k.

2.3.1 Transponder Quality Factor and Resonance Frequency

The terminus Q-factor describes how close a practically realized energy storing component – a capacitor or a coil – is compared to its ideal representation as a network element which can be a capacitance or an inductance. An increasing parasitic series resistance for inductors or a decreasing parasitic parallel resistance for capacitors results in self-discharge, which reduces the quality of the component. This concept can be applied for a network of components to find a total resulting quality factor Q, which is defined as

$$Q = 2\pi \frac{\text{maximum energy stored}}{\text{total energy lost per period}} \quad \text{[Sco87]}. \tag{2.1}$$

2.3.1.1 Series and parallel resonant circuits

Resonant circuits can be easily described by means of these system parameters Q and ω_{RES}, which is exhaustively discussed in the literature for a series or parallel resonant circuit consisting of one resistor, one capacitor and one inductor (see figure 2.3). At the self resonance frequency f_{RES} the reactive part of the energy component is oscillating between the energy storing components, and the resistive part is converted into heat at the resistor. Therefore a series resonant circuit has its smallest impedance $Z = R$ for $f = f_{RES}$, which is also real-valued. The same applies for a parallel resonant circuit accordingly.

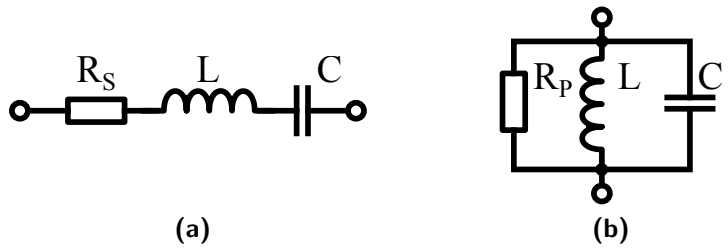

Figure 2.3: Series and parallel resonant RLC circuits

Thus, coming from several possible approaches,

$$\begin{aligned} \text{Angular self resonance frequency: } & \omega_{RES} = \frac{1}{\sqrt{LC}} \\ \text{Series resonant circuit: } & Q_{SERIES} = \frac{\omega_{RES} L}{R_S} = \frac{1}{\omega_{RES} R_S C} \\ \text{Parallel resonant circuit: } & Q_{PARALLEL} = \frac{R_P}{\omega_{RES} L} = \omega_{RES} R_P C \end{aligned} \tag{2.2}$$

Furthermore, it is possible to define an equivalence between a series and parallel resonant circuit, if both Q equations are set equal to another, e.g.

$$R_P = \frac{(\omega_{RES} L)^2}{R_S}, \tag{2.3}$$

which is, of course, valid for $f = f_{RES}$ only.

2.3.1.2 The impact of Q in various domains

Like in the most physical systems there is an inversely proportional relationship between the time and frequency domain. An increased quality factor Q results in a decreased bandwidth B, which defines the broadness of the resonance effect in the frequency domain.

$$Q = \frac{w_{RES}}{B} \tag{2.4}$$

The bandwidth is the frequency range between the two frequency points, where half of the power compared to the resonance frequency is available.

Additionally the envelope $e(t)$ to the step response to a sinusoidal signal with $f = f_{RES}$ is exponentially shaped and can be defined as

$$e(t) \sim 1 - e^{-t \frac{\overbrace{\omega_{RES}}^{=:1/\tau}}{2Q}} \quad \text{[Geb11]}. \tag{2.5}$$

The time constant $\tau \sim Q$ is a measure for the settling time needed after the input step impulse. It can be measured as the time period between 0 % and $1 - \exp(-1) \cong 63$ % of the envelope's maximum. This is one possibility of determining the quality factor of a resonant circuit.

2.3.1.3 Illustrating example

The influence of the quality factor to a transponder-like structure is analysed in figure 2.4 (assuming a constant chip input impedance). Based on an induced voltage in the transponder

antenna of 1 V and a sinusoidal carrier wave with $f_C = 13.56\ MHz \approx f_{RES}$ three Q-values are shown in frequency and time domain and the resulting parameter values are listed in table 2.2. If the quality factor is increased, the time constant will increase as well and the bandwidth will decrease. Additionally a larger Q-value results in a larger voltage rise around f_{RES}.

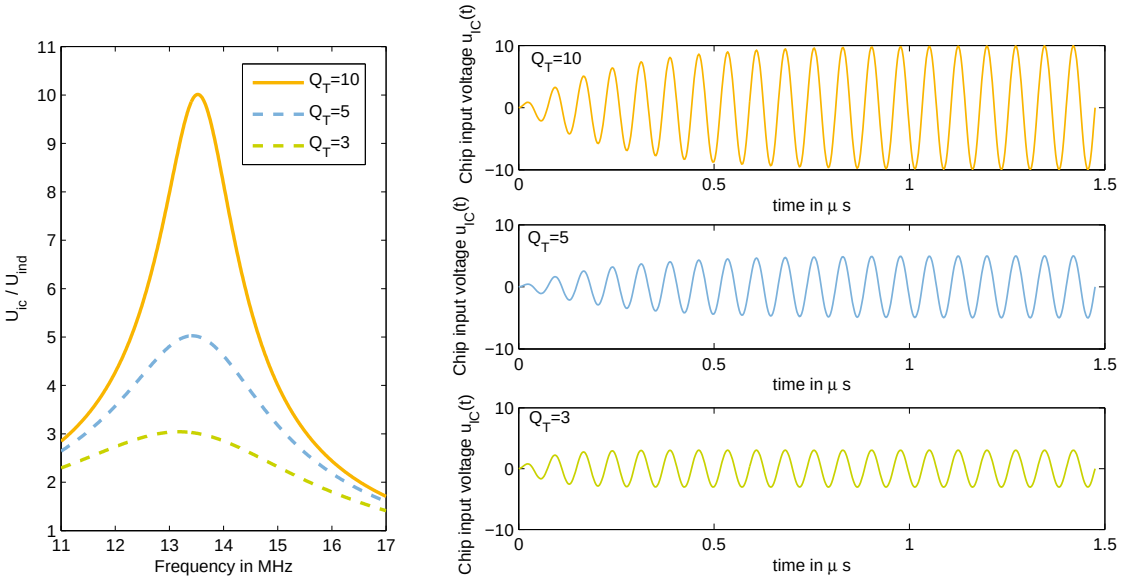

Figure 2.4: Effect of the quality factor exemplarily shown for three quality factor values

Quality factor Q	Bandwidth B in MHz	Time constant τ in μs
3	≈ 4.5	≈ 0.07
5	≈ 2.7	≈ 0.12
10	≈ 1.4	≈ 0.23

Table 2.2: Parameters of the exmaple presented in figure 2.4 ($f_{RES} = 13.56\ MHz$)

2.3.1.4 Equivalent quality factor

Sometimes it is convenient to define an equivalent quality factor Q_f at $f \neq f_{RES}$, for example when analysing a transponder with $f_{RES} \neq f_C$ operated at f_C. This analogy can be done, if (and only if) the resonant voltage rise parameter at specific frequency is of interest. The resistance of an antenna consists of a DC and an AC component. The second one is primarily caused by the frequency depending skin effect, which allows to estimate the resistive component at the frequency f by

$$R_{P,AC}(f) = \sqrt{\frac{f_{RES}}{f}} R_{P,AC}\left(f_{RES}\right), \tag{2.6}$$

and results in the equivalent quality factor $Q(f)$. Note that this is only an approximation.

Although often not explicitly mentioned, it is possible to analyse several resonance circuits at system level [Aik37]. A transponder is often called to be *tuned* if its resonance frequency matches the carrier frequency of the primary reader field, e.g. $f_{RES} = f_C = 13.56\ MHz$.

2.3.2 Coupling between the Reader and the Transponder

To measure the coupling intensity of two inductively coupled circuits the coupling coefficient can be used. From a physical perspective this coefficient $k = \{k \in \mathbb{R} | 0 \leq k \leq 1\}$ gives the proportionality between the causing current in the primary circuit and the induced voltage in the secondary circuit [Sco87], e.g.

$$u_{IND,Transponder} \sim k_{Reader,Transponder} \cdot i_{Reader}. \tag{2.7}$$

2.4 Parameters at the Air Interface

The behaviour of a HF RFID transponder in operation is defined by its air interface parameters, which are based on the system parameters as introduced above. Most of these parameters are defined within international standards and must exceed limit values in order to allow the complete IC to comply.

In an amendment to the proximity base standard ISO/IEC 14443-2 [IE10a] several antenna classes were introduced to define contactless specifications for smaller antenna geometries. Smaller antenna classes feature less restrictive limits in order to allow standard compliance within those demanding constraints. [SG11] includes an overview on the antenna classes and its adopted limits.

2.4.1 Minimum Field Strength

The minimum (magnetic) field strength H_{MIN} defines a lower bound of which the transponder has to be fully functional. It has to be below the operational field strength range (e.g. 1.5 to 7.5 A/m (rms) for ISO/IEC 14443-2 antenna class 1) in which all commands of the specific device have to be fully functional. In order to make this happen the passive transponder IC has to be supplied with sufficient energy and the chip input voltage must exceed the minimum chip voltage, e.g. $U_{IC} \geq U_{IC,MIN}$.

As a first guess it is obvious that the reader-transponder coupling has a crucial importance for this quantity. By increasing the transponder quality factor the minimum field strength is reduced for a tuned transponder.

2.4.2 Maximum Alternating Field

The maximum alternating field defines the strongest magnetic field in which the transponder has to survive – no operation and no limits concerning the modulation shaping have to be fulfilled. In fact this is a test for the current resistivity of the IC and its heat tolerability which are not within the scope of this thesis.

2.4.3 Reader Command Demodulation

The signal modulation of the reader seen from the transponder in time domain is defined in [IE10a] including some tolerance values. Especially the rise and fall times and over- and undershoot limits are defined for the *envelope shaping*. Based on these quantities the worst-case demodulator input signal can be specified.

Within this thesis the reader to transponder communication link is not to be discussed – it is important for reader design to guarantee interoperability with transponders from different vendors. [GWBB08] gives an introduction and presents an automated measurement approach, which was extended with an envelope extraction algorithm presented in [MG09].

2.4.4 Card Loading

A transponder within the vicinity of the reader's H-field will act as a load for the emitting device as it branches off energy. This results in a reduction compared to the unloaded H-field strength. The relevant test standard [IE11] accounts for this fact by defining the H-field with a transponder being present as device under test (DUT). Therefore the card loading effect is compensated by increasing strength of the carrier signal (gain of the amplifier).

To allow interoperability a *"Class 1" PICC maximum loading effect* test was included in the standard. It defines that any transponder with a class 1 antenna size must load the PCD less than a Reference PICC tuned to "maximum loading conditions" at H_{min}.

2.4.5 Load Modulation Amplitude

The transponder performs load switching for transponder to reader communication. The load modulation amplitude is measured within a special measurement setup [IE11] and must exceed a lower bound in the operational field strength range. The values are derived by means of a *Discrete Fourier Transform* DFT at the sideband frequencies $f_C \pm f_{SB}$, e.g. 13.56 MHz $\pm$ 847.5 kHz. These are often called *Lower* and *Upper Side-Band* (LSB and USB). Contrary to the standard, this thesis uses f_{SB} instead of f_S when referring to the sideband carrier frequency to distinguish it from the sampling frequency f_S.

Figure 2.5 gives an impression of the load modulation amplitudes as defined in frequency domain and motivates the importance of the quality factor.

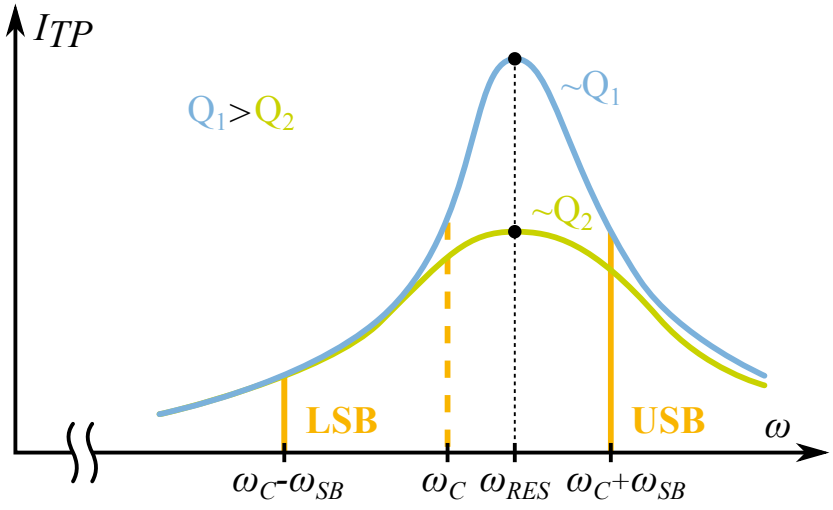

Figure 2.5: Transponder quality factor and sideband amplitudes

2.5 Motivation of Finding a Link between System and Air Interface Parameters

Although a description based on system parameters might seem to be too inaccurate to yield in usable results, it has a long list of benefits: Performing the step to desist from the usage of specific component values and other numerical dependencies, it allows to use the result of a (probably?) more time consuming unique problem solving phase for each and every conceivable system component instantaneously as long as it is allowed within the constraints introduced by the system modelling.

Like it may be be assumed from its name this modelling allows to gain deep access into the system itself and gives first results prior finding specific component values. Furthermore conventional numerical simulations based on measured or even estimated component values often include an unpredictable uncertainty.

The main problem is to find an **analytic** link between system and air interface parameters. If it results to be mathematically infeasible or if further system simplifications are intolerable, an empirical modelling based on an as large as possible set of measurements will be a good possibility to form a link.

Another big advantage of having an analytic description to compute the air interface parameters based on system parameters is the possibility of rearranging the formula. An iterative simulation does not allow this, because this irreversible representation has to be solved recursively, which is connected to a high computational effort. Therefore, an analytic equation allows to estimate the necessary system parameters needed for specific air interface parameters defined in a standard.

In a nutshell system level analysis will never be able to replace component level analysis as it is used, for example, in the development phase of integrated circuits. But the system level approach could and should be used before starting to design an IC and for a coarse and fast possibility for issue analysis regarding the coupled system.

Chapter 3: System Model

"Models are to be used, not believed."

[H. Theil, "Principles of Econometrics"]

3.1 A Discussion on RFID System Models

The main problem when modelling any system is the question what it should contain to be as simple as possible while still reflecting the reality as good as possible or necessary. In fact one has to restrict the aspects of a model in one or the other way. It should be as simple as possible while not degrading the aspects of the desired outcome.

3.1.1 Reasons and Contents of Models

A model should generally be the link between a set of input data and the quantities to be characterized. In terms of HF RFID transponders within this thesis the input data might be a transponder which has to fulfil a set of requirements in order to comply a specific standard to guarantee interoperability. The output of the model should contain the test parameters which are limited by the test standard.

In the early time of HF RFID in application [Foc00] presented one possibility to introduce a system level description but is rather application oriented and does not concern the ISO measurement setup according to [IE11]. Popular and information filled standard texts like [Fin10] or [Par05] don't contain an ISO/IEC specific discussion either – least of all at system level, but on network level. In contrast this thesis tries to build a link between these domains and to emphasize the potential of a system level description.

3.1.2 Overview of the ISO/IEC Standard Measurement Setup Model

The fundamental modelling approach is based on a network model of the complete ISO/IEC measurement setup ascribed to system parameters. First of all the principle structure is presented and an overview on possible sub modelling tasks is given.

As written in the introduction the transponder and the test description build the input data of the model. A schematic block diagram of various description methods is illustrated in figure 3.1. To construct the complete network model a set of intermediate entities is to be defined. The equivalent circuit of the transponder (consisting of an antenna and the RFID chip) and of the measurement setup and the involved couplings can be designed by the various approaches described in the following sections.

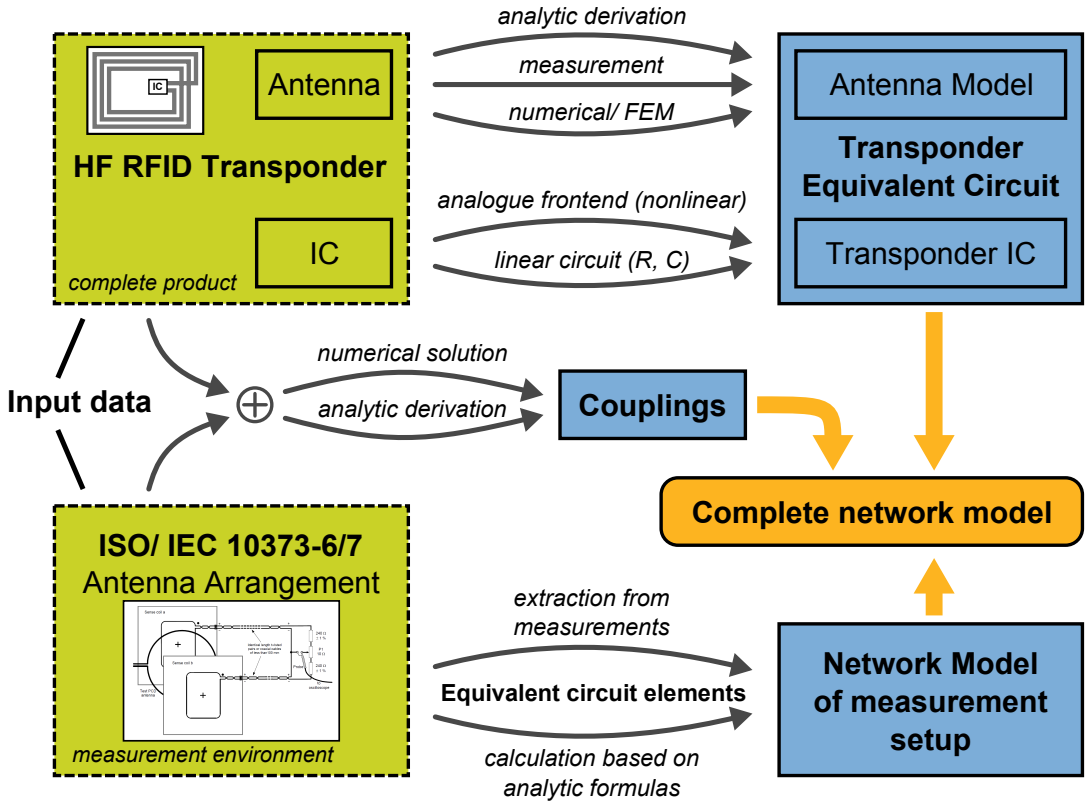

Figure 3.1: Various possible system modelling approaches

3.2 HF RFID Transponder

For standard proximity- and vicinity-style application scenarios a transponder can be seen to be split up to an antenna and an IC only. For the sake of completeness a resonance tuning capacitor is added.

3.2.1 Transponder Antenna

The antenna is typically planar and features a small number of turns. There are several industrial production technologies for such antennas, e.g. etching, winding, galvanic processes, which define the cross section of the conductors and the material of it and the substrate. For mass market applications rectangularly shaped antenna outlines are commonly used, although circular antennas are in place as well. This discussion will be done assuming a rectangular outline with outer dimensions a_0 and b_0, which is no restriction for the generality.

The main property of the antenna is its inductance which is linked with the self resonance frequency of the complete transponder. A typical range for it would be around $1 - 3\ \mu H$.

An in-depth introduction to such spiral coils is given in [Sch10]. A broadband macro model shown in figure 3.2 defines its main components: The coil acts primarily inductive defined by $\underline{Z}_{MQS}$ (magneto-quasi-static) but has additionally an electric energy storing component (C_p) and some dielectric losses (R_p). An internal ladder model characterized by $\underline{Z}_{lad}$ includes the possibility of modelling skin- and proximity-effect losses inside the conductors as well as the frequency-dependent inductance. All together a quasi-static broadband impedance $\underline{Z}_{QS}$ is defined.

The complete broadband model includes an infinite number of self resonance frequencies and

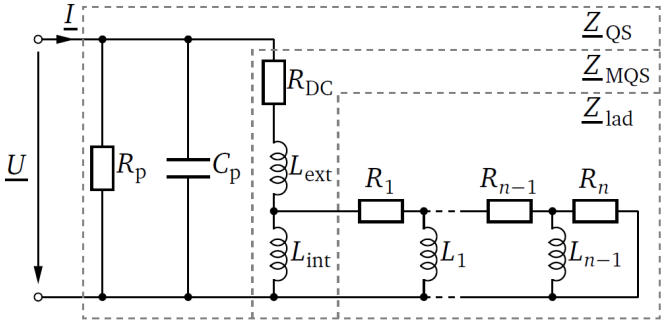

Figure 3.2: Broadband macro model of a printed spiral coil (PSC) according to and taken from [Sch10]. $\underline{Z}_{lad}$ can be removed to get a narrowband macro model.

changes its overall behaviour between inductive and capacitive over frequency (the higher the frequency gets, the more the skin- and proximity-effect losses alter the expected performance). Concerning HF RFID only the frequency range around f_C is of interest. The resonance frequency of the transponder antenna is typically between 40 and 200 MHz and, therefore, $\underline{Z}_{lad}$ can be ignored within this context, which results in a narrowband model.

3.2.1.1 Simplified Equivalent Circuit

If the narrowband macro model from figure 3.2 is simplified by combining R_{DC} and R_p to an overall resistance R_s in series an inductance L_s and both together parallel to the capacitance C_p, the typically used simplified antenna equivalent circuit already included in figure 2.1 is derived.

Note that all components are frequency dependent – even the resistance consists of a DC-value and an AC-value. This has to be kept in mind as a resonant antenna is typically defined at its resonance frequency which is in this context well above the carrier frequency f_C!

Some application environments interfere with the ideal physical context. For example, the performance of HF communication is severely degraded by nearby metal surfaces or components. There are possibilities of shielding or blocking these disturbers (e.g. by the use of ferrite sheets [GNSW11]). If a transponder is exposed to such a dominant load all the time, the values of the equivalent circuit (and its related system parameters) can be defined with the environment already taken into account.

3.2.1.2 Analytic Derivation of Equivalent Circuit Elements

The first possibility to determine the values of the antenna equivalent circuit is to find an analytic equation which allows direct computation. In general it is hard to find an accurate formula as the geometry has to be considered in detail. Simplified approaches can be found, for example in [Sch10, Par05]. Especially the AC component of the series resistor often results in inaccuracies. All in all – assuming the availability of such modelling equations – they give a rough guess of the component values in very short time. Within the numeric simulation series described in chapter 5 such an analytical model will be presented and used.

3.2.1.3 Numerical FEM Antenna Modelling

The antenna geometry can by modelled in 2D or 3D to apply a *Finite Element Method* resulting in the equivalent circuit elements. This is a method of analysing a specific geometry and

is (especially compared with the analytic approach) very time consuming, but can get quite accurate.

Typical examples of FEM-based modelling include HFSS simulations [GNSW11] or mixed approaches like [Cic06], which is quite interesting as it involves a combination of several simulation programs and allows an antenna analysis of a complete range of antenna dimensions. Figure 3.3 gives an impression of this approach.

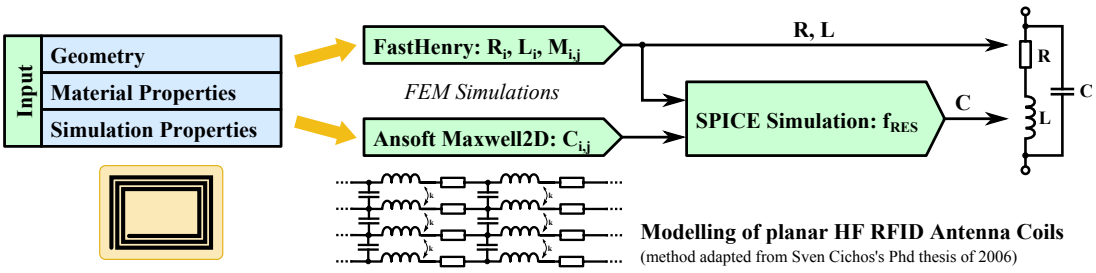

Figure 3.3: Numerical transponder antenna modelling approach presented in [Cic06]

3.2.1.4 Measurement of the Equivalent Circuit Elements

The equivalent circuit elements of an antenna can be measured using an impedance analyser [Geb08]. The recommended procedure is to measure the self inductance and the DC resistance value at low frequency (the self resonance has nearly no impact) and the parallel resistance at resonance frequency. These values can be used to calculate the complete replacement circuit.

Measurements are a good option of characterizing an antenna including all parasitic effects and fabrication process offsets. The drawback is the need of the physical presence of the fabricated antenna. Normally a series of possible antenna geometries is produced by a manufacturer and the best one is chosen based on measurements. All in all this is time consuming and a good and accurate analytical approach would be needed to improve the process.

3.2.2 RFID Transponder IC

The RF frontend of a transponder IC consists of an analogue circuitry which will be simplified to a (non-linear) RC parallel equivalent circuit in order to simplify and speed up the examinations and simulations and to allow system level description.

3.2.2.1 Analogue Frontend of a RFID IC

The analogue frontend of a transponder chip sketched in figure 3.4 consists of several fundamental building blocks which each have an impact on the transponder's air interface parameters. The IC needs a specific operating voltage $U_{IC,MIN}$ at its input pins – typically called L_A and L_B – in order to be fully operational. This input voltage increases with the H-field strength normal to the transponder area. In order not to exceed the maximum input voltage defined by the IC manufacturing process, the antenna voltage is clamped by a limiter by means of decreasing the equivalent input resistance R_{IC}, which results in a decreased quality factor Q_T, a decreased transponder antenna current I_{TP} and a reduced input voltage U_{IC}.

A rectifier and a voltage regulator limiter are needed to derive a stabilized internal DC supply voltage. To allow communication with the reader, load modulation by means of switching a

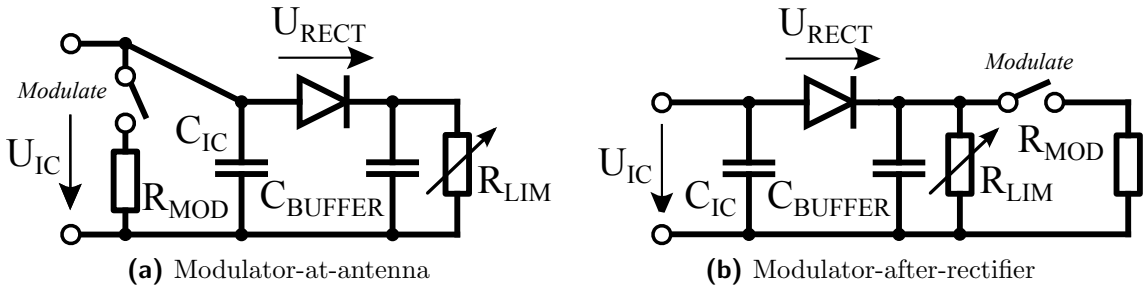

(a) Modulator-at-antenna **(b)** Modulator-after-rectifier

Figure 3.4: Simplified analogue frontend of a HF RFID transponder IC including the main components for understanding the principal behaviour at system level over varying H-field strength and load modulation. Subfigure (a) shows an IC with its modulator at the antenna, whereas subfigure (b) features a *modulator-after-rectifier* design.

load resistor is commonly used. This modulator can be placed directly at the chip's input pins (at the antenna) or at DC domain (after the rectifier). The first one causes a negligible chip input voltage during modulation which results in the largest possible modulation amplitude and sideband amplitudes. In the load modulated state the chip does not see the primary field but still has to stay in sync with f_C at his own, which can be achieved e.g. by using a phase locked loop (PLL) as done in [Kla09]. This is not needed in the second case, because the chip input voltage in the modulated state is at least as high as the voltage drop over the rectifier. The drawback of this configuration is a reduced modulation amplitude, which results in reduced sideband amplitudes.

3.2.2.2 Defining a Chip Input Impedance

The non-linear input impedance of a transponder IC over its input voltage range can be modelled by a parallel resistance R_{IC} and a parallel capacitance C_{IC}. At a glance their static trends are typically somewhat like shown in figure 3.5. The resistive component for the chip in operational

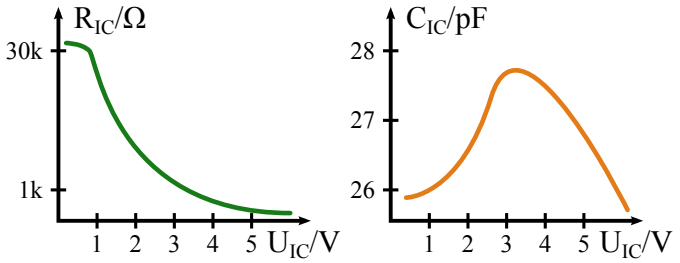

Figure 3.5: Typical trace of a chip input impedance over input voltage consisting of the parallel input resistance and capacitance with a typical $U_{IC,MIN} \approx 3\ V$

state is primarily influenced by the limiter. The reactive component consists of an integrated capacitor and a sum of small parasitic capacitors caused by the rectifier, the package, the chip connection and internal transistors.

3.2.2.3 Chip Impedance Measurement

The chip input impedance can be characterised using a network analyser (NWA) as described in [GBG10], which is a contact based procedure. The chip's input voltage is varied as a voltage

sweep and R_{IC} and C_{IC} are calculated based on the measured reflection coefficients. These curves give a good guess about the various chip activation voltages. Even if the chip is seen as a black box, the voltage drop over the rectifier and $U_{IC,MIN}$ can be extracted easily.

The measurement assumes a "static" or non-modulating chip. The measurement can be repeated for a constantly modulating chip (modulation switch closed), but the results can not directly be used for LMA analysis, as load modulation of the subcarrier frequency is a dynamic process, which may include additional parasitic influences not covered by a switch between two impedance states derived from static measurements.

3.2.2.4 Characterization based on the Chip Input Voltage

Especially for LMA analysis an other or an additional modelling approach can be used to specify the chip input voltage in the modulated and non-modulated state. Figure 3.6 illustrates the effect of the modulator position to the chip input voltage and the modulated rectifier current over H-field for fictitious chip frontends.

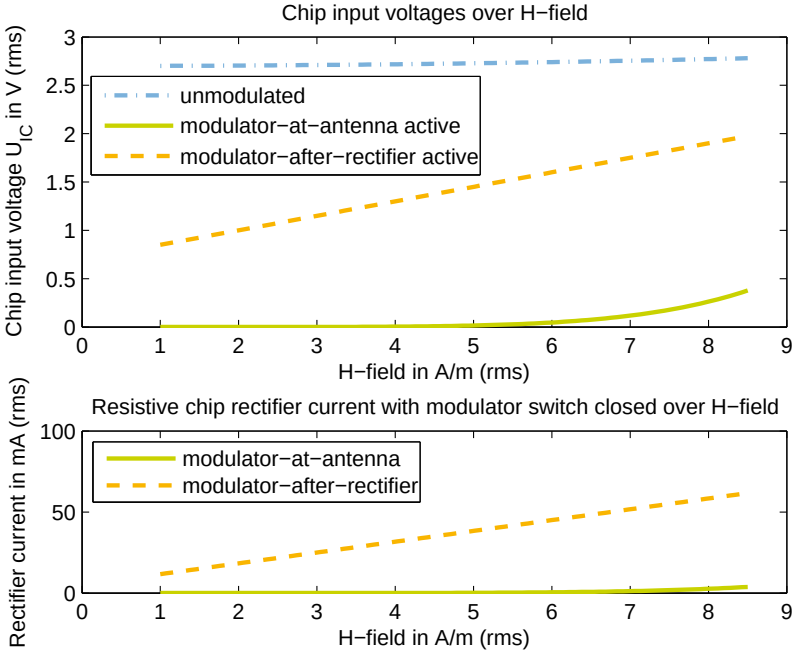

Figure 3.6: Effect of modulator position to chip input voltage for a modulated and unmodulated chip state for fictitious chip frontends assuming $H_{MIN} \approx 1\ A/m(rms)$ and $U_{IC,MIN} \approx 2.7\ V(rms)$

Assuming that the chip is within the energy distance or operated above H_{MIN}, respectively, the chip input voltage may be assumed to be $U_{IC} \approx U_{IC,MIN}$ due to limiter action. Especially for higher field strength values measurements have shown that the value increases slightly – this effect is not that strong and needs not to be implemented to get the overall picture.

The modulated chip input voltage depends on the designed modulator position: If the modulator is placed at the antenna side, this will result in a (nearly) zero valued chip input voltage amplitude, e.g. $U_{IC,MOD} \approx 0\ V$. In contrast to that, the alternative modulator position results in a voltage drop across the rectifier (in a first approximation, there are, of course, more impact factors). This voltage drop is a function of the field strength, as the current through the limiter and therefore through the rectifier increases with the H-field, e.g. $U_{IC,MOD} \approx U_{RECT} + S_{RECT} H$, where S_{RECT} models the increase of voltage drop over H-field strength.

3.2.3 Transponder System Parameters

The simplified equivalent network model of the transponder is shown in figure 3.7. For mathematical simplicity it is reasonable to introduce an overall capacitance $C := C_{TP} + C_{TUNE} + C_{IC}$.

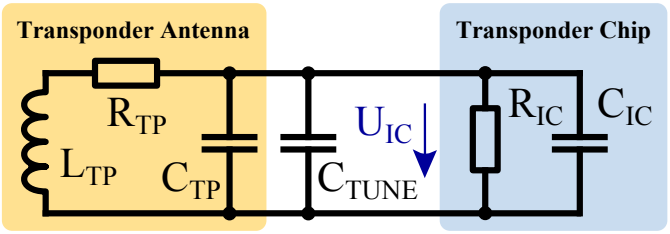

Figure 3.7: Basic transponder equivalent circuit

The network is a mixed series and parallel resonance circuit which isn't discussed normally in literature. First of all the transponder has only one self resonance frequency

$$\omega_{RES} = \frac{1}{\sqrt{L_{TP}C}} \qquad \textit{Thomson Equation.} \tag{3.1}$$

Due to the simplicity of the network it can be seen as a parallel arrangement of a series and a parallel resonance circuit with $Q_A = \omega_{RES} L_{TP} / R_{TP}$ and $Q_B = R_{IC} / (\omega_{RES} L_{TP})$. Thus, as derived in [Fin10],

$$Q_T = \frac{1}{\frac{R_{TP}}{\omega_{RES} L_{TP}} + \frac{\omega_{RES} L_{TP}}{R_{IC}}} = \frac{1}{R_{TP}\sqrt{\frac{C}{L_{TP}}} + \frac{1}{R_{IC}}\sqrt{\frac{L_{TP}}{C_{IC}}}}. \tag{3.2}$$

The value of Q_T is only valid at $\omega = \omega_{RES}$. Sometimes an equivalent value at $\omega = \omega_c$ may be needed. In this case the component values may be adapted to get a coarse estimated value. [Geb08] introduces this concept.

3.3 Network Model of the ISO/IEC 10373-6 Test Setup

The standard compliance of proximity transponders can be verified using a measurement setup described in the following sections. A more in depth discussion with an example of realization can be found in [GBBM08].

3.3.1 Description of the Test Setup

The test setup described in [IE11] defines the coaxial antenna arrangement and measurement methods to verify the standard compliance of a device under test. In principle this test setup for proximity coupling systems (ISO/IEC 10373-6 [IE11]) is equal to that for vicinity coupling systems (ISO/IEC 10373-7 [IE08]) but has other dimensions. Figure 3.8 gives a schematic overview on the antenna arrangement.

The setup consists of a coaxial antenna arrangement built around the emitting loop antenna (PCD antenna). Two co-axial sense coil antennas are positioned such that the primary H-field causes a zero voltage at the Helmholtz bridge point in the unloaded tuned case. The emitted H-field towards the two sides can be assumed to be symmetrical. The potentiometer P1 is available to minimize the residual probe voltage introduced by a real setup and its surroundings prior bringing the test device into the vicinity of the antenna arrangement.

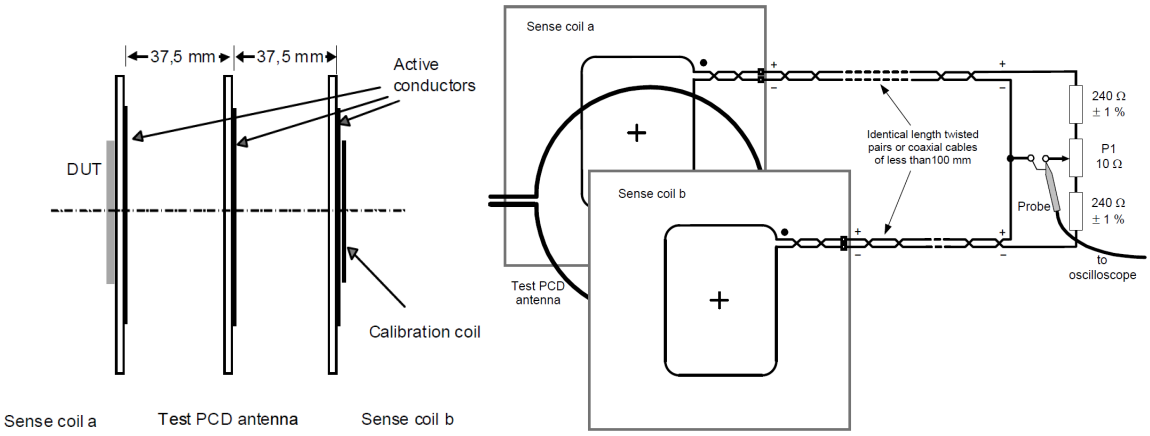

(a) Antenna arrangement **(b)** Principle of the test setup

Figure 3.8: Test setup according to and taken from ISO/IEC 10373-6 [IE11]

The transponder is placed into the DUT position co-axial to the other antennas. The distribution of the PCD's magnetic flux within the area spanned by the transponder antenna can be assumed to be homogeneous. An additional calibration coil opposite to the transponder antenna is used to measure the H-field strength at the DUT position which is proportional to the induced voltage in the calibration coil.

If the transponder changes its load for load modulation, sense coil A will see a reduced H-field resulting in a non zero Helmholtz bridge point voltage. This signal is recorded with a digital sampling oscilloscope and processed offline using a DFT to compute the sideband amplitude values.

One main aspect of this measurement arrangement is the constant coupling between PCD and transponder. In fact this is definitely not a realistic application scenario as in reality a transponder will be brought into the reader's communication range and the coupling will vary with the distance, the orientation and the tilt between the two antennas. The principle of this static test assembly has to be fully understood in order to optimize the transponder entity. The limits given for the standard compatibility are the main focus of this thesis and have to be analysed.

A conventional reader device, which would be found in an application scenario, would read the modulation from the transponder by sensing the (periodic) change of the reader antenna's current (or a proportional voltage). This is the basic principle used as well in the popular contactless payment standard EMVCo [EMV11] where the coupling between reader and transponder is varied within a communication volume. The same applies accordingly for the NFC Forum certification [NFC12].

3.3.2 ISO Setup in S-Domain

The ISO/IEC 10373-6 test setup with its coaxial antenna arrangement can be represented by an equivalent circuit as network model as shown in figure 3.9. The concept can be easily used for numerical network analysis with SPICE or Cadence as presented in [SG11].

If an analytic derivation is desired, the network can be partially combined and has to be extended with additional voltage sources resulting from the couplings [Sco87]. Not each and every coupling link has to be considered in both directions. Especially a static system analysis can be performed on parts of the network exemplarily shown in figure 3.10. The mesh-current-

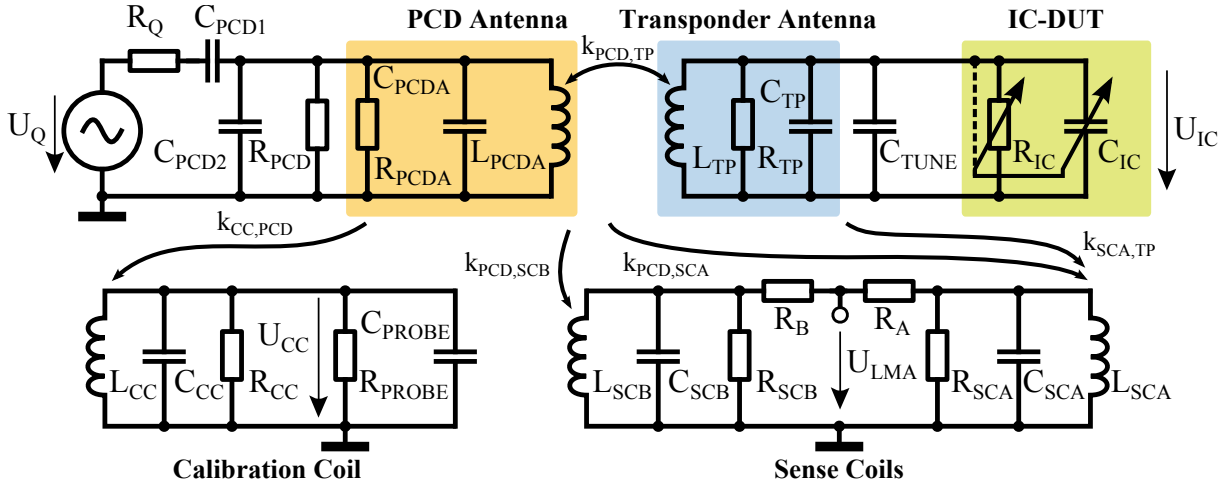

Figure 3.9: Network model of measurement setup according to ISO/IEC 10373-6 [IE11]

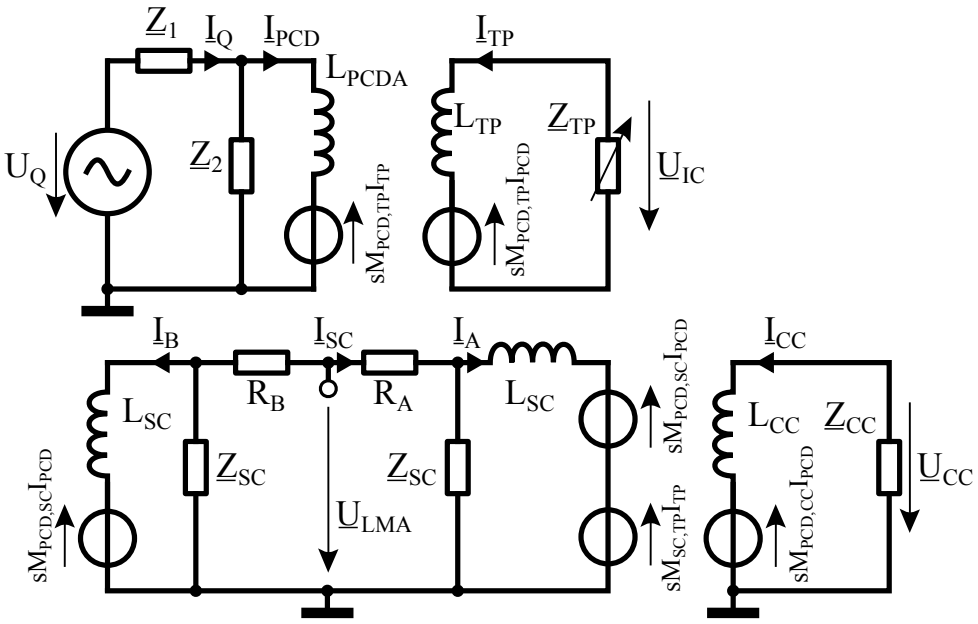

Figure 3.10: Simplified network model

method can be used to extract the impedance matrix of the simplified test setup. Thus,

$$\underline{\mathbf{Z}}(s) = \begin{bmatrix} \underline{Z}_1 + \underline{Z}_2 & -\underline{Z}_2 & 0 & 0 & 0 & 0 & 0 \\ -\underline{Z}_2 & \underline{Z}_2 + sL_{PCDA} & -sM_{PCD,TP} & 0 & 0 & 0 & 0 \\ 0 & -sM_{PCD,TP} & \underline{Z}_{TP}(s) + sL_{TP} & 0 & 0 & 0 & 0 \\ 0 & sM_{PCD,SC} & -sM_{SCA,TP} & sL_{SC} + \underline{Z}_{SC} & 0 & -\underline{Z}_{SC} & 0 \\ 0 & -sM_{PCD,SC} & 0 & 0 & sL_{SC} + \underline{Z}_{SC} & \underline{Z}_{SC} & 0 \\ 0 & 0 & 0 & -\underline{Z}_{SC} & \underline{Z}_{SC} & R_A + R_B + \underline{Z}_{SC} + \underline{Z}_{SC} & 0 \\ 0 & -sM_{CC,PCD} & 0 & 0 & 0 & 0 & \underline{Z}_{CC} + sL_{CC} \end{bmatrix}$$

Due to the time-varying chip input impedance $Z_{TP}(t) = \mathcal{L}^{-1}\{\underline{Z}_{TP}(s)\}$ the network impedance matrix is not constant. This fact complicates the analytic derivation of the inverse matrix needed to compute the mesh currents, e.g.

$$\underline{\mathbf{I}} = \begin{bmatrix} \underline{I}_Q \\ \underline{I}_{PCDA} \\ \underline{I}_{TP} \\ \underline{I}_A \\ \underline{I}_B \\ \underline{I}_{SC} \\ \underline{I}_{CC} \end{bmatrix} = \left(\underline{\mathbf{Z}}(s)\right)^{-1} \begin{bmatrix} \underline{U}_Q \\ 0 \\ 0 \\ 0 \\ 0 \\ 0 \\ 0 \end{bmatrix}. \tag{3.3}$$

The load modulation amplitudes can be computed assuming the knowledge of the sense coil currents. Analytically solving the complete measurement setup seems likely to give a complex, not analysable result caused by the time-varying chip input impedance. Therefore, simplified sub-networks will be used for analytical considerations in this thesis.

3.4 Card Loading

The simplest consideration regarding card loading includes only the transponder and the PCD's antenna current I_{PCD} which is visualized in figure 3.11. The transponder can be seen as the secondary circuit in this coupling link which draws energy from the H-field emitted by the primary circuit . This reduction of energy in the PCD antenna's circuit can be modelled as a (counter-) induced voltage in series to L_{PCDA} (see figure 3.10) or as an additional complex impedance in series to L_{PCDA}. Both methods are well known from power transformer analysis. In general the strength of the card loading effect varies with the coupling (antenna size) and

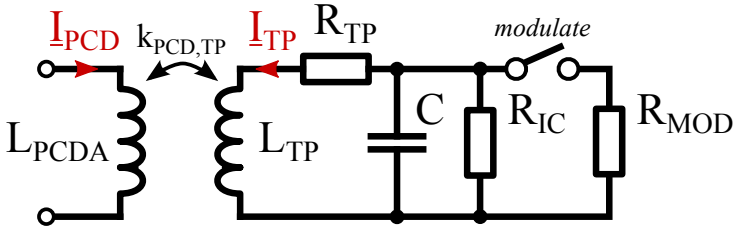

Figure 3.11: PCD to transponder coupling (simplified)

with Q_T, which does also vary during load modulation. The test procedures defined within ISO/IEC 10373-6 account for this effect by defining the H-field strength with the non-modulating transponder in DUT position.

3.5 Load Modulation Analysis

Now what about predicting the load modulation amplitudes in frequency domain? A fully analytic discussion based on the complete measurement setup network model is too complex

due to the dynamic input impedance of the chip. The network may be simplified by a few assumptions based on observations made when analysing measurements. For this first analytic modelling approach a relation between the load modulation amplitude of the envelope of the transient chip input voltage and the load modulation amplitudes in frequency domain is assumed.

3.5.1 Load Modulation Synthesis

(Passive) load modulation is realized by periodically opening and closing a switch which acts as a varying modulation impedance. Typically a resistive load is used, which can be interpreted as changing the transponder quality factor between the regular Q_T and the modulated transponder quality factor Q_M. An other option is to use a capacitive load, which modifies the resonance frequency of the transponder. As described in the introductory section 2.3.1, this change of f_{RES} can be interpreted as a change of the equivalent Q-factor at f_C considering the resonant voltage rise.

3.5.1.1 Classification of the Modulation Type

Load modulation is an *external modulation* because a system of two coupled resonant circuits is periodically modified. The transponder is a complex impedance in series to the PCD's inductance (transformed transponder impedance concept). A change of this load results in a change of the magnitude of the emitting antenna current (change of the card loading effect) and the PCD's resonance frequency, which would not be modified in the case of an *internal modulation*. Such a modulation results in a signal, which is generated, modulated, amplified and emitted into the far field via an antenna. In the case of passive load modulation, the properties of the near field's dominant component (H-field) are changed by varying the parameters of the coupled resonant circuits.

Thus, the PCD antenna emits the primary and the transponder antenna the secondary H-field which are both synchronous with the carrier frequency f_C. Any possible point in space sees the overlap of both H-fields which are phase shifted and differ in amplitude. In general, this results in a complex modulation, which is a combination of amplitude modulation (AM) and phase modulation (PM). Only in special cases pure AM or PM can be detected. This is the reason why no definition of a modulation index can be done in general.

3.5.1.2 Envelope of a Load Modulated Signal

Within the ISO/IEC 10373-6 test setup there are two measurement points of interest concerning the LMA analysis: The first one is the probe voltage trace $u_{LMA}(t)$ between the two sense coils which is related the test criterion. The final product transponder has to exceed the minimum limits specified in the proximity base standard. The other one is the transponder itself, where the envelope signal of the transponder's coil current or the chip input voltage can be used for system analysis. A signal load modulation pulse measured at various points within the test setup and the principal envelope shape are shown in figure 3.12.

While modulating the chip input voltage is reduced to its minimum. The time constant of the falling slope is small and proportional to Q_M. At the Helmholtz balance point a reduced H-field originating from the transponder can be measured and only the residual PCD's H-field – resulting from a not perfectly balanced measurement bridge – is left. When the modulator switch is opened again, the transponder's quality factor increases. This causes a long time constant (small rising slope).

The resulting sideband amplitudes will decrease with an increasing residual chip input voltage in the modulated state, because any point in space sees a reduced relative H-field difference

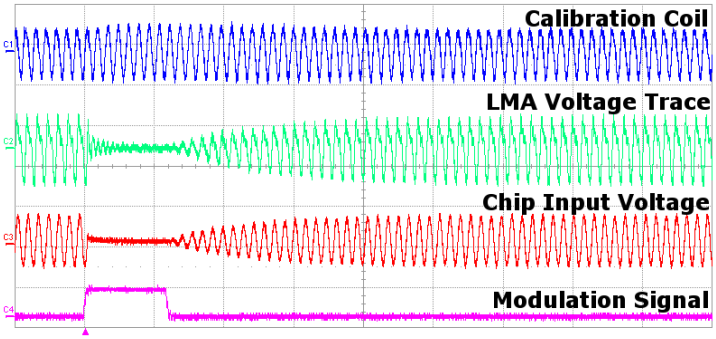

(a) Load modulation as seen at the air interface

(b) Modelled envelope of a load modulated signal

Figure 3.12: Load modulation pulse shape in time domain

between the modulated and unmodulated chip. As already discussed in section 3.2.2.1, this is the reason, why a modulator-at-antenna chip topology is preferable in terms of load modulation amplitudes. In terms of system parameters (resonance voltage rise) the difference between Q_T and Q_M is proportional to the sideband amplitudes.

The emitted field strength of the PCD antenna increases during modulation as indicated by the calibration coil voltage, which is caused by the previously mentioned temporarily reduced card loading effect.

Furthermore it has to be mentioned that this consideration based on the time constants is only possible assuming $f_{RES} \approx f_C$ because within a detuned system over- and undershoots occur and no exponentially shaped envelope is encountered any more.

This concept can be extended for a series of modulation pulses. For visual clarity figure 3.13 shows three modulation pulses for the transponder's coil current I_{TP}. The principle is introduced in [Geb11]. This model assumes a periodical switching between two Q-values. In reality this is a

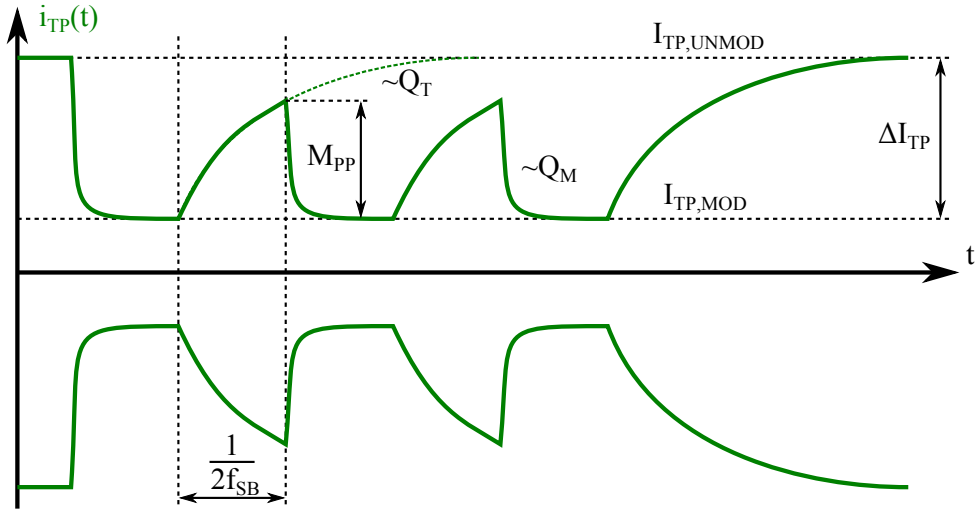

Figure 3.13: Envelope of transponder's coil current $i_{TP}(t)$ assuming three modulated pulses

continuous process what may be accounted for by defining a continuous quality factor function $Q_T(t)$ like introduced in [Kla09]. This thesis will stick to the simplified assumption the periodical Q-factor switching to allow a simplified analytic disussion.

3.5.2 Envelope Signal of Load Modulating Chip

The modulation amplitude can be estimated according to figure 3.13. To derive a formula for the modulation depth M_{pp} the envelope shape of the transponder antenna's current for a rising edge can be defined as

$$\begin{aligned} i_{TP,RISE}(t) &= (I_{TP,UNMOD} - I_{TP,MOD}) \left(1 - e^{-\frac{t}{\tau_{RISE}}}\right) \\ &\text{with } \tau_{RISE} = \frac{2Q_T}{\omega_{RES}} \text{ and } f_{SB} = \frac{f_C}{2k}, k \in \mathbb{N}\backslash 0 \\ \hat{M} &= i_{TP,RISE}\left(\frac{1}{2f_{SB}}\right) = \Delta I_{TP}\left(1 - e^{-\frac{f_{RES}}{f_C}\frac{k\pi}{Q_T}}\right), \end{aligned} \tag{3.4}$$

where f_{SB} denotes the sidecarrier frequency and τ_{RISE} the time constant of the rising edge. For a typical HF RFID communication system based on ASK load modulation the maximum data rate and subcarrier frequency is defined as $f_C/16 \approx 848\ kHz = f_{SB}$ as an OOK coding scheme with one bit per Hertz is used.

Chapter 4: Analytical Description of the coupled Transponder

"One machine can do the work of fifty ordinary men. No machine can do the work of one extraordinary man."

[Elbert Hubbard]

The aim of this chapter is a detailed analysis of the currents within an ISO/IEC 10373-6 measurement setup, which can be partially extended to any typical reader-transponder setup and to discuss a possible relation allowing a coarse estimation of the sideband amplitudes according to the proximity base standard ISO/IEC 14443 [IE10a]. It is desirable to find a purely analytical formula. As noted earlier this can only be as accurate as the underlying model is. To verify the practical usability this discussion is based on simulations in LTspice [Tec12] and analytic derivations of the network equations numerically solved in MATLAB [The12].

4.1 The transponder as a Load

Assuming a noteworthy coupling between DUT and PCD the energy drawn by a transponder reduces the H-field strength of the emitting coil. The magnitude of the antenna coil current is proportional to the emitted H-field strength. As a first step the general relationship between the PCD's and transponder's antenna currents is analysed. This will be extended to discuss the card loading effect. Its concept has already been introduced in the previous chapters.

4.1.1 Simulation Setup

The network shown in figure 4.1 is used to model the transponder. For simplicity a constant input impedance of the IC and a resistive-only modulation impedance are assumed for simplicity. Whereas the SPICE simulation includes the complete antenna arrangement as specified in the

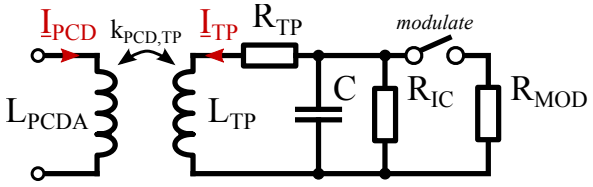

Figure 4.1: Coupling network consisting of the primary emitting coil and the transponder

proximity test standard ISO/IEC 10373-6 [IE11], the analytical description is simplified to the emitting PCD antenna coupled to the transponder. As it will be seen later, this yields a marginal

deviation in the simulation results caused by the additional loading of the PCD antenna by the calibration and sense coils.

Simulations were performed using a typical transponder within an ISO/IEC measurement setup using a $Q_{PCD} = 12$ matching. Table 4.1 lists the selected values. As defined in the test standards, a PCD1 measurement setup network is used for transponder antennas of Class 1 to 3 and PCD2 to Class 4 to 6 respectively. This results in a larger coupling factor between PCD and the transponder for the smaller Class 4 antenna compared with the larger Class 2 antenna as the PCD2 antenna radius is 50 mm compared with 75 mm using a PCD 1 antenna.

Section	Name	Symbol	Value	Unit
Transponder Antenna Class 1	Serial Inductance	L_{TP}	3	μH
	Serial Resistance	R_{TP}	2.45	Ω
	Parallel Capacitance	C_{TP}	4.64	pF
Transponder Antenna Class 2	Serial Inductance	L_{TP}	1.86	μH
	Serial Resistance	R_{TP}	1.51	Ω
	Parallel Capacitance	C_{TP}	2.41	pF
Transponder Antenna Class 4	Serial Inductance	L_{TP}	1.67	μH
	Serial Resistance	R_{TP}	4.07	Ω
	Parallel Capacitance	C_{TP}	1.59	pF
Coupling Factor	Class 1 Transponder	$k_{PCD,TP}^{\text{Class 1}}$	0.063	
	Class 2 Transponder	$k_{PCD,TP}^{\text{Class 2}}$	0.039	
	Class 4 Transponder	$k_{PCD,TP}^{\text{Class 4}}$	0.058	

Table 4.1: Component values used for simulations

4.1.2 PCD Transponder Coupling

For a fundamental analysis of the coupling system an incremental approach was chosen:

1. Discuss the basic physics behind magnetic coupling.
2. Derive a relation for a short-circuited transponder coil current.
3. Relate the transponder's and the PCD's coil currents to find a phase relation between them.
4. Calculate and verify the transponder's and the PCD's coil currents based on the amplifier's output voltage.
5. Correlate the ratio between the unmodulated and the modulated transponder's coil currents to the ISO/IEC sideband amplitudes for different subcarrier frequencies.
6. Vary the resistances in the transponder network to check the impact compared to the smallest transponder's coil current. This current in the short-circuited case shall be the lower bound.

4.1.2.1 Inductive Coupling System

The principle of a general RFID inductive coupling arrangement is shown in figure 4.2. According to *Ampere's Law* $\nabla \times \mathbf{B} = \mu_0 \mathbf{J}$ the current in the reader coil I_{PCD} generates a magnetic field $\mathbf{B}_{PCD}$ and a magnetic flux ϕ_{PCD} respectively. The transponder's antenna spans an area A_{TP} which acts as a cross section for ϕ_{PCD}. If the secondary loop is closed (e.g. $R_2 < \infty$), a voltage will be induced as defined by *Faraday's Law of Induction* $\nabla \times \mathbf{E} = -\partial \mathbf{B}/\partial t$. As the primary reader current I_{PCD} is sinusoidal and therefore time varying, there will always be an induced voltage. With this voltage a current I_{TP} will arise that is inversely proportional to the induced voltage by the factor R_2. In the case of a zero-valued load resistor this defines the short-circuit current $I_{TP,0}$. The current in the secondary loop itself generates a magnetic field $\mathbf{B}_{TP}$ which

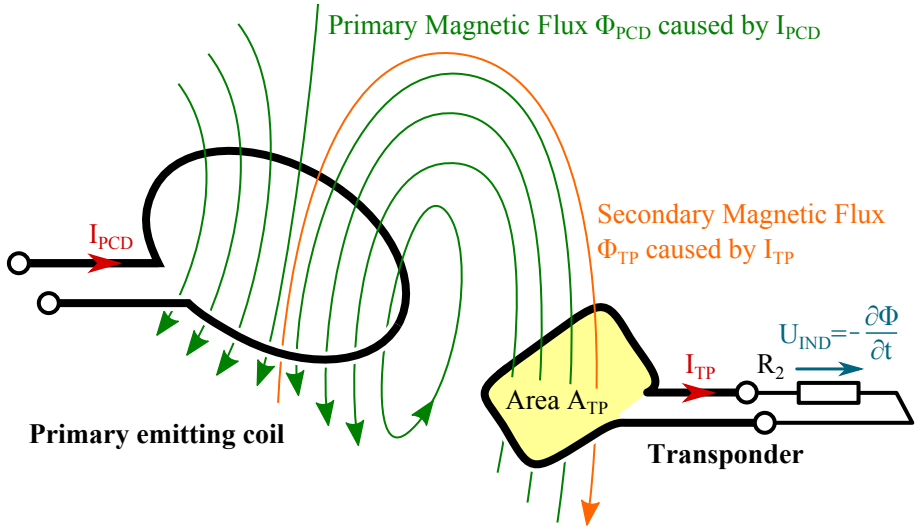

Figure 4.2: Inductive coupling between reader and transponder

cancels out the primary H-field within the transponder loop in the case of $R_2 = 0$ (*Lenz's Law*). A portion of the total secondary flux goes through the primary coil and results in a current that reduces the primary reader current I_{PCD}. The phase difference between these two currents is 180°. The strength of this effect is depending on the inductance of and the coupling between these two loops.

To represent the induced voltage on network level, a modified topology shown in figure 4.3 should be used. The mutual inductance is defined as

$$M_{PCD,TP} = k_{PCD,TP}\sqrt{L_{TP}L_{PCD}}. \tag{4.1}$$

4.1.2.2 Short Circuited Transponder

According to *Lenz's Law* there arises a secondary H-field that cancels the primary field at the transponder's position. Knowing the estimated emitted H-field of a rectangular spiral transponder antenna, the required current can be estimated knowing the field strength applied to the

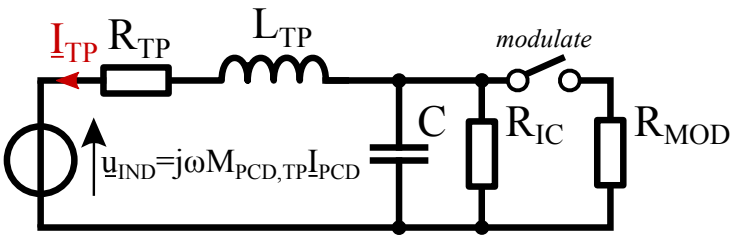

Figure 4.3: Modified equivalent circuit of the transponder including the induced voltage caused by the PCD. The total parallel capacitance is defined as $C = C_{TP} + C_{TUNE} + C_{IC}$.

transponder [Gri99].

$$
\begin{aligned}
H(x) &= \frac{INab}{4\pi\sqrt{\left(\frac{a}{2}\right)^2 + \left(\frac{b}{2}\right)^2 + x^2}} \left[\frac{1}{\left(\frac{a}{2}\right)^2 + x^2} + \frac{1}{\left(\frac{b}{2}\right)^2 + x^2} \right] \\
H(0) &= \frac{INab}{4\pi\frac{1}{2}\sqrt{a^2+b^2}} 4\frac{a^2+b^2}{a^2b^2} = \frac{2IN\sqrt{a^2+b^2}}{ab\pi} \\
\rightarrow I &= \frac{ab\pi}{2N\sqrt{a^2+b^2}} H
\end{aligned}
\tag{4.2}
$$

This equation is true for a perfectly rectangular single loop antenna with width a and height b which span the transponder antenna area A_{TP}. equation 4.2 has to be extended to reflect the reality.

4.1.2.3 Phase Relation between Currents

In the general case the PCD and transponder coil currents are related to each other. Properties of this relation are of interest as these are linked to the amount of energy (*energy distance*) and the properties of the load modulated return link (*communication distance*).

4.1.2.4 Vector Diagrams of Transponder Network

To analyse the phase relations between the two coil currents, one has to examine all the voltages and currents within the transponder network shown in figure 4.3. Assuming an arbitrate current I_C and resonance (e.g. $f = f_{RES}$), a vector diagram can be created as illustrated in figure 4.4 (a). In the case of a high-Q transponder the chip input resistance R_{IC} can be neglected and the transponder acts as a pure series resonance circuit. The corresponding vector diagram is shown in figure 4.4 (b). The energy oscillates between the reactive elements and their component voltages cancel out. The complete induced voltage can be measured over the resistor R_{TP}.

As the quality factor of the transponder decreases, the resistive chip input current increases compared to the capacitor current which is illustrated in figure 4.4 (c). This results in an increasing phase difference between the two coil's currents, which gets as high as -180 ° in the case of a short circuited transponder. This extreme case will occur if the capacitance is short-circuited by a zero-valued R_{IC}.

Note that the absolute value of the induced voltage U_{IND} is nearly the same for all three vector diagrams in figure 4.4 although the length of the vectors indicate something else. Therefore the IC is supplied with less energy in the low-Q case.

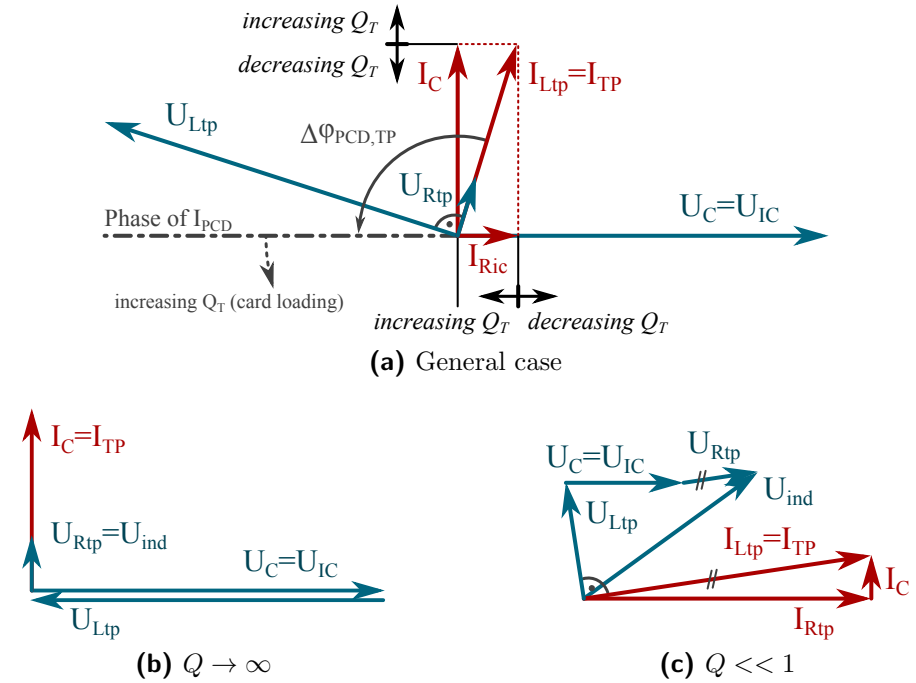

Figure 4.4: Vector diagrams of voltages and currents within the transponder network for different transponder quality factors Q_T assuming $f = f_{RES}$ to explain the phase relations to the PCD's coil current I_{PCD}. Diagrams in general and compared to each other are not to scale.

4.1.2.5 Transformed Transponder Impedance

According to *Faraday's Law of Induction* the phase of this voltage would lag the exciting current by 90 ° in the high-Q case (series resonance case). In a first approximation the phase orientation of the PCD's coil current can be assumed to be constant over a varying transponder quality factor. A more detailed discussion has to consider a loading of the PCD caused by the transponder, which is often called *card loading*. It is reasonable to introduce the concept of a transformed transponder impedance known from power transformers and presented for HF RFID systems in [Fin10]. The transponder impedance

$$\underline{Z}_{TP} = R_{TP} + j\omega L_{TP} + \frac{R_{IC}}{1 + j\omega C R_{IC}} \tag{4.3}$$

acts as an additional series impedance to the primary PCD's coil. The transformed transponder impedance can be calculated by

$$\begin{aligned} \underline{Z}'_{TP} &= \frac{(\omega M_{PCD,TP})^2}{\underline{Z}_{TP}} \\ &= \frac{R_{TP} + R_{IC} - \omega^3 R_{IC}^2 L_{TP} C^2 + \omega^2 R_{IC}^2 R_{TP} C^2 + j\omega\left(R_{IC}^2 C - L_{TP}\right)}{\left(R_{TP} + R_{IC} - \omega^2 R_{IC} L_{TP} C\right)^2 + \omega^2 \left(L_{TP} + R_{IC} R_{TP} C\right)^2} \left(\omega M_{PCD,TP}\right)^2 \end{aligned} \tag{4.4}$$

and was calculated for the three considered antenna classes. In the modulated case and for practical transponder quality factors Q_T exceeding 1, R_{IC} can be replaced by R_{MOD} as they are in parallel. This additional transformed impedance is acting in series to the PCD's coil, e.g.

$$\underline{Z}_{PCD} = \underline{X}_{PCD} = j\omega L_{PCD} \;\rightarrow\; \widetilde{\underline{Z}}_{PCD} = \underline{X}_{PCD} + \underline{Z}'_{TP}. \tag{4.5}$$

The impedance-over-Q plot is shown in figure 4.5. The transformed transponder's impedance has always to be seen in comparison with the impedance of the transmitting PCD coil which is

$$\underline{Z}_{Lpcd}^{f=13.56\ MHz} = \begin{cases} j39.362\ \Omega & \dots \quad \text{PCD1 for antenna classes 1 to 3} \\ j27.605\ \Omega & \dots \quad \text{PCD2 for antenna classes 4 to 6.} \end{cases} \tag{4.6}$$

A higher transponder Q-factor reduces the magnitude of the PCD's coil current and therefore the emitted H-strength.

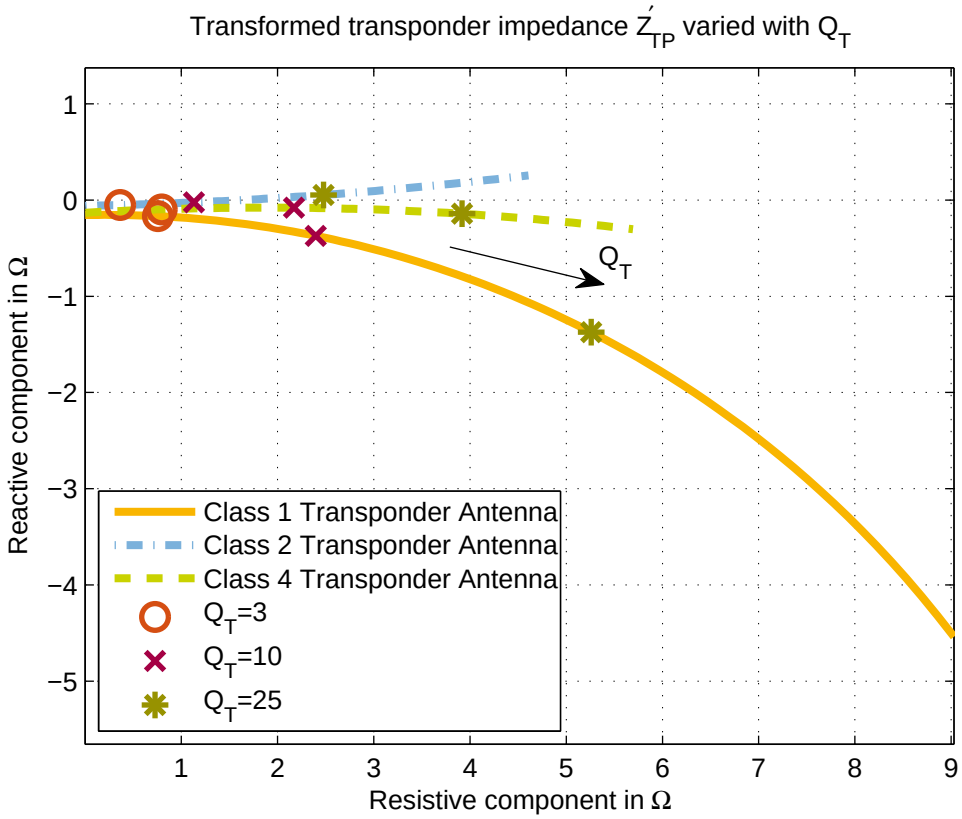

Figure 4.5: Transformed transponder impedance $\underline{Z}'_{TP}$ varied with the transponder quality factor Q_T from 0 to 60 for three antennas at $f_C = 13.56\ MHz$

It can be seen clearly from equation 4.4 and figure 4.5 that the coupling has a crucial impact on the card loading. As a rough guess one can postulate the proportionality

$$\underline{Z}'_{TP} \propto k^2_{PCD,TP} L_{TP}. \tag{4.7}$$

As a summary of this subsection it can be observed that the phase of the transformed transponder impedance has an impact on the PCD's coil current which can be neglected for smaller antenna sizes (small coupling coefficient and smaller inductance) when considering realistic transponder quality factors below 60.

For an even more deep insight towards the loading effect the transformed transponder impedance can be expressed in terms of system properties. Under the constraint $R_{TP} <<$

R_{IC} or $Q_{TP,ANT} << Q_{IC}$ this impedance can be expressed as

$$\begin{aligned} \underline{Z}_{TP} &\approx \frac{R_{IC} - \omega^2 R_{IC} C L_{TP} + j\omega L_{TP}}{\left(1 + j\omega R_{IC} C\right)\left(\omega M_{PCD,TP}\right)^2} = \frac{\left(1 - \frac{\omega^2}{\omega_{RES}^2}\right) + j\frac{\omega}{\omega_{RES}}\frac{1}{Q_T}}{\frac{1}{Q_T} + j\frac{\omega}{\omega_{RES}}}\omega_{RES} L_{TP} \\ \rightarrow \underline{Z}'_{TP} &\approx \frac{1 + j\frac{\omega}{\omega_{RES}} Q_T}{\left(\frac{\omega_{RES}}{\omega} - \frac{\omega}{\omega_{RES}}\right) Q_T + j} k_{PCD,TP}^2 \omega L_{PCD}. \end{aligned} \tag{4.8}$$

4.1.2.6 Simulations Results

The phase differences have been extracted from simulations of three antenna classes and are shown in figure 4.6. For a transponder circuit with a low quality factor close to the carrier frequency a transponder current arises with a 180 ° phase shift to the primary PCD's current. With an increasing quality factor the phase difference decreases as the phase of the transponder current I_{TP} increases while the PCD's current I_{PCD} stays (nearly) constant. But as the preceding paragraphs have shown this PCD's current phase is slightly increasing for higher coupling coefficients and larger transponder coil inductances as $\widetilde{Z}_{PCD}$ is getting more capacitive (a decreasing impedance phase results in an increasing current phase).

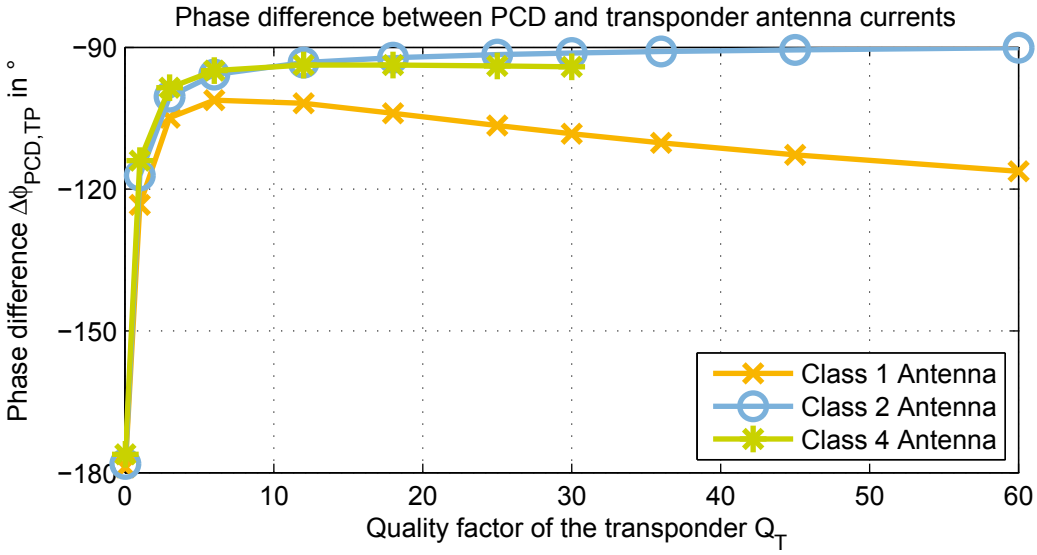

Figure 4.6: Phase difference between PCD and transponder currents as a function of the quality factor of the transponder Q_T for tuned antennas ($f_C = f_{RES}$). Note that the quality factor of the Class 4 antenna system is physically limited to about 34.

4.1.3 Estimation of H_{MIN} for Chip Operation

The (simplified) transponder impedance can be used to estimate the chip voltage U_{IC} based on the induced voltage U_{IND}. Under the constraint of $R_{TP} \rightarrow 0$ the circuit in figure 4.3 results in a voltage ratio defined by

$$\frac{\underline{U}_{IC}}{\underline{U}_{IND}} = \frac{R_{IC}}{1 + j\omega R_{IC} C} \underline{Z}_{TP}^{-1} = \frac{1}{1 - \frac{\omega^2}{\omega_{RES}^2} + j\frac{\omega}{\omega_{RES}}\frac{1}{Q_T}}. \tag{4.9}$$

Under the assumption of a purely sinusoidal induced voltage caused by a homogeneous magnetic flux, its magnitude can be estimated to be

$$|\underline{U}_{IND}| \approx \mu_0 \omega_C H \underbrace{N A}_{=:A_{TPant}} \cos\alpha, \tag{4.10}$$

as described in [TSG08]. Thus,

$$|\underline{U}_{IC}| = \frac{\mu_0 \omega_C H A_{TPant} \cos\alpha}{\sqrt{\left(1 - \frac{\omega^2}{\omega_{RES}^2}\right)^2 + \frac{\omega^2}{\omega_{RES}^2}\frac{1}{Q_T^2}}} \tag{4.11}$$

can be reformulated to give a value for the H-field strength

$$H = \frac{\sqrt{\left(1 - \frac{\omega^2}{\omega_{RES}^2}\right)^2 + \frac{\omega^2}{\omega_{RES}^2}\frac{1}{Q_T^2}}}{\mu_0 \omega_C A_{TPant} \cos\alpha} U_{IC}. \tag{4.12}$$

This equation is the basis for understanding the transponder at system level and is discussed in detail within [Geb11]. It gives a prediction about the minimum H-field strength H_{MIN} in DUT position if $U_{IC,MIN}$ is plugged in. Field strength values greater than H_{MIN} still result in $U_{IC} \approx U_{IC,MIN}$ as the quality factor is decreased (limiter action). The coarse estimation of $Q_T = R_{IC}/(\omega_{RES} L_{TP})$ can be used to get a value for the chip input resistance in operational state.

For the tuned case $\omega_{RES} = \omega_C$ the quality factor can be interpreted as a gain factor, e.g.

$$|U_{IC}| = Q_T |U_{IND}| \quad \forall\ \omega_{RES} = \omega_C, \tag{4.13}$$

which can be used to extract the modulated quality factor based on the knowledge of the magnitude of the chip input voltage in the modulated and non-modulated state, i.e.

$$Q_M = Q_T \frac{|U_{ic,mod}|}{|U_{IC}|} \quad \forall\ \omega_{RES} = \omega_C. \tag{4.14}$$

This section implicitly used the absolute value operator $|.|$ for clarity reasons. It will be neglected in further discussions as it can be seen from the context.

4.1.4 Analytical Derivation of Currents

The next step in this approach of modelling the RFID HF coupling system is to consider the complete PCD network between the amplifier output and the primary transmitting antenna. Simulations have shown that it is useful to consider the complete network, which consists of two capacitors C_{PCD1} and C_{PCD2} to achieve a matching between the 50 Ω output of the amplifier and the antenna. An additional damping resistor R_{PCD} is used to control the quality factor Q_{PCD}. This network is shown in subfigure 4.7 (a) which can be simplified introducing

$$\begin{aligned} R_\delta &= \frac{R_{PCD} R_{PCDA}}{R_{PCD} + R_{PCDA}}, \quad C_\delta = C_{PCD2} + C_{PCDa} \\ \underline{Z}_Q &= R_q + \frac{1}{j\omega C_{PCD1}}, \quad \underline{Z}_\alpha = \underline{Z}'_{TP} + j\omega L_{PCDA} \quad \text{and} \quad \underline{Z}_\delta = \frac{R_\delta}{1 + j\omega R_\delta C_\delta} \end{aligned} \tag{4.15}$$

resulting in the network shown in subfigure 4.7 (b). The PCD's current follows with

$$\underline{I}_{PCD} = \underline{U}_q \frac{\underline{Z}_\delta}{\underline{Z}_Q (\underline{Z}_\alpha + \underline{Z}_\delta) + \underline{Z}_\alpha \underline{Z}_\delta} \tag{4.16}$$

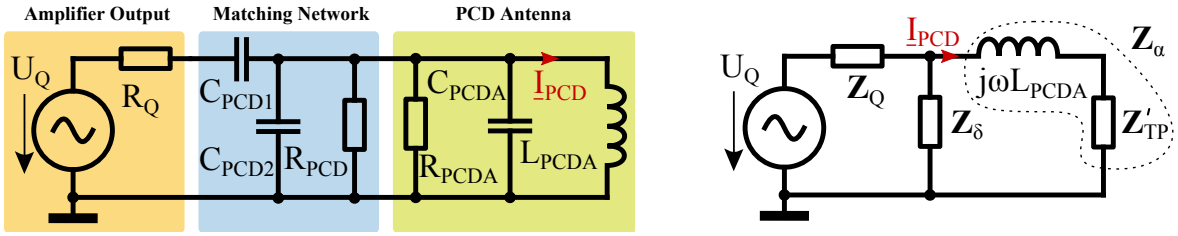

(a) PCD network **(b)** Simplified network

Figure 4.7: Standard PCD network and the simplified version of it

and the transponder coil current with

$$\underline{I}_{TP} = \frac{\underline{U}_{IND}}{\underline{Z}_{TP}} = \frac{j\omega k_{PCD,TP}\sqrt{L_{TP}L_{PCDA}}}{\underline{Z}_{TP}}\underline{I}_{PCD}. \tag{4.17}$$

Comparisons between the analytical considerations with numerical MATLAB simulations and SPICE simulations of the complete ISO/IEC 10373-6 measurement setup were performed with a Class 2 antenna configuration. Figure 4.8 includes the results of the comparison, which show a good match between them. Note that the analytical model only considers the PCD to transponder coupling link, whereas the SPICE model includes couplings between all the antennas in the ISO measurement setup. So it can be concluded that this additional loading to the PCD antenna (*measurement setup loading*) introduced by these sense and calibration coils can be neglected. Two additional verification measurements out of the SPICE simulation were done to verify this to explain the difference between the *LTspice I* and *Matlab I* curves in figure 4.8.

4.1.5 Estimation of the Card Loading Effect

Equation 4.16 introduced a mathematical model describing the impact of the presence of the transponder to the PCD's coil current I_{PCD}. This relation can be used to estimate the card loading effect, which is expressed in terms of the card loading factor (CLF)

$$CLF = \frac{\text{H-field with transponder} - \text{H-field without transponder}}{\text{H-field without transponder}}. \tag{4.18}$$

The CLF is defined negatively, because increased loading decreases the H-field strength. As the magnitude of the PCD's coil current causes the measured H-field, the card loading factor can be related to this current in the loaded and unloaded state. Thus,

$$CLF \approx \text{abs}\left\{\frac{I_{PCD}}{I_{PCD}|_{\underline{Z}'_{TP}\to 0}}\right\} - 1. \tag{4.19}$$

Although this deviation neglects the effect of any other resonant networks within the vicinity of the PCD-transponder coupling system, it reflects the main and dominant effects in the complete test setup. Introducing equation 4.16 results in

$$CLF \approx \text{abs}\left\{\frac{\underline{Z}_Q\left(j\omega L_{PCDA} + \underline{Z}_\delta\right) + j\omega L_{PCDA}\underline{Z}_\delta}{\underline{Z}_Q\left(\underline{Z}'_{TP} + j\omega L_{PCDA} + \underline{Z}_\delta\right) + \left(\underline{Z}'_{TP} + j\omega L_{PCDA}\right)\underline{Z}_\delta}\right\} - 1, \tag{4.20}$$

which can be realigned and simplified to

$$CLF \approx \text{abs}\left\{\frac{\underline{Z}_Q\underline{Z}_\delta + j\omega L_{TP}\left(\underline{Z}_Q + \underline{Z}_\delta\right)}{\underline{Z}_Q\underline{Z}_\delta + \underline{Z}'_{TP}\left(\underline{Z}_Q + \underline{Z}_\delta\right) + j\omega L_{TP}\left(\underline{Z}_Q + \underline{Z}_\delta\right)}\right\} - 1 = \frac{1}{\text{abs}\left\{1 + \frac{\underline{Z}'_{TP}}{\underline{Z}_{PCD}}\right\}} - 1 \tag{4.21}$$

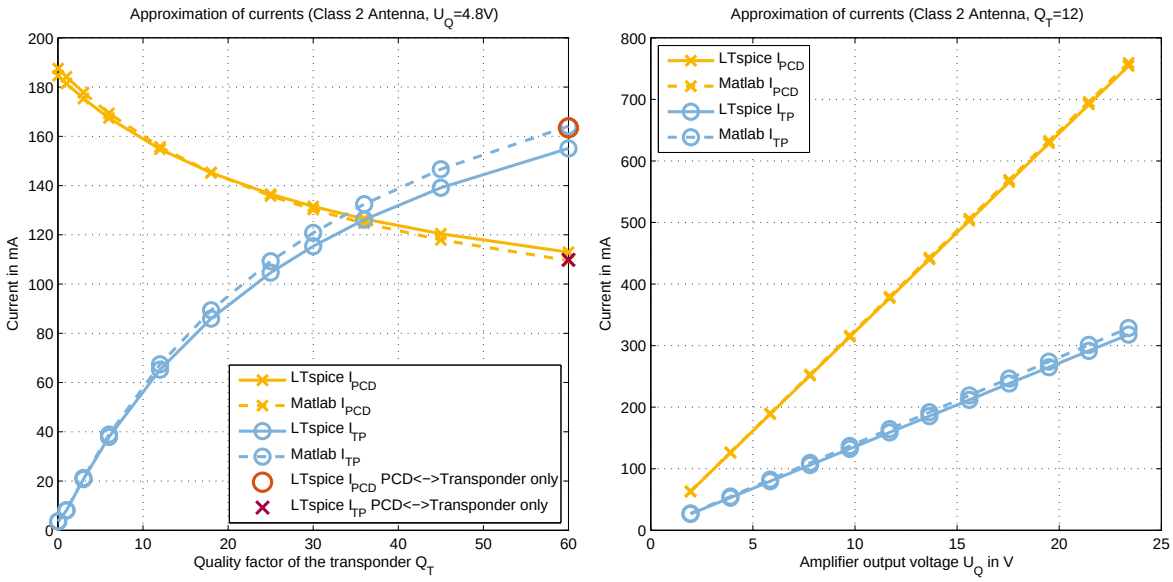

(a) Currents over Q_T **(b)** Currents over U_Q

Figure 4.8: PCD and transponder coil currents as a function of the transponder quality factor Q_T and the amplifier output voltage U_Q generated from SPICE and MATLAB simulations. Subfigure (a) shows two measurement points derived from a SPICE simulation including only the PCD to transponder coupling link. The amplifier output voltage range relates to a field strength at DUT position between 0.25 to 2.5 $A/m(rms)$.

by defining a constant PCD network impedance

$$\tilde{\underline{Z}}_{PCD} := \frac{\underline{Z}_Q \underline{Z}_\delta}{\underline{Z}_Q + \underline{Z}_\delta} + j\omega L_{TP}. \tag{4.22}$$

Equation 4.8 can be applied to predict the card loading factor for any arbitrary coupling, transponder quality factor or resonance frequency. The strongest loading effect is to be expected for $f_{RES} = f_C$, e.g.

$$\underline{Z}'_{TP}|_{f_{RES}=f_C} = k^2_{PCD,TP}\ \omega_C\ L_{PCDA}\ \ (Q_T - j)\,. \tag{4.23}$$

Based on these equations the strength of the expected card loading can be calculated. Figure 4.9 shows the maximum loading for $f_{RES} = f_C$ for six typical couplings originating from all six Reference PICC antennas (coupled to a PCD 1 antenna).

4.2 Introduction to an Analytical Model for the Load Modulation Amplitudes

This section describes one possibility of defining an analytic relation between system parameters and values for the lower and upper sideband amplitude.

4.2.1 Definition of a Simplified Coupling Network

Chapter 3 already started a discussion on the difficulty of including the complete ISO measurement network into the analytical LMA modelling. Here it is restricted to the fundamental

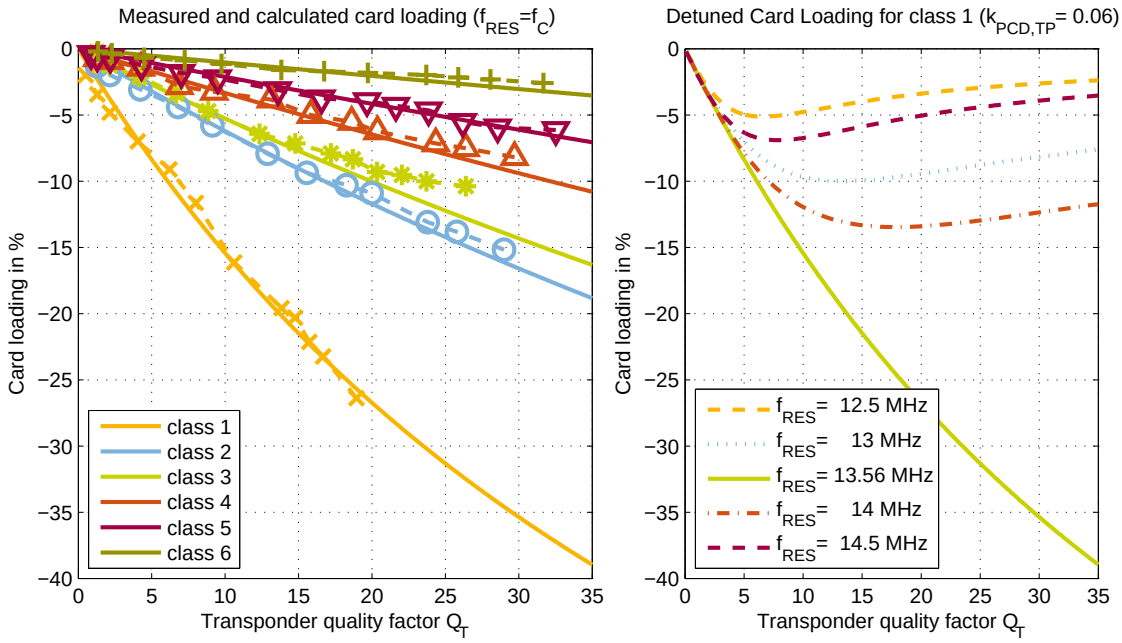

Figure 4.9: Maximum card loading ($f_{RES} = f_C$) plotted for all six Reference PICC antennas coupled to a PCD 1 antenna within the ISO/IEC test setup compared to measurement data (dashed lines). On the right hand side the expected card loading over transponder quality factor for detuned transponders with a class 1 antenna is shown.

parts which deal with the transponder backlink measurement shown in figure 4.10: A passively powered transponder performs load modulation by periodically switching a load resistor parallel to its input ports to vary the quality factor between two values. A current proportional to the transponder's coil current is induced in the sense coil A which itself is proportional to the resulting probe voltage $u_{LMA}(t)$. In this simplified quasi-static consideration sense coil B can be neglected completely as the coupling between it and the transponder is almost zero. Its main purpose is to cancel the primary PCD's H-field. The series resistance of the transponder antenna

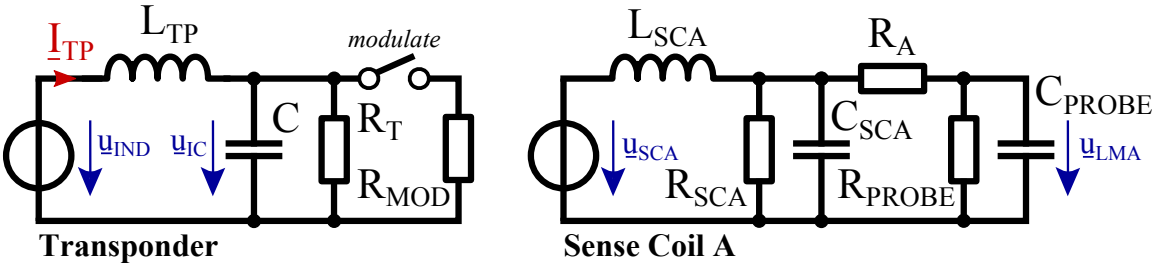

Figure 4.10: Simplified network to allow analysis of load modulation amplitudes in frequency domain consisting of the active parts within the transponder and the sense coils

R_{TP} is included in R_T for simplicity [Geb11]. For a compact notation the parallel resistance of the transponder is called R_T in the unmodulated case (proportional to Q_T) and $R_T^{(mod)}$ in the modulated case (proportional to Q_M).

The problem of deriving the LMA strengths can be divided into two separate sub-problems which are linked by the transponder's coil current I_{TP} in only one direction:

1. Transponder network: Derive an equation for I_{TP} assuming R_T is periodically varying
2. Sense coils/ Helmholtz network: Relate u_{LMA} or LSB and USB based und I_{TP}

The second task is the by far simpler as it includes only a voltage divider of constant elements. But the transponder in contrast is a linear time-variant network which is not always analytically solvable.

4.2.2 Part I: The Linear Time-Variant Transponder Network

A steady-state system description of the transponder network will be used to analyse the LMA values. First the representation at system level will be derived. Afterwards time Q-switching will be introduced and analytic solution methods will be presented.

4.2.2.1 Definition of the Steady State System

One possibility of describing the transponder network from figure 4.10 is the definition of a steady state system. Using the component's laws

$$i_C = C\dot{u}_{IC} \quad \text{and} \quad u_C = L_{TP}\dot{i}_{TP} \tag{4.24}$$

where $\dot{\alpha}$ denotes the time derivative of α, it is possible to extract the differential equations in time domain

$$\begin{aligned} \text{(I)}\ U_{IND} &= L_{TP}\dot{i}_{TP} + u_{IC} \\ \text{(II)}\ i_{TP} &= \frac{u_{IC}}{R_T} + C\dot{u}_{IC} \end{aligned} \tag{4.25}$$

out of the network. Therefore it is reasonable to define the state variable vector describing the time signal of the energy storing components and their derivatives with respect to time, i.e.

$$\mathbf{x} := \begin{bmatrix} i_{TP} \\ u_{IC} \end{bmatrix} \quad \text{and} \quad \dot{\mathbf{x}} := \begin{bmatrix} \dot{i}_{TP} \\ \dot{u}_{IC} \end{bmatrix}, \tag{4.26}$$

which yields to the definition of the steady state system

$$\begin{aligned} \dot{\mathbf{x}} &= \begin{bmatrix} 0 & -\frac{1}{L_{TP}} \\ \frac{1}{C} & -\frac{1}{R_T C} \end{bmatrix} \mathbf{x} + \begin{bmatrix} \frac{\hat{U}_{IND}}{L_{TP}} \\ 0 \end{bmatrix} u \\ y &= [1 \quad 0]\,\mathbf{x} \end{aligned} \tag{4.27}$$

The system can be represented at system level by using the characteristic properties of a resonant circuit (see section 2.3.1). Thus,

$$\begin{aligned} \dot{\mathbf{x}} &= \underbrace{\begin{bmatrix} 0 & -\frac{1}{L_{TP}} \\ \omega_{RES}^2 L_{TP} & -\frac{\omega_{RES}}{Q} \end{bmatrix}}_{=:\mathbf{A}(Q)} \mathbf{x} + \underbrace{\begin{bmatrix} \frac{\hat{U}_{IND}}{L_{TP}} \\ 0 \end{bmatrix}}_{=:\mathbf{b}} u \\ y &= \underbrace{[1 \quad 0]}_{=:\mathbf{c}^T} \mathbf{x} \end{aligned} \tag{4.28}$$

4.2.2.2 Including the Time-Variant Transponder Quality Factor

In the simplest case equation 4.28 has to be extended with

$$Q \rightarrow Q(t) = \begin{cases} Q_T & \dots \quad 0 \leq t < \frac{1}{2f_{SB}} \\ Q_M & \dots \quad \frac{1}{2f_{SB}} \leq t < \frac{1}{f_{SB}} \end{cases} . \tag{4.29}$$

As noted in the first chapters the Q-factor has to change continuously, which is here not the case. But in general the assumption of equation 4.29 is said to be accurate enough.

One possible way to find a solution for y or the load modulation amplitudes is to find a solution for this system of inhomogeneous linear differential equations of first order with non-constant coefficients or to combine both equations to a single inhomogeneous linear differential equation of second order with non-constant coefficients. The variation of the quality factor $Q(t)$ can be approximated by the first element of a Fourier series expansion. Thus,

$$Q(t) = \underbrace{\frac{Q_T + Q_M}{2}}_{\text{offset}} + \underbrace{\frac{Q_T - Q_M}{2}}_{\text{amplitude}} \underbrace{\frac{4}{\pi} \sum_{k=1}^{\infty} \frac{\sin\left((2k-1)\omega_{SB}t\right)}{2k-1}}_{\text{Fourier series expansion}} \approx \frac{2\left(Q_T - Q_M\right)}{\pi} \sin\left(\omega_{SB}t\right) . \tag{4.30}$$

This is definitely an extensive assumption. There are books containing lists of possible solutions for such differential equations [PZ03], but this specific differential equation could not be found in there. A solution solving these differential equations using this general workflow seems to be infeasible.

4.2.2.3 Switched Steady States Systems

As an alternative approach for a simplified solution for LMA analysis the system described in equation 4.28 can be seen to have two periodically switched system matrices, e.g.

$$\begin{aligned} \mathbf{A}_1 = \mathbf{A}(Q_T) \quad \dots \quad & \text{unmodulated phase } 0 \leq t < \frac{1}{2f_{SB}} \\ \mathbf{A}_2 = \mathbf{A}(Q_M) \quad \dots \quad & \text{modulated phase } \frac{1}{2f_{SB}} \leq t < \frac{1}{f_{SB}} = T_{SB} \end{aligned} \tag{4.31}$$

Even the variation of the induced voltage due to card loading resulting from the change of the quality factor can easily be included in the discussion by switching between two values of the induced voltage in vector $\mathbf{b}$. The increased H-field strength during modulation can be computed by the set of equations defined in section 4.1.5.

After defining two time invariant steady state system matrices (constant coefficients) and a switching interval an analytic solution for the load modulation amplitudes at $\omega_C \pm \omega_{SB}$ can be found following an approach like described in [Lio72]. This allows to get analytic results, which are still too complex to be understood. One main problem is the nature of the system matrix $\mathbf{A}(Q)$: To solve the differential equations system the matrix has to be diagonalised using a complex exponential transition matrix $e^{\mathbf{A}}$. But the "nature" of the complete system changes with Q as seen by $\mathbf{A}$'s eigenvalues:

$$\begin{aligned} \det\left\{\lambda\mathbf{E} - \mathbf{A}\right\} = \lambda^2 + \frac{\omega_{RES}}{Q}\lambda + \omega_{RES}^2 &\stackrel{!}{=} 0 \\ \rightarrow \text{eigenvalues } \lambda_{1,2} = \frac{\omega_{RES}}{2Q}\left(-1 \pm \sqrt{1-4Q^2}\right) & \end{aligned} \tag{4.32}$$

A quality factor $Q < \frac{1}{2}$ results in two real-valued eigenvalues on the left pane and a $Q \geq \frac{1}{2}$ results in a complex conjugated pair of eigenvalues. Depending on the choice of the eigenvalues the structure of the transition matrices changes. A good guide for calculating these transition matrices can be found in [BS93].

4.2.3 Part II: Helmholtz Network

The sense coil network shown on the right hand side of figure 4.10 includes only constant components which allows to apply the voltage division rule [Sco87]. To reduce the number of quantities in the derivation process, the impedances

$$\underline{Z}_{SCA} := \frac{R_{SCA}}{1 + sR_{SCA}C_{SCA}} \quad \text{and} \quad \underline{Z}_{PROBE} := \frac{R_{PROBE}}{1 + sR_{PROBE}C_{PROBE}} \tag{4.33}$$

are introduced. The induced voltage in sense coil A is defined as

$$\underline{U}_{SCA} = s \underbrace{k_{SCA,TP}\sqrt{L_{SCA}L_{TP}}}_{=\underline{M}_{SCA,TP}} \underline{I}_{TP}. \tag{4.34}$$

After some steps of derivation the desired relation can be found. Thus,

$$\underline{U}_{LMA}(s) = \frac{\underline{Z}_{SCA}\underline{Z}_{PROBE}}{sL_{TP}\left(R_A + \underline{Z}_{SCA} + \underline{Z}_{PROBE}\right) + \underline{Z}_{SCA}\left(R_A + \underline{Z}_{PROBE}\right)} s\underline{M}_{SCA,TP}\underline{I}_{TP}. \tag{4.35}$$

This equation can be used to relate each frequency component of the transponder current to the resulting components as seen at the probe point. For illustration the frequency response $\underline{H}_{SCA}^{(\text{PCD1,class1})}(j\omega) = \underline{U}_{LMA}/\underline{I}_{TP}$ for a PCD 1 measurement setup with a class 1 transponder antenna is shown in figure 4.11. The component values of the sense coils are taken from [SG11]. Note that the transponder antenna size or class acts just as a frequency-constant gain factor. The

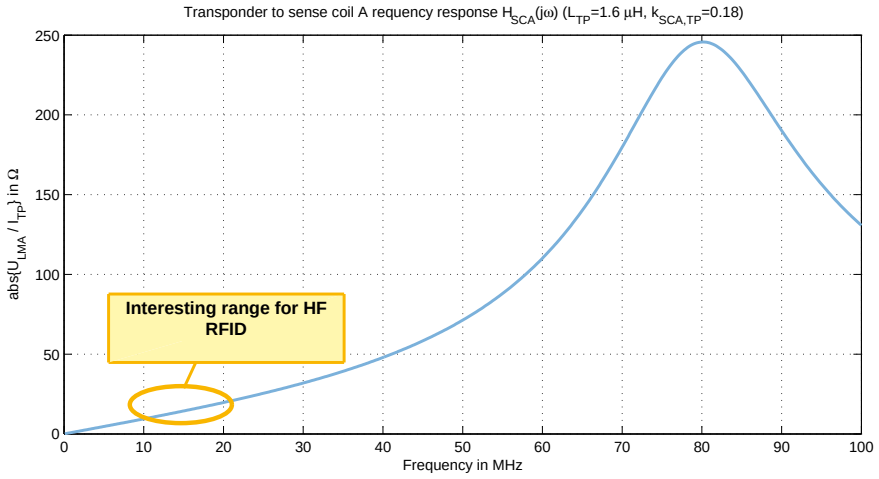

Figure 4.11: Transponder current to LMA voltage transfer function for a typical PCD 1 class 1 transponder setup ($R_{PROBE} = 10\ M\Omega$, $C_{PROBE} = 4.7\ pF$)

upper sideband is preferred compared to the lower sideband due to the sense coil self resonance frequency $f_{RES,SCA} \approx 80\ MHz$.

4.2.4 Numerical Solution of the Switched State System

Using this framework the lower and upper sideband amplitude values can be easily computed following some steps:

1. Compute the coupling coefficients $k_{PCD,TP}$ and $k_{SCA,TP}$
2. Calculate the induced voltage in the transponder coil in the unmodulated state U_{IND}

3. Approximate the the induced voltage in the modulated case by using the card loading factor equations in section 4.1.5 with

$$U_{IND,MOD} \approx \frac{1 + CLF(Q_M)}{1 + CLF(Q_T)} U_{IND} \tag{4.36}$$

4. Use the steady state model for the transponder and the solution path introduced in section 4.2.2 to calculate the signal energy of the transponders coil current I_{TP} at $\omega = \omega_C \pm \omega_{SB}$

5. The LMA values are finally computed applying the transfer function $\underline{H}_{SCA}(j\omega)$ from section 4.2.3 and analysing abs $\{u_{LMA}(j(\omega_C \pm \omega_{SB}))\}$

Figure 4.12 includes the load modulation amplitudes of the numerically solved switched state system model for the resonant (maximum loading) and two detuned cases.

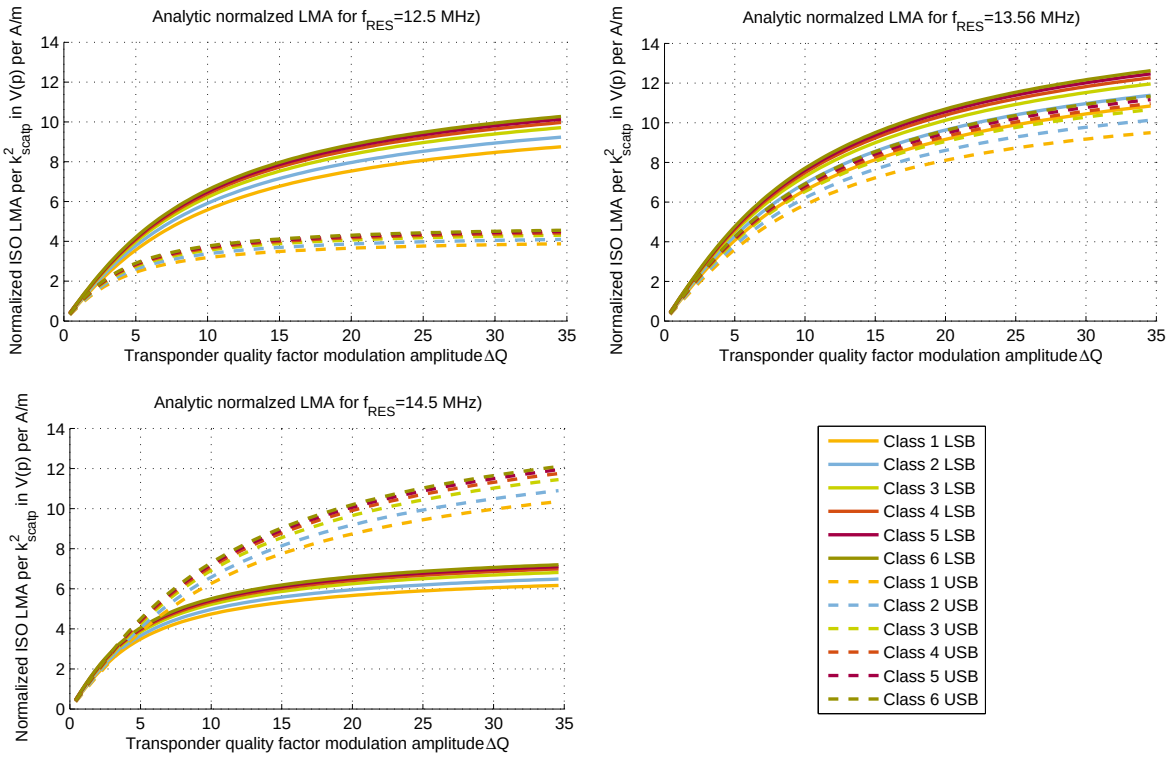

Figure 4.12: Effect of detuning to the LMA values

As shown in figure 4.13 this numerically solved analytical model matches the measurement results and the empirical model presented in chapter 6 quite well. The numerically computed values were bandwidth compensated by a factor factor of $\sqrt[4]{1 + Q_T^2 \left(\frac{\omega_{RES}}{\omega} - \frac{\omega}{\omega_{RES}}\right)^2}$.

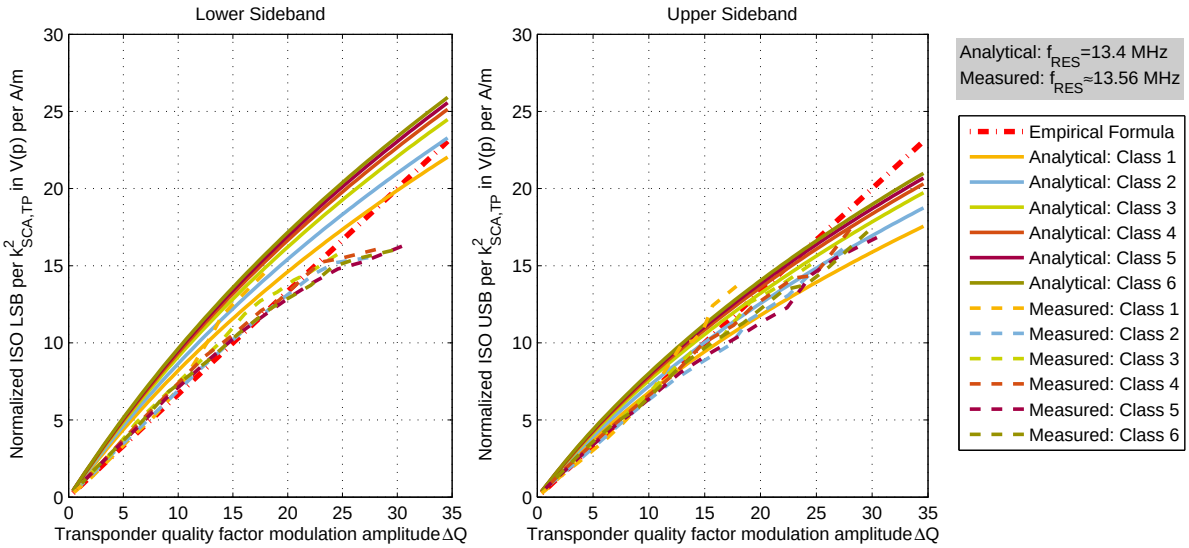

Figure 4.13: Comparison between numerically solved and bandwidth corrected analytical LMA model with empirical model based on measurements from chapter 6.

Chapter 5: Numerical Simulations on the Load Modulation Amplitude Analysis

"Computers are useless. They can only give you answers."

[Pablo Picasso]

Within this section a simulation environment using MATLAB [The12] and LTspice [Tec12] is presented and discussed in detail. It is used for a series of simulations to optimize the transponder antenna area with respect to the ISO sideband amplitudes.

5.1 Designing a Simulation Environment

Figure 5.1 shows the basic process flow as a block diagram. Beside some boundary conditions like a conventional PCD1 high datarate ISO measurement setup a typical transponder antenna like a rectangular planar spiral coil with rectangular conductor cross-section is assumed. Based on a targeted transponder inductance L_{TP} all further considerations are made and result in a transponder antenna equivalent circuit. The transponder can be tuned to the have a specific resonance frequency f_{RES} and quality factor Q_T using two degrees of freedom (tuning capacitor C_{TUNE} and chip input resistance R_{IC}). After calculation of all network components a LTspice simulation can be started which outputs the transient voltage trace at the Helmholtz point between the two sense coils. These data can be analysed using a DFT and results in the ISO sideband amplitudes. The whole process can be cycled for a set of transponder quality factors $Q_T^{(i)}$ and a set of transponder antenna turns $N^{(i)}$. All these action points will be discussed in more detail in the following subsections.

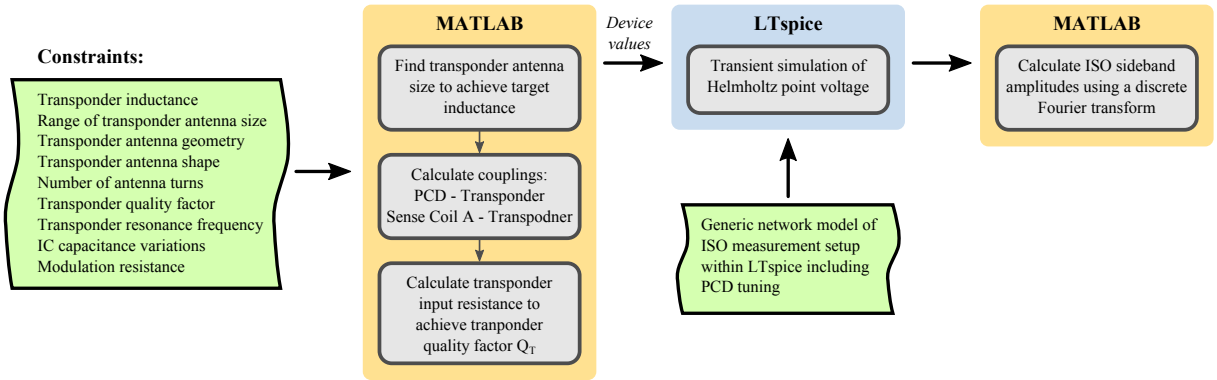

Figure 5.1: Block diagram of the simulation environment to relate the ISO sideband amplitudes with the transponder antenna area

The transponder network is defined within this simulation setup as shown in figure 5.2. Compared with the classical transponder circuit it includes in addition a small capacitor which is active if the transponder IC is properly powered, e.g. $U_{IC} \geq U_{IC,min}$. This models the resonance frequency shift which can be observed between the modulated and unmodulated state. That means the simulation uses two operating points of the transponder IC (active and not active) depending on its supply or input voltage U_{IC}. An example for the resulting input impedance is shown in figure 5.3.

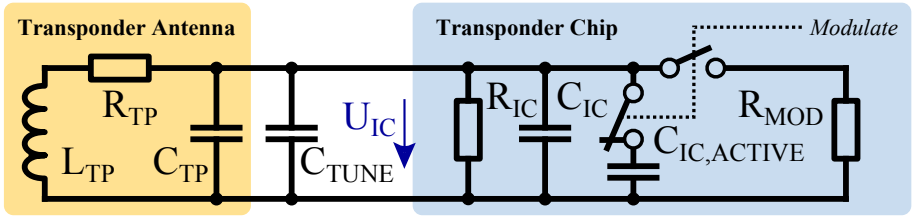

Figure 5.2: Transponder equivalent circuit including a load modulator

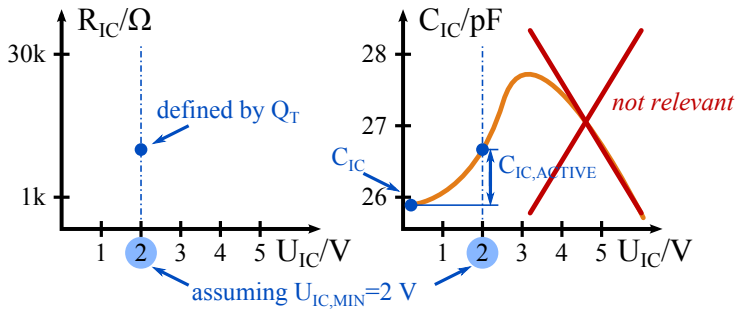

Figure 5.3: Example including the operating points of the chip input impedance as used by the LTspice simulation

5.2 Numerical Modelling

Based on the simplified network model of the coaxial antenna arrangement of the test setup defined in ISO/ IEC 10373-6 including the transponder the load modulation amplitudes can be estimated. This section describes the iterative approach which performs this task for a specific transponder antenna and a typical smartcard chip compliant to the proximity standard.

5.2.1 Antenna Equivalent Circuit

The transponder equivalent circuit components L_{TP}, R_{TP} and C_{TP} are calculated based on the geometry and a correction exponent α derived from empirical observations (measurements done in the laboratory). The shape of the considered transponder antenna is a rectangular spiral loop of outer length a_0 and an outer width b_0, respectively (figure 5.4). The antenna conductor tracks have a width w, a thickness t and a conductivity σ_{track}. The gap between two tracks of a rectangular cross section is defined by g. The substrate is assumed to have a relative permittivity constant ϵ_r. Note that this antenna type can be generalized to cover round conductor cross sections, which are commonly used for embedded wire antennas that can typically be found on card inlays.

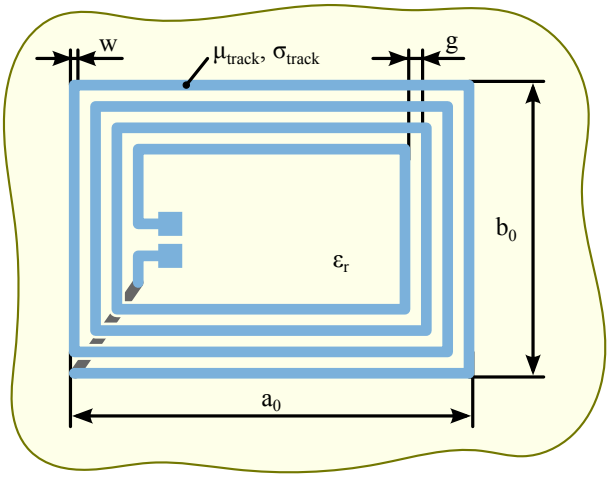

Figure 5.4: Sketch of the geometry of a rectangular planar loop antenna with four turns

In the literature there are many approximations to estimate the equivalent circuit model of an antenna. The equations which are used within this simulation environment are adopted from [Geb08]. Numerical finite element methods have shown that the current distributions of the conductors' cross sections are not equal [RSJH07]. There is a larger current density in the inner turns, which results in a reduced effective antenna area denoted by a_{AVG} and b_{AVG} respectively. Prior investigations showed a good match when using the quadratic mean of all turns' dimensions.

$$\begin{aligned} a_{AVG} &= \frac{1}{2}\left[(w+g)(2N-1)+w+\sqrt{4a_0^2-((2N-1)+w)^2}\right] \\ b_{AVG} &= \frac{1}{2}\left[(w+g)(2N-1)+w+\sqrt{4b_0^2-((2N-1)+w)^2}\right] \end{aligned} \tag{5.1}$$

Defining the equivalent conductor diameter

$$d = 2\frac{t+w}{\pi} \tag{5.2}$$

the series inductance of an antenna of this shape can be estimated with

$$\begin{aligned} \tilde{L}_{TP} = \frac{\mu_0}{\pi}\Bigg[& a_{AVG}\ln\left(\frac{2a_{AVG}b_{AVG}}{d\left(a_{AVG}+\sqrt{a_{AVG}^2+b_{AVG}^2}\right)}\right) + b_{AVG}\ln\left(\frac{2a_{AVG}b_{AVG}}{d\left(b_{AVG}+\sqrt{a_{AVG}^2+b_{AVG}^2}\right)}\right) \\ & - 2\left(a_{AVG}+b_{AVG}-\sqrt{a_{AVG}^2+b_{AVG}^2}\right)+\frac{a_{AVG}+b_{AVG}}{4}\Bigg] N^{\alpha} \approx L_{TP} \end{aligned} \tag{5.3}$$

and $\alpha = 1.73$. The parallel capacitance of the antenna's conductor arrangement can be approximated by

$$\tilde{C}_{TP} = \epsilon_0\epsilon_r\frac{2\left(a_{AVG}+b_{AVG}\right)tN}{g} \approx C_{TP}. \tag{5.4}$$

Note that this only covers the turn-to-turn parasitic capacitances and not these generated by the crossing or bridge which is needed to connect the inner end of the loop with the IC (see figure 5.4). The serial resistance is composed of a low frequency resistance R_{DC} and a high frequency component R_{AC} which takes the skin effect into account. The equivalent total resistance is

hard to find because the effective conductor cross-section varies between the turns as mentioned above. However an estimation of this component at the carrier frequency f_c can be made using

$$\tilde{R}_{TP} \equiv R_{AC+DC} = \frac{2\,(a_{AVG} + b_{AVG})\,N}{w+t}\sqrt{\frac{f_c \pi \mu_0 \mu_{track}}{\sigma_{track}}} \approx R_{TP}, \tag{5.5}$$

but comparisons with measurements have shown that this equation for the serial resistance tends to be too small. In general this fact has no big impact on the whole system, as R_{TP} has only a minor impact on the transponder quality factor Q_T which – for the case of proximity smartcards – is typically dominated by the chip equivalent resistance in operation. Improved numerical antenna modelling strategies can be found in the literature, e.g. [Cic06].

To find a geometry (width and height of antenna) having a desired inductance, a set of possible dimensions within the constraints is checked and the best match is used for further computations. Of course, it is possible that this specific inductance can not be realized using the constraints. In this case the rest of this iteration is skipped and the simulation continues with the next parameter set.

5.2.2 Estimation of the Coupling Coefficients

After finding an antenna geometry the couplings between the transponder antenna and PCD antenna and the sense coils in the coaxial antenna arrangement of the ISO/IEC 10373-6 setup are computed. The analytic derivation is quite tedious and complicated. The coupling coefficient between to inductances L_1 and L_2 shown in in figure 5.5 is defined as

$$k = \frac{M}{\sqrt{L_1 L_2}}, \qquad 0 \leqslant |k| \leqslant 1 \tag{5.6}$$

where M denotes the mutual inductance, which can be derived by solving the double integral

$$M = \frac{\mu_0}{4\pi} \oint_{\mathcal{C}_1} \oint_{\mathcal{C}_2} \frac{\mathrm{d}\mathbf{s}_2 \cdot \mathrm{d}\mathbf{s}_1}{|\mathbf{s}_2 - \mathbf{s}_1|}. \tag{5.7}$$

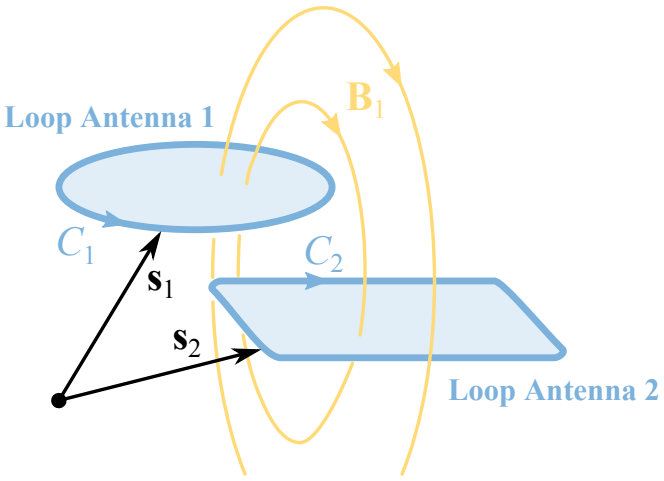

Figure 5.5: Coupling system of two general loops in arbitrary space

5.2.2.1 Coupling between Transponder and Sense Coil A

These two antennas have both a (nearly) rectangular shape, have the same normal vector and have coaxial orientation. The sense coil has only one turn, e.g. $N_{SC} = 1$. These properties simplify the solution of the integral. Nevertheless the result is computed by a numerical calculation of the integrals.

By introducing the width and height of the sense coil a_{SC} and b_{SC} respectively and the distance between the coils $R_{SCA,TP}$, equation 5.7 can be expanded to

$$
\begin{aligned}
k_{SCA,TP} = \frac{\mu_0 N}{4\pi\sqrt{L_{SC}L_s}} \Bigg[& \int_{-\frac{a_{AVG}}{2}}^{\frac{a_{AVG}}{2}} \int_{-\frac{a_{SC}}{2}}^{\frac{a_{SC}}{2}} \Bigg(\frac{1}{\sqrt{(\xi-\zeta)^2 + \left(\frac{b_{SC}}{2} - \frac{b_{AVG}}{2}\right)^2 + R_{SCA,TP}^2}} \\
& - \frac{1}{\sqrt{(\xi-\zeta)^2 + \left(-\frac{b_{SC}}{2} - \frac{b_{AVG}}{2}\right)^2 + R_{SCA,TP}^2}} - \frac{1}{\sqrt{(\xi-\zeta)^2 + \left(\frac{b_{SC}}{2} + \frac{b_{AVG}}{2}\right)^2 + R_{SCA,TP}^2}} \\
& + \frac{1}{\sqrt{(\xi-\zeta)^2 + \left(\frac{b_{AVG}}{2} - \frac{b_{SC}}{2}\right)^2 + R_{SCA,TP}^2}} \Bigg) \mathrm{d}\zeta \mathrm{d}\xi \\
& + \int_{-\frac{b_{AVG}}{2}}^{\frac{b_{AVG}}{2}} \int_{-\frac{b_{SC}}{2}}^{\frac{b_{SC}}{2}} \Bigg(\frac{1}{\sqrt{(\xi-\zeta)^2 + \left(\frac{a_{SC}}{2} - \frac{a_{AVG}}{2}\right)^2 + R_{SCA,TP}^2}} \\
& - \frac{1}{\sqrt{(\xi-\zeta)^2 + \left(-\frac{a_{SC}}{2} - \frac{a_{AVG}}{2}\right)^2 + R_{SCA,TP}^2}} - \frac{1}{\sqrt{(\xi-\zeta)^2 + \left(\frac{a_{SC}}{2} + \frac{a_{AVG}}{2}\right)^2 + R_{SCA,TP}^2}} \\
& + \frac{1}{\sqrt{(\xi-\zeta)^2 + \left(\frac{a_{AVG}}{2} - \frac{a_{SC}}{2}\right)^2 + R_{SCA,TP}^2}} \Bigg) \mathrm{d}\zeta \mathrm{d}\xi \Bigg] .
\end{aligned}
\tag{5.8}
$$

5.2.2.2 Coupling between Transponder and PCD Antenna

The PCD antenna has a radius of r_{PCD} and the distance between the two coaxial parallel antennas is $R_{PCD,TP}$. Deriving the coupling coefficient between a circular and a rectangular loop antenna is even more complicated than between sense coil and transponder antenna. To simplify the calculation, the rectangular transponder antenna can be approximated by a circular loop antenna of equal antenna area. This allows to use the analytical equation for the computation of a coupling coefficient between two circular antennas. Thus,

$$
k_{PCD,TP} = \frac{\mu_0 \pi N a_{AVG} b_{AVG}}{2\sqrt{L_{PCDA} L_{TP}}} \frac{r_{PCD}^2}{\left(r_{PCD}^2 + R_{PCD,TP}^2\right)^{\frac{3}{2}}}. \tag{5.9}
$$

5.2.3 Transponder Tuning and Quality Factor

To get a specific transponder resonance frequency f_{RES} the total parallel capacitance has to be set to

$$
C = \frac{1}{\left(2\pi f_{RES}\right)^2 L_{TP}} \qquad \text{(Thomson's Equation)}, \tag{5.10}
$$

which requires the value of the tuning capacitor to be

$$C_{TUNE} = C - C_{IC} - C_{TP}. \tag{5.11}$$

The quality factor of the transponder Q_T is limited by the parallel input resistance of the transponder IC, which can be estimated according equation 5.12 for the intended transponder quality factor.

$$Q_T = \frac{1}{R_{TP}\sqrt{\frac{C+C_{IC,ACTIVE}}{L_{TP}}} + \frac{1}{R_{IC}}\sqrt{\frac{L_{TP}}{C_{IC}+C_{IC,ACTIVE}}}} \quad \rightarrow \quad R_{IC} = \frac{\sqrt{\frac{L_{TP}}{C_{IC}+C_{IC,ACTIVE}}}}{\frac{1}{Q_T} - R_{TP}\sqrt{\frac{C+C_{IC,ACTIVE}}{L_{TP}}}} \tag{5.12}$$

Note that this equation includes the additional capacitance $C_{IC,ACTIVE}$ (see section 3.2.2.2), as the resonance frequency is tuned at a low chip input voltage, whereas the quality factor should be defined while the chip is operating, e.g. $U_{IC} \geq U_{IC,MIN}$.

Additionally the chip input voltage in the unmodulated state $U_{IC,MIN}$ and in the modulated state $U_{IC,MOD}$ over the H-field range (see section 3.2.2.4) are a constraint to the simulation. These voltages are guaranteed by an iterative finetuning of R_{MOD} in terms of repeated simulations.

5.2.3.1 Description of the Simulation Schematic

The complete ISO measurement setup [IE11] was modelled at network level in LTspice based on [SG11]. The schematic is shown in figure 5.6. To allow a maximum amount of flexibility all component values and simulation settings like the modulation pattern are read from three external text files, which contain simple SPICE directives. The content of these files with example data is shown in listings A.2, A.3 and A.1.

5.2.3.2 Starting the LTspice Simulation from MATLAB

To automate the simulation LTspice has to be parametrized and started via MATLAB. As described in the previous section all the component values and simulation settings are read from three configuration files which can be written easily from the MATLAB workspace. The *net listing* of the network can be created by starting the simulation within the LTspice workspace which generates a `.net` file. This should be renamed to a `.cir` file to avoid automatic deletion after program execution.

The simulation itself is started via a system or console command using

```
1 system([LTSPICE_PATH ' -b ..\ltspice\isosetup.cir']);
```

LTspice is started without opening a graphical user interface and simulation results are written to a `.raw` and a `.log` file respectively. In the next step a MATLAB function reads this transient raw output data file, which have to be resampled because the discretized SPICE simulation points are not equidistant in time.

5.2.4 Calculation of the ISO Load Modulation Amplitudes

Finally the transient voltage record at the Helmholtz point can be fed into a DFT algorithm to compute the ISO sideband amplitudes. To achieve the best compatibility with the standards and real life measurements, the DFT algorithm presented in the International Standard [IE11] was also implemented in MATLAB (see listing A.4). It was extended to allow arbitrate subcarrier frequencies (integer fractional of the carrier frequency).

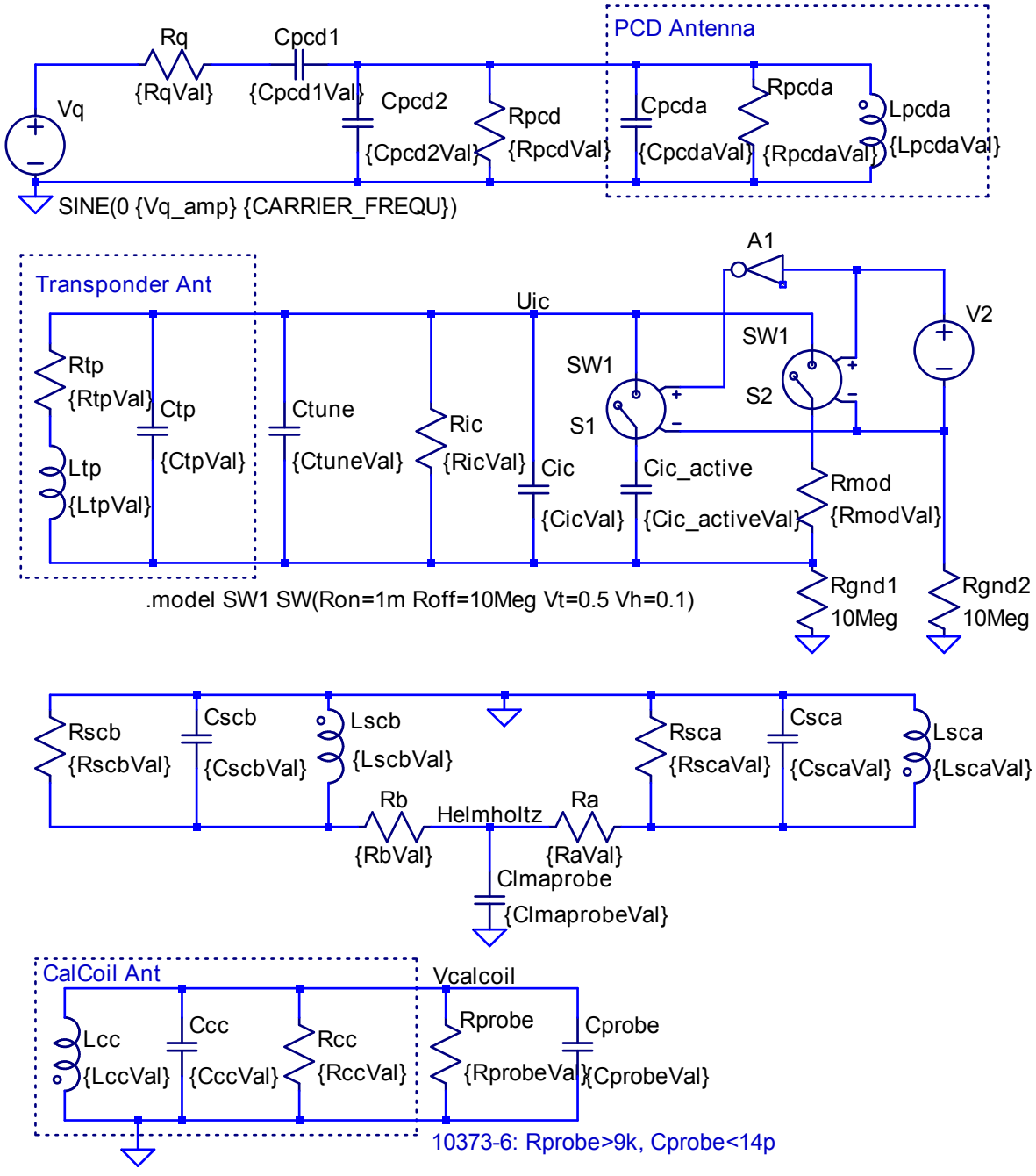

Figure 5.6: Circuit diagram of LTspice simulation

5.2.5 Discussion of the Consequences of the Simplified Modelling

Every modelling introduces errors caused by various simplifications. Prior using the results based on a model the impact of the errors has to be discussed. One major problem is the representation of the antenna geometry with a network model. A purely rectangular transponder antenna shape is assumed – but this is surely not the case (bended edges). The average antenna dimensions a_{AVG} and b_{AVG} cause further modelling problems.

Another inaccuracy is the computation of the coupling coefficients. Especially the PCD to transponder antenna coupling is problematic due to the fact that their shapes differ. As long as the H-field can be assumed to be homogeneous this error should be small enough to be tolerated.

In the beginning of this chapter the concept of two operating points of the input chip impedance was presented (compare with the example shown in figure 5.3). In cases where the chip is just not yet properly powered the unmodulated operating point is not reached. This has to be observed when applying the results of this general simulation series with a real chip.

5.3 Comparison with Real-Life Measurement Data

The simulation environment is the basis for all further analysis. A plot of ISO load modulation amplitudes per field strength over transponder area gives some fundamental information on the principally desired system design. To adapt this information to the real qualification criteria further simulations have to be done. For example, the proximity base standard ISO/IEC 14443-2 [IE10a] defines a minimum limit for the ISO sideband amplitudes measured at the Helmholz point for a class 1 antenna size DUT H-field operating range of 1.5 to 7.5 A/m (rms).

A comparison between real life measurement data and output of the simulation is presented in figure 5.7. The chip voltages are the control parameter to get a good match. Although there is a set of possible measurement uncertainties (antenna positioning, environment) the simulation reflects the measurements quite well.

Side results of the simulation are the quality factors over H-field strength which usually can't be measured. The corresponding values to the presented curves of LMA over H-field are shown in figure 5.7. Note that these values must be seen as the equivalent quality factor at ω_C, as Q is normally only defined at the self resonance frequency!

The key statement of figure 5.7 is the fact that the quality factors at ω_{RES} are a function of the H-field strength (due to limiter action), the resonance frequency of the transponder (only equivalent quality factor), and the coupling coefficient (more resonance voltage rise due to an increased quality factor is needed to get enough chip voltage for operation for the same H-field strength values).

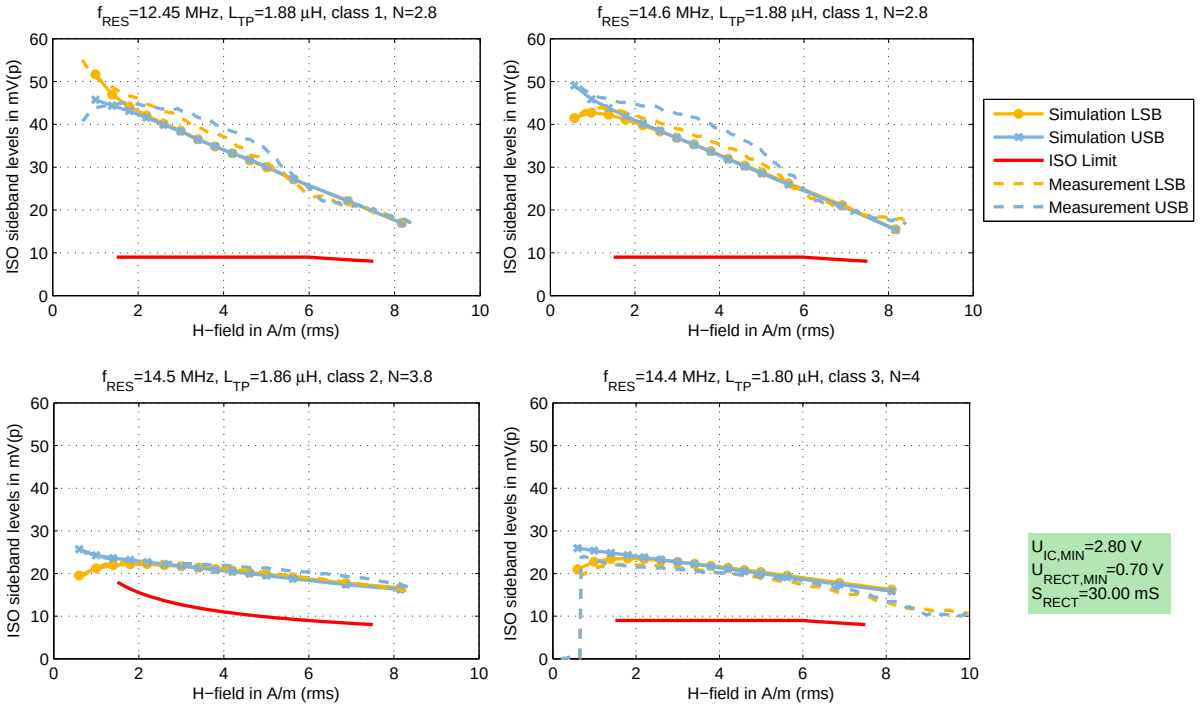

Figure 5.7: Accuracy of the numerical simulation environment by comparing real life measurements with results from the MATLAB/SPICE co-simulation framework. The proximity chip in question has a parallel input capacitance of about 70 pF (courtesy of NXP Semiconductors)

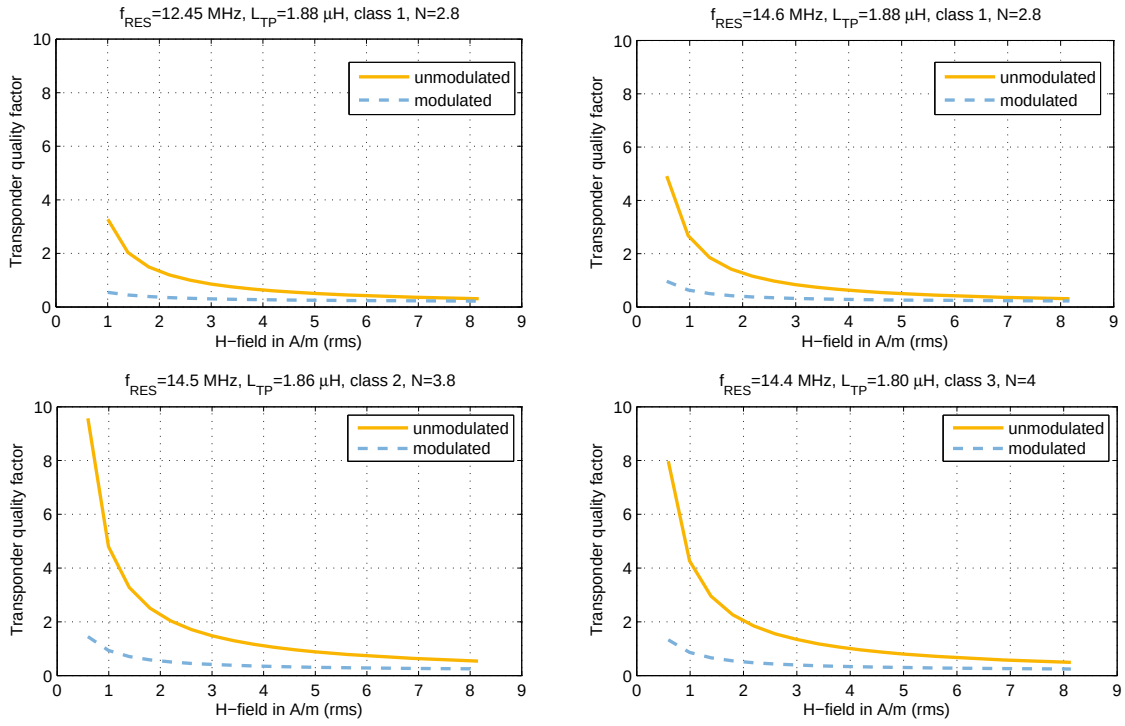

Figure 5.8: Simulated transponder quality factors Q_T and Q_M coming from the same simulation series as the LMA results shown in figure 5.7

Chapter 6: Empirical System Model based on Measurements

"Any sufficiently advanced technology is indistinguishable from magic. "

[Sir Arthur C. Clarke]

Another quite obvious way to find a link between system parameters and parameters at the air interface is to characterize the general behaviour based on a large set of measurement results. The problem in this work was that there were not any of such measurements performed with respect to the system parameters in the past. Therefore this chapter will present a test environment which served as a platform for gaining a data basis. This is analysed in a second step and results in an empirical model for predicting the load modulation amplitude as a function of the system parameters.

6.1 Description of the Measurement Setup

The measurement environment used for this empirical modelling was designed according to the test standard [IE11]. The idea behind this evaluation is quite contrary to a normal product orientated evaluation series in the laboratory: The task is not to characterize a specific product, but to gain as much as possible measurement data at system level. Therefore, the transponder antenna size and the transponder quality factor were selected to cover a large range of possible values.

6.1.1 Scope of the Measurement Series

The outcome of this measurement series should include quantities that are normally not relevant for product characterization. This analysis only covers the topics load modulation amplitude and card loading. The first would normally be measured over the specified H-field range of the appropriate antenna class. There is a separate maximum loading test specified in the test standard. The here used transponder configurations are designed to pass this test.

6.1.2 Definition of the Tasks

A typical testboard for transponder characterization consisting of an antenna, a tuning capacitor and the IC is extended with an additional (quality factor limiting) parallel resistor $R_{Q,LIM}$, which allows to set Q_T to a desired value (see figure 6.1). To guarantee consistent results the IC is operated at the same internal "operating point". This is achieved by operating the chip at an antenna voltage which is just below its start of operation, e.g. $U_{IC,MEAS} \approx 0.99\, U_{IC,MIN}$. This is achieved by adjustment of the H-field of the setup, while the antenna voltage is measured

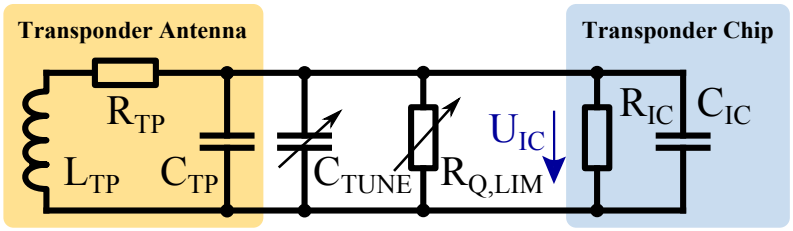

Figure 6.1: Varying the transponder quality factor with an external resistor $R_{Q,LIM}$

with a low-capacitance probe. This results in a (nearly) inactive limiter and gives the highest possible chip quality factor.

The transient voltage trace of the chip input voltage $u_{IC}(t)$ and of the LMA probe voltage $u_{LMA}(t)$ during a load modulation sequence are measured and recorded with a digital sampling oscilloscope and then processed offline with MATLAB. Additionally the H-field strength in the loaded and unloaded case are recorded to allow compute the card loading factor. Three approaches to estimate Q_T are performed and discussed in section 6.2.1.

To get the strongest response a tuned transponder was forced by varying C_{TUNE} for $f_{RES} = f_C$. This can be seen as the optimum case on the one hand (strongest response) and as the worst case on the other (strongest loading). Note that this resonance tuning was done at the measurement operating point $U_{IC,MEAS}$ as the slight capacitance change for different chip input voltages detunes the transponder and disturbs the measurement especially for larger values of Q_T.

The subcarrier was selected to be $f_C/16 = 847.5\ kHz$ and $f_C/8 = 1695\ kHz$. The first one is the test related subcarrier according to ISO/IEC 10373-6 and the second one allows an outlook for very high bit rate systems (VHBR) and is interesting with respect to its increased bandwidth requirements. Note that the selected test chips were only designed to perform load modulation at $f_C/16 = 847.5\ kHz$ subcarrier frequency but are able to switch faster by supplying an external modulation clock signal.

6.1.3 Transponder IC

Section 3.5.1 explained, why the residual chip input voltage during modulation has a limiting impact on the load modulation amplitude values. This is related to the fact whether the modulator of the IC is placed at the input port (*modulator-at-antenna*) or after the rectifier (*modulator-after-rectifier*). To cover both cases two different designs were analysed. Table 6.1 includes the main characteristic properties of both test chips.

	Test Chip A (TC A)	**Test Chip B (TC B)**
Modulator position	antenna side	after rectifier
Minimum chip supply voltage $U_{IC,MIN}$	1.8 $V(rms)$	2.6 $V(rms)$
Selected operating point $U_{IC,MEAS}$	1.7 $V(rms)$	2.3 $V(rms)$

Table 6.1: Key facts of the analysed transponder test chips

To extend the range of possible transponder quality factors the current consumption of the digital part of the IC was reduced to zero by either powering it externally or disabling it completely. A reduced amount of energy or antenna current, respectively, results in an increased chip input resistance at $U_{IC,MIN}$ will be, which is proportional to Q_T. Therefore, at lower H-field strength values a larger resonant voltage rise or Q-factor is needed to power the chip.

6.1.4 Transponder Antenna

For this measurement series a set of well known and characterized antennas was chosen. The proximity test standard specifies the antennas for the Reference PICC antenna geometry classes 1 to 6, which give a realistic range of possible antennas within applications. Figure 6.2 gives an impression of how the antenna classes are related to each other with respect to the outer border.

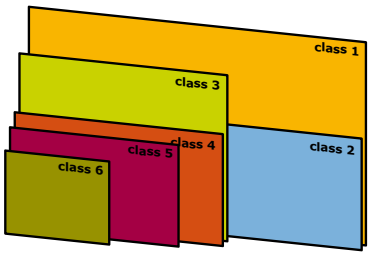

Figure 6.2: Impression of the maximum outer antenna dimensions according to the proximity antenna classes defined by ISO/IEC

Normally classes 4 to 6 are measured with a slightly adopted antenna arrangement called PCD 2. This measurement series was performed with the classical PCD 1 configuration only to cover the largest possible range of couplings to the transponder. Note that there are less restrictive qualifications limits for smaller antenna classes specified within the measurement standards (amendments to ISO/IEC 14443-2 and ISO/IEC 10373-6) and are listed in table 6.2.

Antenna Class	**PCD**	**Max. Outline** mm	H_{MIN} $A/m\ (rms)$	H_{MAX} $A/m\ (rms)$	**Min. LMA** $mV(p)$
1	1	89×49	1.5	7.5	$22/\sqrt{H}$
2	1	81×27	1.5	8.5	$\min\left\{14; 22/\sqrt{H}\right\}$
3	1	50×40	1.5	8.5	$\min\left\{14; 22/\sqrt{H}\right\}$
4	2	50×27	2	12	$\min\left\{18; 40/\sqrt{H}\right\}$
5	2	40.5×24.5	2.5	14	$\min\left\{14; 34/\sqrt{H}\right\}$
6	2	25×20	4.5	18	$\min\left\{7; 26/\sqrt{H}\right\}$

Table 6.2: ISO antenna classes and their corresponding LMA limit values

6.1.5 Test Setup

The main components of the measurement setup were introduced in the previous sections. Figure 6.3 includes the interconnection block diagram of all elements of the test system. A function generator providing the carrier frequency of $f_C = 13.56\ MHz$ and a HF power amplifier connected to the PCD 1 antenna generate the H-field which powers transponder or – to be more precise – the analogue part of the IC. The digital part of the IC is externally powered. The chip internal modulation switch is controlled with a square wave generated by a second function generator which shares its time base with the other one. Otherwise sideband carriers do not occur exactly at $f_C \pm f_{SB}$. A real chip would relate its modulation base clock directly from the

H-field.

An active differential probe is used to measure the chip input voltage trace $u_{IC}(t)$. The big advantage of this measurement device is a negligible input capacitance (typ. $< 1\ pF$) and high input resistance to load the measured point as little as possible. All quantities relevant to be measured are acquired with a digital sampling oscilloscope. The values are read from the display and the important traces are recorded and imported in MATLAB for offline processing.

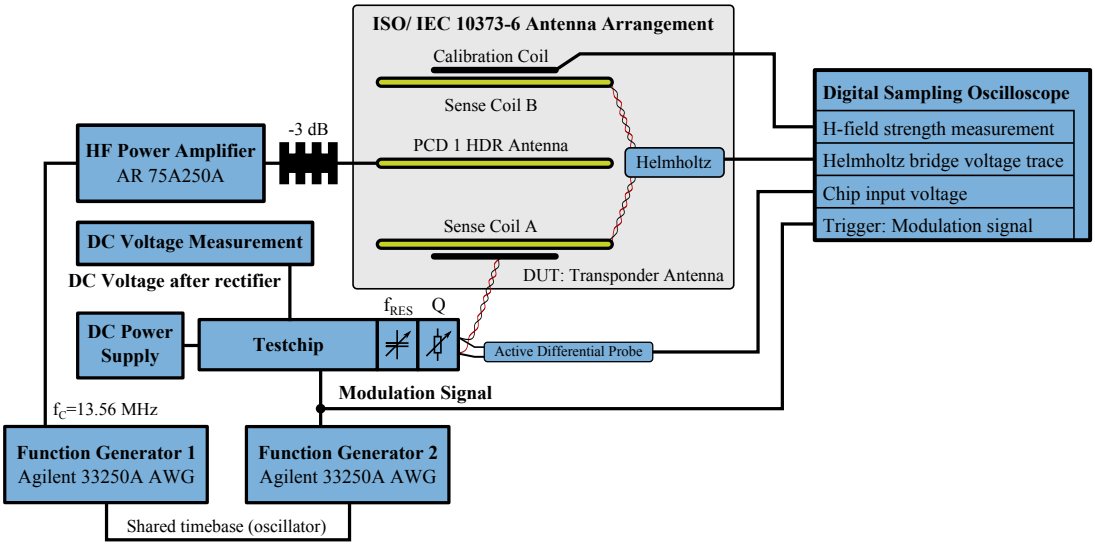

Figure 6.3: Block diagram of the measurement setup

6.1.6 Measurement Procedure

Each fundamental measurement sequence is repeated for both test chips and transponder antennas. To simplify the execution of the tasks not a range of specific quality factors is forced, but a list of equivalent additional parallel resistor values that cover the desired range as well as possible.

The procedure can be summarized into the following steps:

1. Tune the transponder to f_{RES} by finding a setting for C_{TUNE} that results in $U_{IC} = U_{IC,MEAS}$ at the lowest H-field strength without any $R_{Q,LIM}$ being present.

2. Measure the time constant τ_{UNMOD} of the envelope of $u_{IC}(t)$ after a single load modulation pulse to estimate the transponder quality factor with

$$Q_T^{max} \approx Q_{T,MEAS}^{max} = \frac{\tau_{UNMOD}\ \omega_{RES}}{2} \tag{6.1}$$

   following the discussion in [Geb11]. The equivalent chip input resistance R_{IC}^{calc} can be expected using equation 3.2

3. Repeat for a range of Q-limiting resistor values $R_{Q,LIM}$ proportional to Q_T:

   (a) Measure actual transponder quality factor $Q_{T,MEAS} \approx Q_T$ by measuring the time constant τ_{UNMOD} of the envelope of $u_{IC}(t)$ after a load modulation pulse and equation 6.1

   (b) Calculate transponder quality factor $Q_{T,CALC} \approx Q_T$ with R_{IC}^{calc} and $R_{Q,LIM}$ with equation 3.2 for comparison

(c) Measure the peak-to-peak chip input voltage in the modulated and unmodulated states

(d) Capture the transient voltage traces $u_{IC}(t)$ and $u_{LMA}(t)$ for at least eight subcarrier cycles for five times to allow measurement averaging

(e) Calculate ISO load modulation amplitude using the DFT program defined in the appendix of [IE11]

(f) Determine the H field strength with and without the transponder in DUT position to analyse the card loading effect

A preceding chip input characterisation over its input voltage using the NWA method (section 3.2.2.3) is optional but can improve the determination of Q_T. This allows to have a third approximation method for Q_T: The chip input resistance measured with the network analyser at the related voltage can be seen to be parallel with $R_{Q,LIM}$ and results in $Q_{T,NWA} \approx Q_T$.

6.1.7 Discussion of Measurement Inaccuracies

This section should be seen as a list of possible sources leading to measurement uncertainties. Most of them are caused by the realistic behaviour of the measurement setup itself. The others are caused by necessary simplifications.

One obvious problematic fact is the measurement at high values of Q_T: This is linked to a very small H-field strength which is associated with to a comparatively high noise level which limits the reading accuracy. Furthermore an active differential probe is to be used but does not have a very high measurement accuracy.

Resonance tuning is done without any $R_{Q,LIM}$. Measurements with a LCR meter have shown that the used resistors have parallel capacitance of about 200 fF, which results in a slight detuning which should be neglectable compared with the manual tuning process. Even the control process to get $U_{IC} = U_{IC,MEAS}$ has a certain variance and drift.

Of course, there is some influence by the environment of the measurement area even within a laboratory. The setup includes several ground loops (e.g. modulation clock) which are known to cause problems within wireless communication links especially for large field strengths.

Although there is quite a long list of minor detected measurement inaccuracies, the results show a good general correlation. The discussion in the section serves as a base to discuss measurement outliers and can be the base for improvements in further measurements.

6.2 Selected Results

A listing of all measurement results would exceed the scope of this work. The main idea is to show the fundamental links between system and air interface parameters and to present an empirical model.

6.2.1 Determination of the Quality Factor

Section 6.1.6 explained the methods used to approximate Q_T. As NWA measurements were not available for test chip A, Q_{NWA} was neglected for further considerations. The main element in approximating the quality factor is to measure the time constant of the envelope of the rising edge of chip input voltage and to apply equation 6.1. Note that this implicitly assumes a purely exponential shape of the edge – of course, this will not be the case in reality, but it is a good approximation. In the literature there is a Phd thesis [Kla09] which introduced a more

sophisticated discussion on a time variant quality factor, but it does not mention the derivation of its argumentation.

A MATLAB function is used to extract τ. The envelope trace of the time signal is extracted using the algorithm presented in [MG09]. An additional notch filter is used to suppress some ripple. The result is shown in figure 6.4, where the modulation pulse durations for both considered frequencies are added. It is obvious that the modulation amplitude in time domain for 1695 kHz denoted as Δ_{1695} is smaller than for 847.5 kHz as long as $\tau > \Delta_{1695}$.

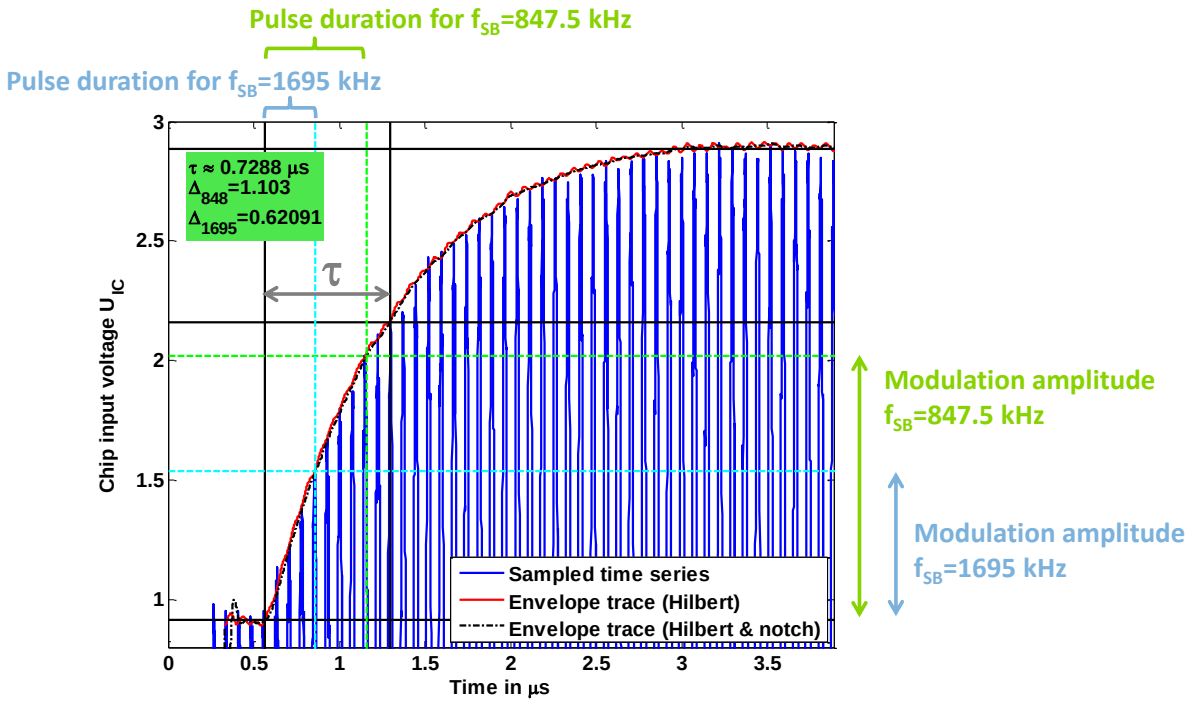

Figure 6.4: Extraction of the time constant τ of the envelope of the chip input voltage trace $u_{IC}(t)$ to allow a quality factor approximation

Figure 6.5 compares the other approximations. The match is quite good for both chips but Q_{MEAS} tends to be too small for larger values of Q_T. All further measurement results are based on the calculated transponder quality factor, e.g. $Q_T \equiv Q_{MEAS}$ is assumed. It can be seen from the plot, the achieved values for Q_T are well above the normally used $< 1 - 5$.

6.2.2 Chip Input Voltage Modulation Amplitudes over Quality Factor

The modulation amplitudes in time domain are connected with the sideband amplitudes in frequency domain. To understand the influence of the coupling and the quality factor to these quantities, a more detailed discussion is done within this section.

6.2.2.1 Modulator-At-Antenna (Test Chip A)

First the more simple case, where the envelope of the modulated residual chip voltage goes to zero, e.g. $\hat{U}_{IC,MOD} \rightarrow 0$, is shown in figure 6.6. Whereas the antenna size doesn't have any influence on the modulation amplitude of the chip voltage as an increased H field compensates the smaller coupling coefficient, the modulation amplitude of $u_{LMA}(t)$ decreases with $k_{SCA,TP}$.

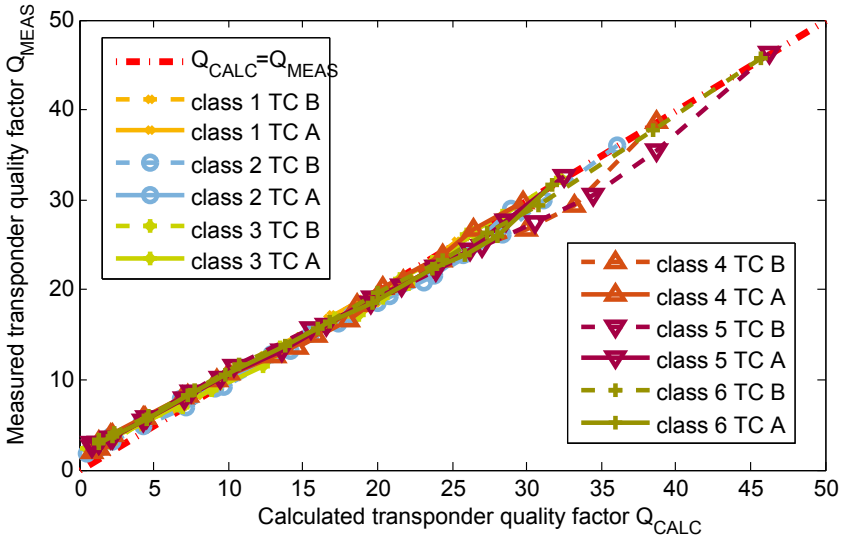

Figure 6.5: Comparison between the two transponder quality factor approximations Q_{CALC} and Q_{MEAS} for both test chips

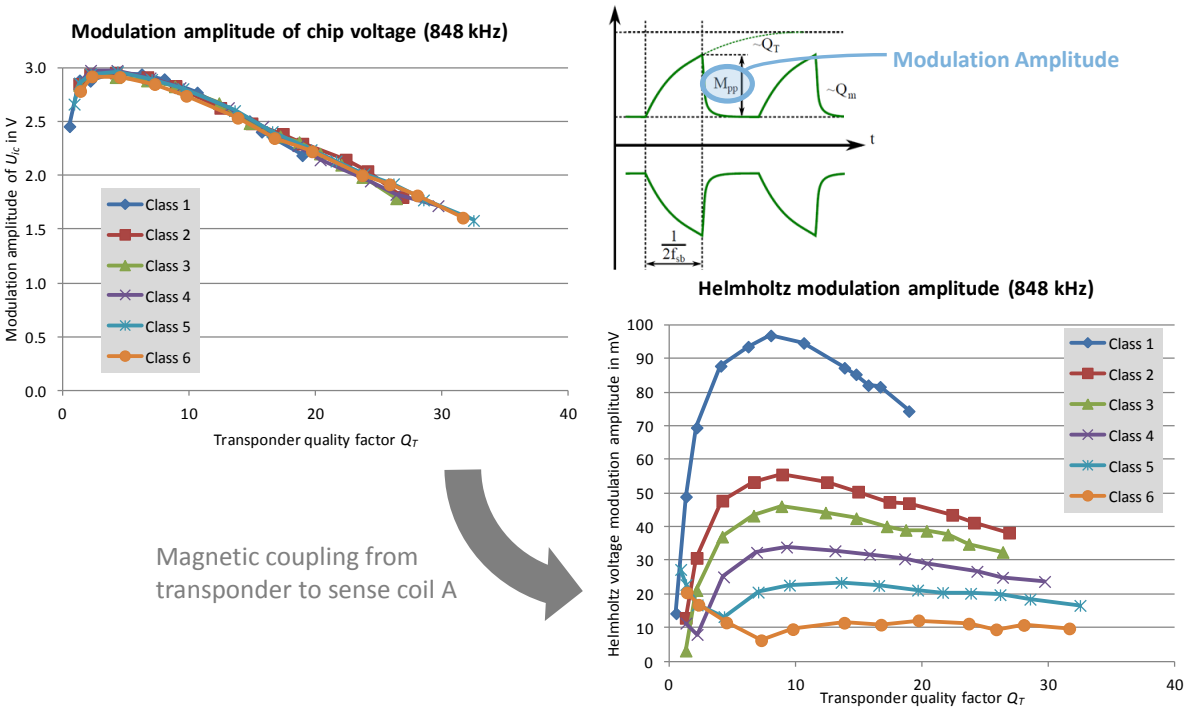

Figure 6.6: Measured modulation amplitudes in time domain of test chip B for $f_{SB} = 847.5\ kHz$ over Q_T shown for the chip input voltage $u_{IC}(t)$ and the Helmholtz bridge point voltage $u_{LMA}(t)$

6.2.2.2 Modulator-Before-Rectifier (Test Chip B)

What happens if $\hat{U}_{IC,MOD}$ is non-zero and increases with the H-field strength (like seen for the architecture represented by test chip A)? It can be seen best by an example shown in figure 6.7. Low field strength values are connected to higher quality factors (less limiter activity), which results in a decreased modulated chip input voltage. Thus, $\hat{U}_{IC,MOD}$ decreases with Q_T starting from $Q_T = 0$. For $f_{SB} = 847.5\ kHz$ the time constant (proportional to Q_T) is smaller than the modulation pulse length for approximately $Q_T < 8$. Above the voltage value at the end of the unmodulated pulse length $\hat{U}_{IC,848}$ starts to decrease with the quality factor. This second modulation amplitude limiting influence does also occur for the other architecture, whereas the first influence is caused by the modulator-after-rectifier design.

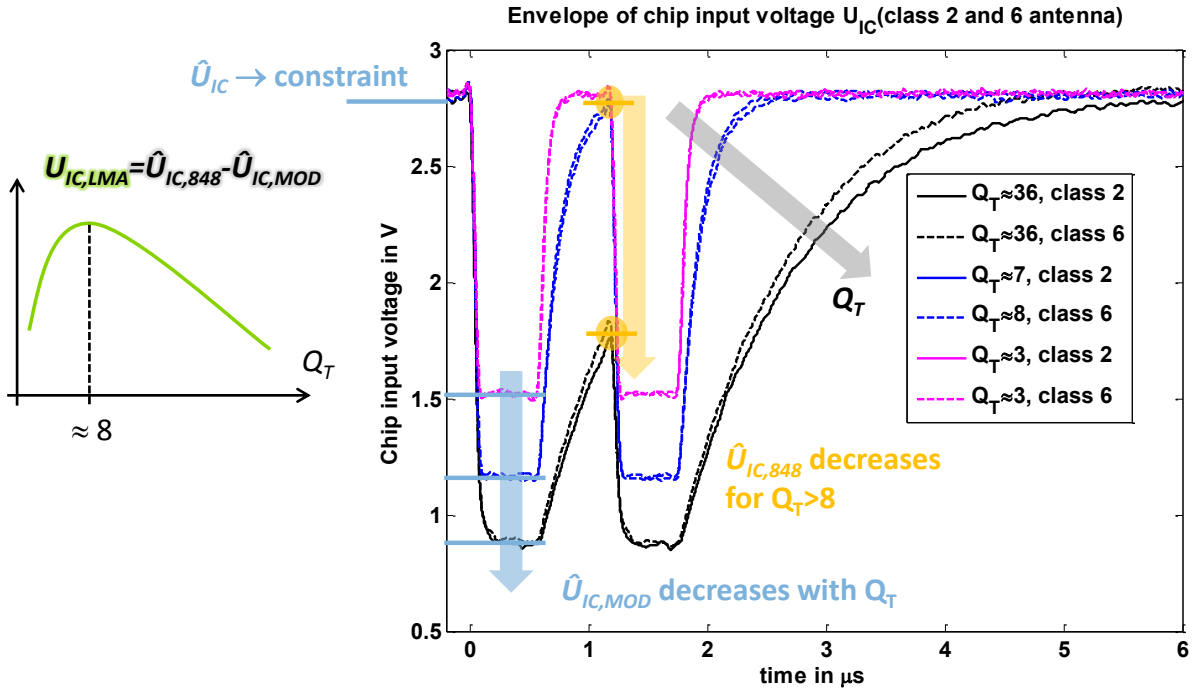

Figure 6.7: Influence of the transponder's quality factor to the modulation amplitude in time domain

All together the impact of this additional loss can be seen if the modulation amplitudes are compared between the two frontend designs shown in figure 6.6 for TC A and figure 6.8 for TC B. The second design has significantly smaller modulation amplitude values for small quality factors. But as earlier discussions showed, the quality factors used within applications are small as well! Therefore, a simple conclusion: Place the modulator directly at the antenna and increase the quality factor!

6.2.3 Card Loading

The previous chapter concerning an analytical description already included a discussion on a good model for the card loading factor. In section 4.1.5 the approximation equation 4.21ff at system level was derived. For comparison purposes the results of this measurement series were already included there in figure 4.9.

The measurement results allowed a more simplified linear interpolation model for smaller

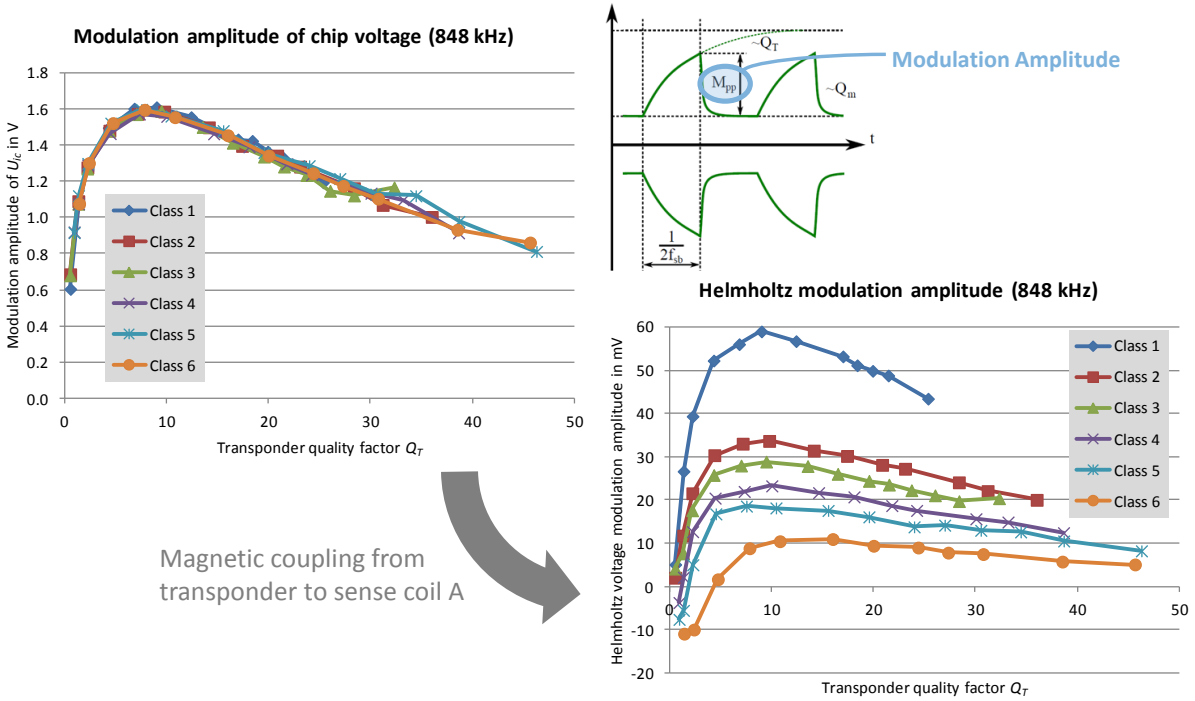

Figure 6.8: Measured modulation amplitudes in time domain of test chip B for $f_{SB} = 847.5\ kHz$ over Q_T shown for the chip input voltage $u_{IC}(t)$ and the Helmholtz bridge point voltage $u_{LMA}(t)$

quality factors as well. A rough approximation for the tuned case can be made using

$$CLF \approx -437\ k_{PCD,TP}^2\ Q_T, \tag{6.2}$$

although equation 4.21ff should be preferred in any case.

6.2.4 Load Modulation Amplitudes

The measured load modulation amplitudes normalized to their corresponding H-field values over the measured transponder quality factor Q_{CALC} are shown in figure 6.9. TC A has a smaller minimum chip input current compared to TC A, which results in a larger maximum quality factor. As theoretically explained in section 3.5.1, if the modulator is not placed at the antenna, this will reduce the LMA values. The same applies for an increased subcarrier frequency, which is related to the increased signal bandwidth compared to the bandwidth of the coupled resonant networks (see section 2.4.5). In general, an increased Q-factor is connected with increased normalized sideband amplitudes.

6.3 Empirical Model for the Load Modulation Amplitudes

This section concerns the task of finding an empirical link between the system parameters and the load modulation amplitude based on the measurement data.

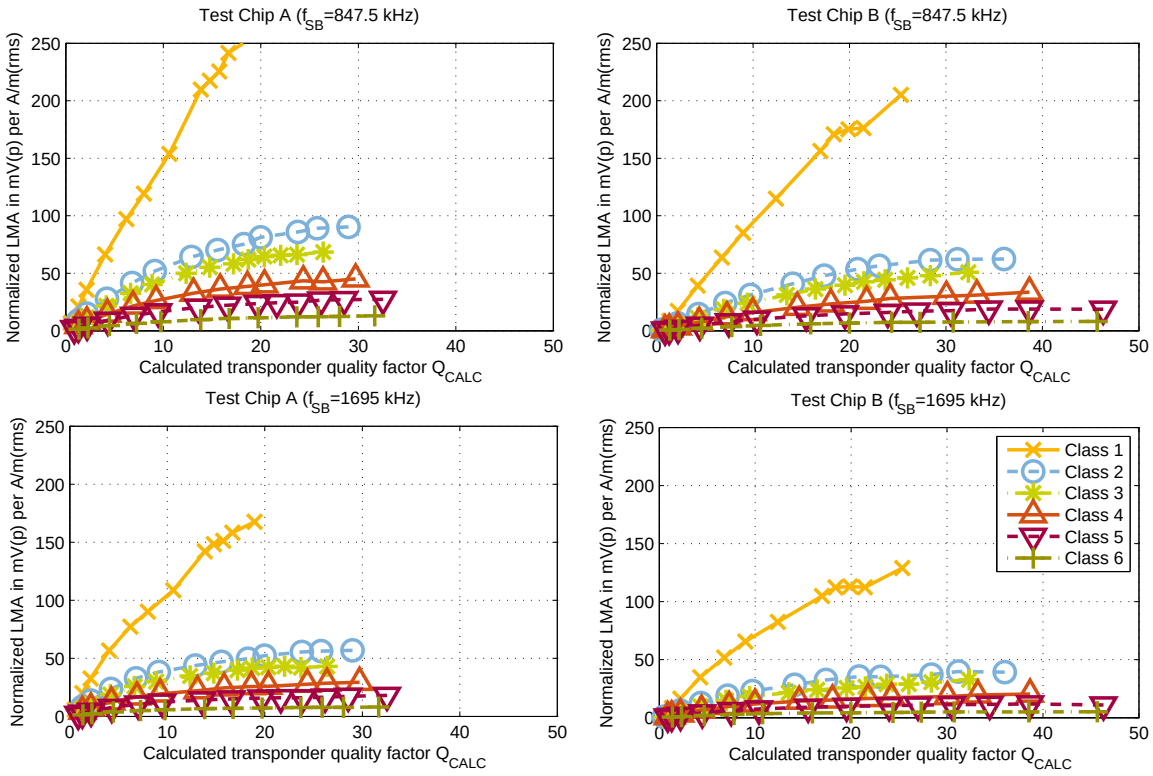

Figure 6.9: Normalized LMA results for both test chips and sideband carrier frequencies

6.3.1 Derivation of the Formula

Based on the acquired measurement data a good empirical approximation formula could be found

$$SBA_{V(p)} \approx \frac{2}{3} k_{SCA,TP}^2 \; H_{\mathrm{A/m}} \Delta Q_T \frac{1}{\sqrt[4]{1 + Q_T^2 \left(\frac{\omega_{RES}}{\omega} - \frac{\omega}{\omega_{RES}} \right)^2}}, \tag{6.3}$$

which is basically derived from the linear fit exemplarily shown in figure 6.10. Up to a high Q_T a good match can be assumed. The subcarrier frequencies are defined with ω. The formula introduces a transponder quality factor modulation amplitude $\Delta Q = Q_T - Q_M$.

Now what does this formula basically consist of? Apart from a constant coefficient 2/3, which may originate in the measurement setup (PCD 1), there is the proportionality factor $k_{SCATP}^2 H_{\mathrm{A/m}} \Delta Q_T$ and a mainly frequency dependent second factor, which is linked to the resonance frequency of the transponder and its bandwidth and the position of the sideband carriers.

Note that this formula is based on measurements with $f_{RES} = f_C$ only – but it can be used for detuned cases quite well as further sections will show. The "strength of detuned-ness" is expected to result in an additional (currently unknown) correction factor in equation 6.3.

To fully understand this formula and its driving factors, the impact of all main system components are discussed with respect to the sideband amplitudes.

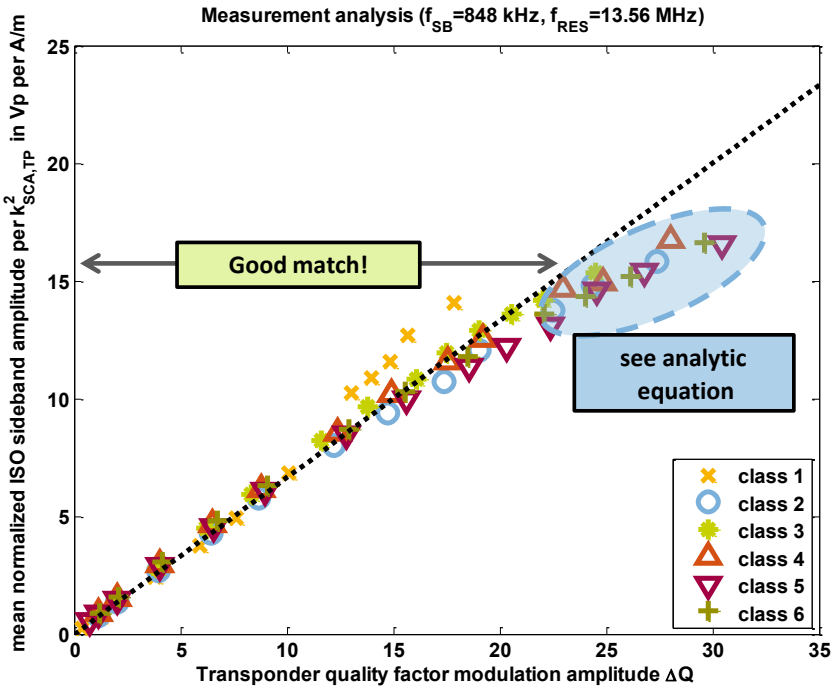

Figure 6.10: Accuracy of the empirical model (exemplarily for TC A)

6.3.1.1 Antenna Coupling/ Antenna Size

There is nothing as effective as a larger antenna regarding optimizing the LMA values. Of course, this is limited by the application and other factors like the card loading factor.

6.3.1.2 Resonance Frequency

The subcarriers will be found at $f_C \pm f_{SB}$ irrespective of resonance frequency of the transponder. The strongest levels will be gained with $f_{RES} = f_C$.

6.3.1.3 Quality Factors and H-field Strength

The quality factor is the tricky component within equation 6.3. First of all the larger the modulated transponder quality factor Q_M will be, the less LMA can be expected. This matches the observation done with both test chips. TC A has a $Q_M \to 0$ due to its optimized modulator position and the LMA are larger than for TC B.

Q_T does also occur in the frequency dependent factor in the numerator. As said above it should be seen linked to the bandwidth of the resonant circuit, as $Q_T = \omega_{RES}/B$ and its LMA limiting influence vanished the farther away ω is compared to ω_{RES}. Nevertheless: Even for the tuned case equation 6.3 states that the LMA can be maximized if Q_T approaches infinity.

The last component in this equation is the H-field strength, which is linked to Q_T. The higher the H field gets, the stronger the limiter will get active and reduces Q_T. It should be mentioned here as a remark that this might not be the case for battery powered transponders. That means that Q_T can be controlled in spite of the H-field strength. The strength of the impact of the limiter can be reduced by using a more sophisticated matching network between antenna and transponder like done in NFC card mode [NFC12]. But even for these more complicated cases it

is assumed that equation 6.3 can be used with some restrictions as long as conventional passive load modulation is performed.

6.3.2 Modelling Capabilities

As a verification for the accuracy of equation 6.3 LMA over H-field strength curves are calculated based on the empirical model and are compared to actual chip classification results (courtesy of NXP Semiconductors).

This is a good application of the empirical formula as it allows to reconstruct the system parameters of an existing product. The input parameters of the model can be varied until the measurements are matched. This can be seen as an adaptive system which performs a system identification task.

The characteristic chip input voltages, namely $U_{IC,MIN}$ and $U_{IC,MOD}$, are parameters that describe the chip. By knowing the resonance frequency and the size of the antenna, both the modulated and unmodulated quality factors and the load modulation amplitudes can be computed over H-field strength (based on equations 4.12ff).

$$Q_T\left(U_{IC}\right) = \left[\left(\frac{\mu_0 \omega_C A_{TP,ANT} \cos\alpha}{U_{IC}} H\right)^2 - \left(1 - \frac{\omega_C}{\omega_{RES}}\right)^2\right]^{-\frac{1}{2}} \tag{6.4}$$

The examination of *standard* and *high input capacitance* chip options (SC with about 17 pF and HC with about 70 pF) is chosen as a good example for system level analysis. The larger capacitance value is used to simplify the tuning to $f_{RES} = f_C$ for transponders with smaller antennas, which usually feature smaller inductances (physically described within the *Thomson Equation* introduced in section 3.2.3). A higher valued input capacitance requires more chip area – which is really expensive – but may allow to use a transponder without a tuning capacitor. This component cannot be added within a transponder card due to cost and space reasons.

Figure 6.11 contains such a comparison between a SC chip option with a class 1 antenna and a HC chip option with a class 2 antenna. Note that transponders are usually tuned to a resonance frequency well above f_C, as the resulting resonance frequency in a real life system with more than one card and other factors is decreasing [WM08]. Note the good match although equation 6.3 does not include the detuned case implicitly and the measurement parameters can never be known exactly (actual couplings, antenna parameters).

The transponder to sense coil A coupling coefficient for a class 1 antenna is roughly twice that of a class 2 antenna. If the HC chip had the same quality factor as the SC chip, the LMA values would be expected to decrease by a factor of four (directly following from 6.3! The 70 pF versions also have a decreased $U_{IC,MIN}$ and the slope of the fictitious rectifier equivalent resistor is divided by a factor of two.

Two very interesting other observations can be made: The modulated transponder quality factor 10 to 30 % of Q_T and the additional voltage drop over the rectifier at higher field strength values while modulating decreases the LMA. Furthermore the upper sideband is stronger as the lower one as the transponders are tuned to $f_{RES} > f_C$.

6.3.3 Lower Antenna Area Bound for LMA Compliance

These good modelling capabilities using this empirical approach will be used for an application specific design criterion. Application scenarios are primary restricted by the cost of the final product and the available space or area. The question arises what is the smallest possible transponder antenna size that will comply with [IE11] assuming passive load modulation?

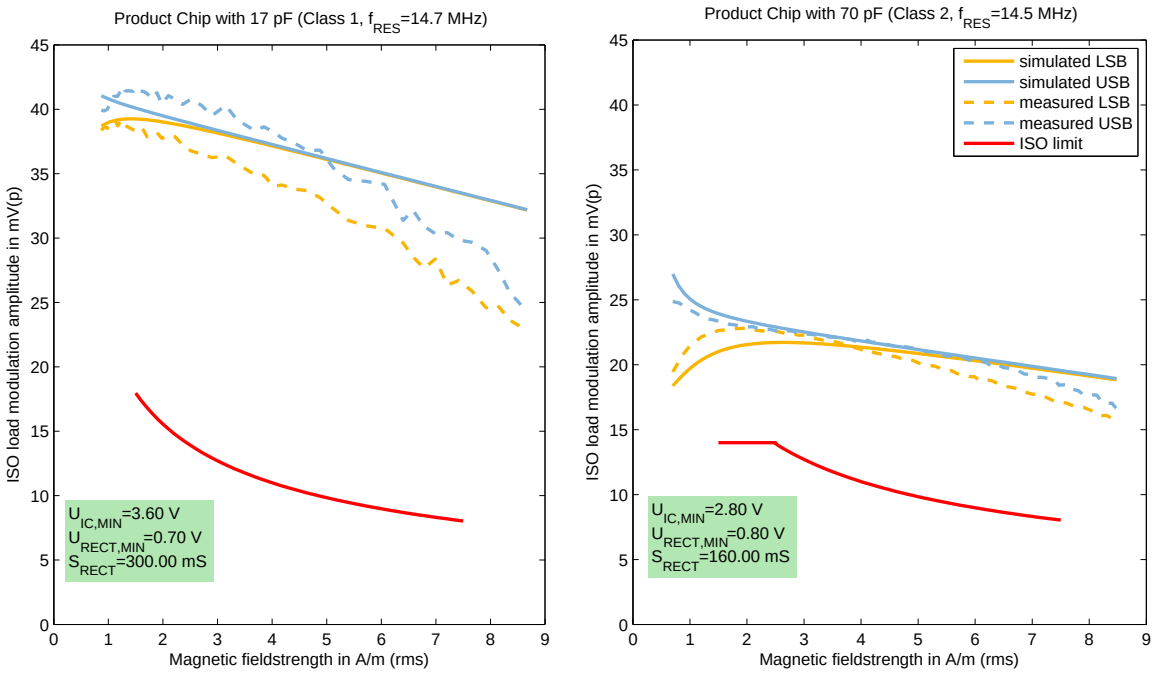

(a) ISO load modulation amplitudes over H-field strength

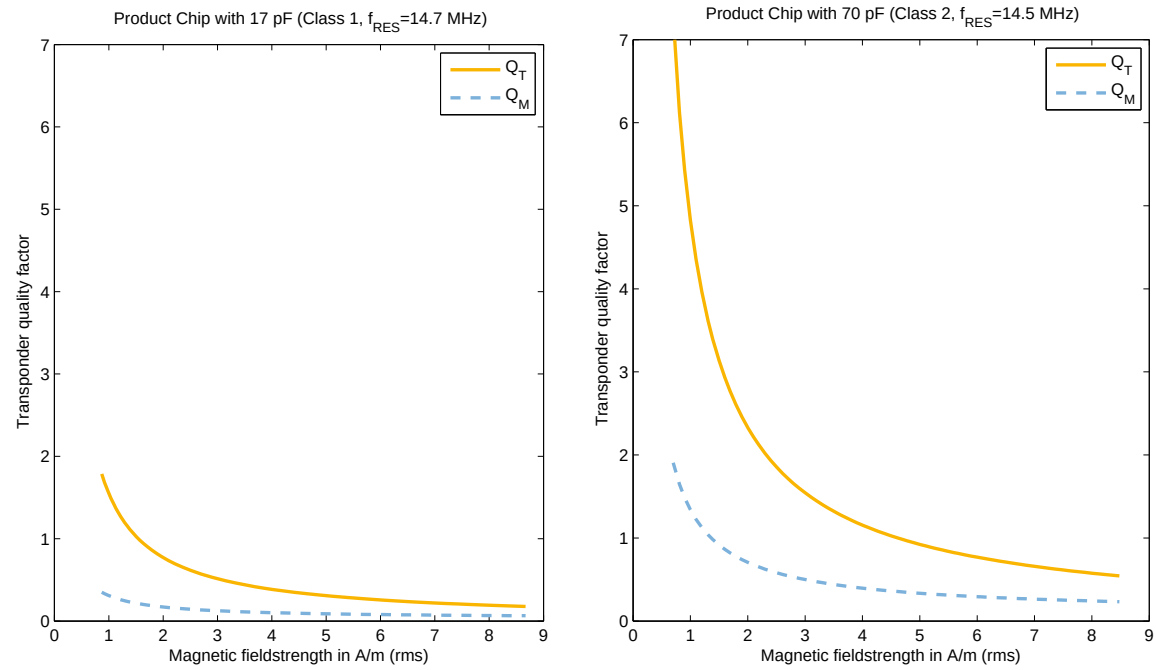

(b) Reconstructed quality factors over H-field strength

Figure 6.11: Simulated load modulation amplitudes based on equation 6.3 compared to results from a product measurement and the according reconstructed quality factors.

6.3.3.1 Simplified Criterion for Class 1 Antennas only

Coupling coefficients were increased for a set of values for Q_T until the pass criterion for the LMA values was exceeded at H_{min}, which is the toughest criterion on general (largest Q-factor needed). The result is shown in figure 6.12, which postulates a lower outer antenna area under some constraints, e.g. $f_{RES} = f_C$. This border curve does only consider the class 1 LMA limit $22\ mV(p)/\sqrt{H}$. No antenna area below this curve is said to be able to comply the ISO standard.

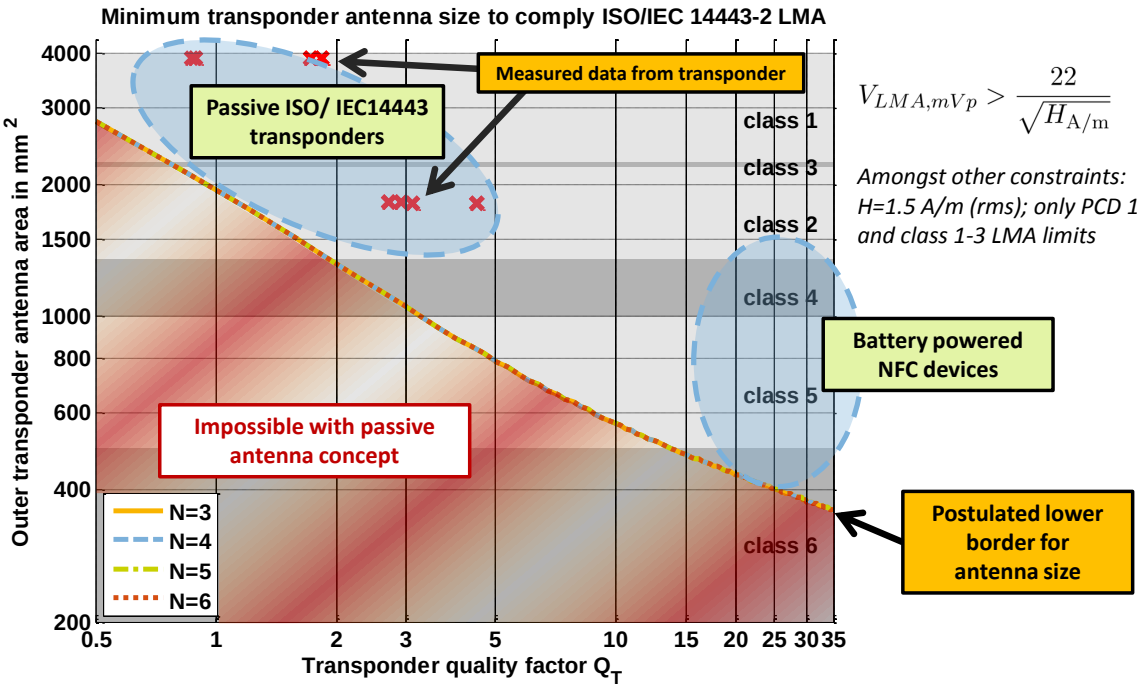

Figure 6.12: Postulated lower bound for the antenna size for LMA compliance within some constraints assuming $Q_M \to 0$ and $f_{RES} = f_C$

The plot also includes the corresponding antenna classes assuming an equivalent area criterion. The antennas that are used for this simulation are quadratic, which would result in unrealistic antenna class mappings. The quadratic shape does not influence the results that much because a homogeneous H-field in the DUT position is to be excepted. Furthermore section 6.1.4 already described that smaller antenna classes have less restrictive LMA limits or feature a larger required minimum field strength.

This plot it gives a fast and easy estimation on the expectable performance. Figure 6.12 additionally includes some real measurement results from section 6.3.2, which had LMA values above the limit. Like mentioned above passive transponders according to [IE10a] have a comparatively small transponder quality factor (nowadays?) and battery powered ISO certified NFC devices in card mode have larger quality factors which allow smaller antenna sizes.

This leads to the question what possible performance is lost by having a chip with $Q_M > 0$. Typically a more or less constant relationship between Q_M and Q_T can be specified. Figure 6.13 shows the consequence of having a non zero residual voltage during modulation. For completeness the other subplot includes the lower antenna area bound for the complete range of field strength values for a class 1 transponder. Remember that the quality factor of a passive transponder decreases with increasing H-field strength due to the limiter.

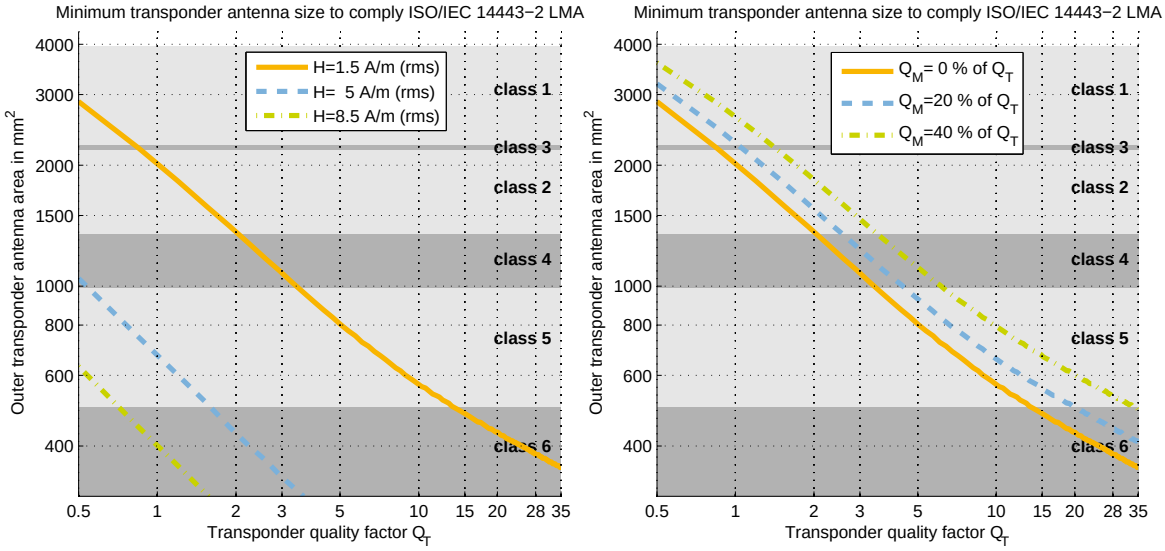

Figure 6.13: Lower bound for the antenna size for LMA compliance over H-field strength (with $Q_M \rightarrow 0$) and varying modulated transponder quality factor (at $H = 1.5\ A/m\ (rms)$)

6.3.3.2 Antenna Size Lower Bound for all ISO Antenna Classes

The concept described in the previous section can be extended to include the limit criterion's of all proximity antenna classes. A lower bound is found for the strongest coupling configuration, e.g. $f_{RES} = f_C$. In this simulation for each antenna size a limit Q factor was calculated based on equation 6.3 that results in the smallest allowed LMA values with the corresponding minimum H-field. Again, no antenna size below the curve shown in figure 6.14 is said to be capable of producing ISO/IEC 14443-2 compliant sideband amplitudes. In the case of a detuned transponder, larger transponder quality factors will be needed to pass the limit criterion. Two different quality factor modulation amplitudes were defined to see the impairment introduced by having a modulator after the rectifier. Note that this simulation takes the PCD 2 setup for antenna classes 4 to 6 into account.

In principle the simulation reflects the expected performance, because the LMA limits where defined to allow standard compatibility even for smaller antenna sizes.

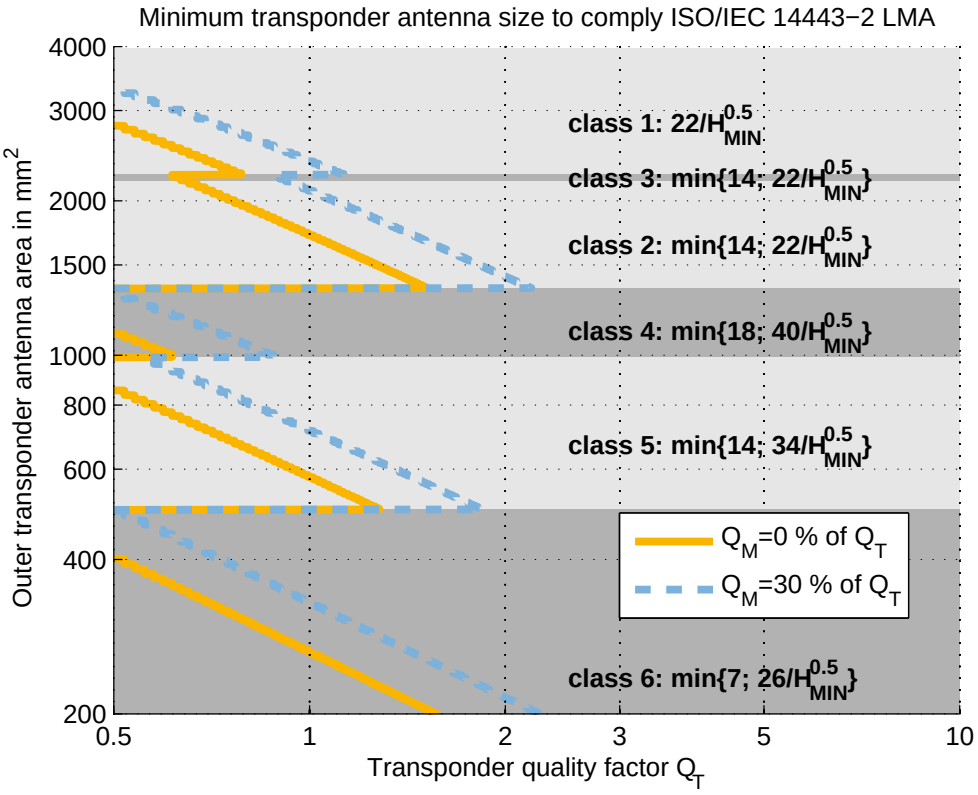

Figure 6.14: Lower bound for the antenna size for LMA compliance over H-field strength including the limits of all antenna classes at their corresponding H_{MIN} values

Chapter 7: Conclusion

"Anyone who has never made a mistake has never tried anything new."

[Albert Einstein]

7.1 Review of the Thesis

This thesis motivated the use of system parameters to analyse contactless passive proximity ISO/IEC 14443-2 HF RFID transponders and provided an access by various approaches. The focus was to analyse the transponder as a constant load (card loading effect) and the load modulation amplitudes. Based on a simplified network model of the ISO/IEC 10373-6 measurement setup both analytical and numerical considerations were made to get a theoretical insight into the coupled system. A measurement series provided an empirical model for predicting the load modulation amplitudes based on the system parameters.

7.2 Physical Limits of HF RFID Transponders with Loop Antennas

Beside a numerical MATLAB/ LTspice cosimulation framework, which allows a fast test system simulation on circuit level and a collection of analytical equations on system level, limit curves defining a lower outer antenna size over the transponder quality factor Q_T were proposed. It has been shown that if the coupling coefficient is doubled, the load modulation amplitudes will increase by a factor of four. This confirms the fact that the antenna (size) is the best amplifier. Additionally an analytic derivation of the card loading factor on system level was given.

The load modulation amplitudes are continuously increasing with the transponder quality factor. Above $Q_T > 20 - 30$ only a limited improvement is observable. Especially for larger quality factors $Q_T > 8$, the resonance frequency of the transponder has an important influence on the system performance. The LMA compliance is tested with a complete market-ready transponder, which should be tuned to $f_{RES} = f_C$ as well as possible concerning the sideband amplitudes. The final application scenario might get a better performance with a different configuration as it does not only include the "synthetical" measurement setup but also other materials and other cards in the vicinity of the resonant coupling system.

The theoretical considerations in this thesis are based on an ideal coupling system and define the theoretical optimum. Other objects in the vicinity of the reader-transponder coupling network and fluctuations in mass production degrade the overall performance. Therefore, practically realized systems have to exceed the physical limits clearly. But without the knowledge of the absolute limits, it is not possible to define a safety margin.

7.3 Outlook

Future work may improve the empirical model presented in chapter 6 by performing additional measurements to find an even more accurate interpolation function. The empirical LMA equation could be combined with the simplified switched state model used in chapter 4. Additionally it would be possible to introduce a weighting function to find an optimized transponder quality factor which allows a fair balance of the card loading effect (lower Q_T results in less loading) and the load modulation amplitudes (higher Q_T improves LMA values). The numerical considerations are based on a simplified RLC antenna model which includes some geometry related limiting assumptions. Further research in this area might improve the accuracy of this work's models.

The outcome of this thesis may provide a basis for analysing other compliance tests like EMVCo or NFC Forum by using the concept behind the analytic derivation of the card loading effect. Furthermore, a transponder coupling network between the chip and the antenna could be included in the model to consider an actively powered NFC device.

Bibliography

[Aik37] C.B. Aiken. Two-mesh tuned coupled circuit filters. *Proceedings of the Institute of Radio Engineers*, 25(2):230 – 272, Feb. 1937. (Cited on page 8.)

[BS93] D.S. Bernstein and W. So. Some explicit formulas for the matrix exponential. *Automatic Control, IEEE Transactions on*, 38(8):1228 –1232, aug 1993. (Cited on page 37.)

[Cic06] S. Cichos. *Verfahren zur Modellierung von planaren Spulen für den Entwurf und die Optimierung von Antennenspulen induktiv gekoppelter RFID-Transponder (German only)*. Dissertation, TU Berlin, 2006. (Cited on pages 15 and 44.)

[EMV11] EMV® Contactless Specifications for Payment Systems. *Book D – EMV Contactless Communication Protocol Specification, Version 2.1*. EMVCo, LLC, March 2011. (Cited on pages 5, 19 and 71.)

[Fin10] K. Finkenzeller. *RFID Handbook: Fundamentals and Applications in Contactless Smart Cards, Radio Frequency Identification and Near-Field Communication*. John Wiley & Sons, 3rd edition, 2010. (Cited on pages 1, 3, 12, 18 and 29.)

[Foc00] T. W. H. Fockens. System model for inductive ID systems. Technical report, Nedap, 2000. (Cited on page 12.)

[GBBM08] M. Gebhart, S. Birnstingl, J. Bruckbauer, and E. Merlin. Properties of a test bench to verify standard compliance of proximity transponders. In *Communication Systems, Networks and Digital Signal Processing, 2008. CNSDSP 2008. 6th International Symposium on*, pages 306 –310, july 2008. (Cited on page 18.)

[GBG10] M. Gebhart, J. Bruckbauer, and M. Gossar. Chip impedance characterization for contactless proximity personal cards. In *Communication Systems Networks and Digital Signal Processing (CSNDSP), 2010 7th International Symposium on*, pages 826 –830, july 2010. (Cited on page 16.)

[Geb08] M. Gebhart. *Lecture notes "RFID Systems" at Graz University of Technology (German only)*. `http://www.iks.tugraz.at/lehre/unterlagen/rfid-systems/`, 2008. (online; accessed August 19th, 2011). (Cited on pages 15, 18 and 43.)

[Geb11] M. Gebhart. Analytical considerations for an ISO/IEC14443 compliant smartcard transponder. In *Telecommunications (ConTEL), Proceedings of the 2011 11th International Conference on*, pages 9 –16, june 2011. (Cited on pages 7, 23, 32, 35 and 53.)

[GNSW11] M. Gebhart, R. Neubauer, M. Stark, and D. Warnez. Design of 13.56 MHz smartcard stickers with ferrite for payment and authentication. In *Near Field Communication (NFC), 2011 3rd International Workshop on*, pages 59 –64, feb. 2011. (Cited on pages 14 and 15.)

[Gri99] D.J. Griffiths. *Introduction to electrodynamics*. Prentice Hall, 1999. (Cited on page 28.)

[GSM10] M. Gebhart, R. Szoncso, and M. Münzer. Improving contactless technology by increase of transponder load modulation with serial capacitor. In *MELECON 2010 - 2010 15th IEEE Mediterranean Electrotechnical Conference*, pages 1253–1258, April 2010. (Cited on page 5.)

[GWBB08] M. Gebhart, M. Wienand, J. Bruckbauer, and S. Birnstingl. Automatic analysis of 13.56 MHz reader command modulation pulses. In *Second International EURASIP Workshop on RFID Technology*, 2008. (Cited on page 9.)

[IE06] ISO/IEC 15693-2:2006(E). *Identification cards – Contactless integrated circuit cards – Vicinity cards – Part 2: Air interface and initialization*. ISO, Geneva, Switzerland, 2006. (Cited on pages 5 and 71.)

[IE08] ISO/IEC 10373-6:2008(E). *Identification cards – Test methods – Part 7: Vicinity Cards*. ISO, Geneva, Switzerland, 2008. (Cited on page 18.)

[IE10a] ISO/IEC 14443-2:2010(E). *Identification cards – Contactless integrated circuit cards – Proximity cards – Part 2: Radio frequency power and signal interface*. ISO, Geneva, Switzerland, 2010. (Cited on pages 1, 5, 9, 25, 48, 63 and 71.)

[IE10b] ISO/IEC 18000-3:2010(E). *Information technology – Radio frequency identification for item management – Part 3: Parameters for air interface communications at 13,56 MHz*. ISO, Geneva, Switzerland, 2010. (Cited on page 5.)

[IE11] ISO/IEC 10373-6:2011(E). *Identification cards – Test methods – Part 6: Proximity Cards*. ISO, Geneva, Switzerland, 2011. (Cited on pages 10, 12, 18, 19, 20, 25, 46, 50, 54 and 61.)

[ISO03] ISO/IEC 7810:2003(E). *Identification cards – Physical characteristics*. ISO, Geneva, Switzerland, 2003. (Cited on page 4.)

[Kla09] C. Klapf. *LinkAnalysis and improvements of operational distance, power dissipation and chip area of passive HF RFID transponder systems*. PhD thesis, Graz University of Technology, 2009. (Cited on pages 16, 23 and 54.)

[Lio72] Ming-Lei Liou. Exact analysis of linear circuits containing periodically operated switches with applications. *Circuit Theory, IEEE Transactions on*, 19(2):146 – 154, mar 1972. (Cited on page 37.)

[MG09] U. Muehlmann and M. Gebhart. Automated analysis of ISO/IEC14443A interrogator command pulse shapes. In *Software, Telecommunications Computer Networks, 2009. SoftCOM 2009. 17th International Conference on*, pages 75 –79, sept. 2009. (Cited on pages 9 and 55.)

[NFC12] NFC Forum. *Consortium Homepage*. `http://www.nfc-forum.org/`, 401 Edgewater Place, Suite 600, Wakefield, MA 01880, USA, 2012. (online; accessed March 13th, 2012). (Cited on pages 3, 5, 19 and 60.)

[Par05] D. Paret. *RFID and contactless smart card applications*. Wiley, 2005. (Cited on pages 12 and 14.)

[PZ03] A.D. Poliyanin and V.F. Zaitsev. *Handbook of exact solutions for ordinary differential equations*. Chapman & Hall/CRC, 2003. (Cited on page 37.)

[RSJH07] C. Reinhold, P. Scholz, W. John, and U. Hilleringmann. Efficient Antenna Design of Inductive Coupled RFID-Systems with High Power Demand. *ACADEMY PUBLISHER – Journal of Communications*, 2(6):14–23, 2007. (Cited on page 43.)

[Sch10] P. Scholz. *Analysis and Numerical Modeling of Inductively Coupled Antenna Systems*. PhD thesis, TU Darmstadt, 2010. (Cited on pages 13 and 14.)

[Sco87] D.E. Scott. *An introduction to circuit analysis: a systems approach*. McGraw-Hill series in electrical engineering. McGraw-Hill, 1987. (Cited on pages 6, 9, 19 and 38.)

[SG11] R. Stadlmair and M. Gebhart. Cadence simulation environment for contactless near-field communication tags. In *Proceedings of the 2011 11th International Conference on Telecommunications (ConTEL)*, pages 39 –46, June 2011. (Cited on pages 9, 19, 38 and 46.)

[Skl01] B. Sklar. *Digital communications: fundamentals and applications*. Prentice Hall Communications Engineering and Emerging Technologies Series. Prentice-Hall PTR, 2001. (Cited on page 4.)

[Tec12] Linear Technology. *LTspice IV Simulation Software*. `http://www.linear.com/designtools/software/`, 2012. (online; accessed March 13th, 2012). (Cited on pages 25 and 41.)

[The12] The MathWorks, Inc. *MATLAB*. `http://www.mathworks.com/products/matlab/`, 2012. (online; accessed March 13th, 2012). (Cited on pages 25 and 41.)

[TSG08] U. Tietze, C. Schenk, and E. Gamm. *Electronic Circuits: Handbook for Design and Application*. Springer, 2008. (Cited on page 32.)

[WM08] H. Witschnig and E. Merlin. Modeling of multilabel scenarios of 13.56 MHz RFID systems. In *Microwave Conference, 2008. EuMC 2008. 38th European*, pages 59 –62, oct. 2008. (Cited on page 61.)

Glossary

AFC	Automated Fare Collection System
DFT	Discrete Fourier Transform
DUT	Device Under Test
EEPROM	Electrically Erasable Programmable Read Only Memory
FEM	Finite Element Method
HF	High Frequency (ITU radio band between 3 and 30 MHz)
IC	Integrated Circuit
ISM	Industrial, Scientific and Medical (radio band)
ITU	International Telecommunications Union
LSB	Lower Sideband Carrier
NFC	Near Field Communication
NWA	Network Analyser
OOK	On Off Keying
PCD	Proximity Coupling Device (used in [IE10a] and [EMV11])
PICC	Proximity Card or Object (used in [IE10a] and [EMV11])
Q	Quality Factor
RFID	Radio Frequency Identification
USB	Upper Sideband Carrier
VCD	Vicinity Coupling Device (used in [IE06])
VICC	Vicinity Integrated Circuit Card (used in [IE06])

Appendix A: MATLAB/LTspice Co-Simulation

A.1 LTspice Configuration Scripts

```
;=============================================================================
; Values of the transponder components (example file)
; To be generated automatically by a MATLAB script file
;=============================================================================

.param LtpVal 1.86u      ; parallel inductance of the transponder antenna
.param RtpVal 1.51       ; parallel resistance of the transponder antenna
.param CtpVal 2.41p      ; parallel capcitance of the transponder antenna

.param CtuneVal 54.6p    ; tuning capacitor of the transponder network
.param RicVal 4481.53    ; input resistance of the transponder IC (Qt=12)
.param CicVal 17p        ; input capcitance of the transponder IC
.param Cic_activeVal 1p  ; additional input capcitance of the transponder
                         ; IC when active (Uic>Uic,min)
.param RmodVal 10        ; modulator resistor

K1 Lpcda Ltp 0.039       ; PCD <-> transponder
K2 Ltp Lsca 0.115        ; transponder <-> sense coil a
```

Listing A.1: Example for `TransponderValues.cir`

```
;=============================================================================
; Values of the ISO Setup components (PCD 1 HDR configuration, Qpcd=12)
; Data taken from measurements documented in various reports and papers
;=============================================================================

;- PCD network ---------------------------------------------------------------
.param RqVal 50          ; output resistance of the amplifier
.param Cpcd1Val 80.77p   ; series capacitor of the matching network
.param Cpcd2Val 200.9p   ; parallel capacitor of the matching network
.param RpcdVal 531.3     ; resistor defining the PCD quality factor
.param CpcdaVal 25.05p   ; parallel capacitance of the PCD antenna (Q=12)
.param RpcdaVal 4257     ; parallel resistance of the PCD antenna (Q=12)
.param LpcdaVal 462n     ; parallel inductance of the PCD antenna (Q=12)

;- Sense coils ---------------------------------------------------------------
.param RaVal 245         ; balance point connection resistor, side A
.param RbVal 245         ; balance point connection resistor, side B
.param CscaVal 5.26p     ; parallel capacitance of sense coil antenna A
.param RscaVal 5653.1    ; parallel resistance of sense coil antenna A
.param LscaVal 422n      ; parallel inductance of sense coil antenna A
.param CscbVal 5.26p     ; parallel capacitance of sense coil antenna B
```

```
22 .param RscbVal 5653.1    ; parallel resistance of sense coil antenna B
23 .param LscbVal 422n      ; parallel inductance of sense coil antenna B
24 .param ClmaprobeVal 10p ; capacitive load of the Helmholtz point (probe)
25
26 ;- Calibration coil ------------------------------------------------------
27 .param CccVal 9p          ; parallel capacitance of the calibartion coil
28 .param RccVal 1766        ; parallel resistance of the calibartion coil
29 .param LccVal 204n        ; parallel inductance of the calibartion coil
30 .param RccpVal 1Meg       ; resistive load to the calibration coil (probe)
31 .param CccpVal 10p        ; capacitve load to the calibration coil (probe)
32
33 ;- Antenna couplings within the ISO network (excl. transponder) ----------
34 K3 Lpcda Lsca 0.09        ; PCD <-> sense coil A
35 K4 Lpcda Lscb 0.09        ; PCD <-> sense coil B
36 K5 Lsca Lscb 0.024        ; sense coil A <-> sense coil B
37 K6 Lpcda Lcc 0.056        ; PCD <-> calibration coil
38 K7 Lscb Lcc 0.175         ; sense coil b <-> calibration coil
```

Listing A.2: Example for `ISOSetupValues.cir`

```
1  ;=============================================================================
2  ; Simulation settings for LTspice simulation (transient)
3  ;=============================================================================
4
5  .param CARRIER_FREQU 13.56Meg    ; carrier frequency
6  .param SUBCARRIER_QUOT 16        ; subcarrier quotient (16 for 848 kHz)
7  .param NUM_OF_PULSES 8           ; number of pulse to be generated for
8                                   ; ISO sideband levels calculation
9
10 .param OFFSET_CYCLES 8           ; preceeding settling time offset (8@848
11                                  ; results to 8*16/13.56Meg=9.44us)
12 .param SHIFTED_SEQ 1             ; if 1: modulation sequence starts
13                                  ; between two edges
14 .param NO_MOD 0                  ; if 1: disable modulation in observed
15                                  ; time frame
16
17 .param MAX_TIMESTEP 5n           ; maximum allowed simulation timestep
18
19 .param Vq_amp 10                 ; voltage amplitude of the amplifier
20                                  ; output in Volts
21
22 .save V(Helmholtz)               ; restrict to save only the voltage at
23                                  ; the Helmholtz point
```

Listing A.3: Example for `SimulationSettings.cir`

A.2 MATLAB Function to Compute LMA Values

```
function [c0_abs c0_phase c1_abs c1_phase c2_abs c2_phase] =
    iso10373_dftexe(vtime, vd, fsb_scaler, count)
%ISO10373_DFTEXE is a ported version of the DFT for sideband analysis
% defined in ISO/IEC 10373-6.
% Input:
%   vtime       Time Vector
%   vd          Data Vector (LMA voltage)
%   fsb_scaler  fsb=fc/fsb_scaler (default 16 for 848 kHz, optional)
%   count       FFT length (optional, default: length(vtime))
% Output:
%   c0_abs      Magnitude of carrier in V
%   c0_phase    Phase of carrier in rad
%   c1_abs      Magnitude of USB in V
%   c1_phase    Phase of USB in rad
%   c2_abs      Magnitude of LSB in V
%   c2_phase    Phase of LSB in V

if nargin<2
   error('iso10373_dftexe: Expecting at least two parameters');
end

if nargin<3
   fsb_scaler = 16;     % assume 848 kHz
end

if nargin<4
    count = length(vtime);
end

fc=13.56e6;
w0=double((fc*2.0)*pi); % carrier 13.56 MHz
wu=double((1.0+1.0/fsb_scaler)*w0); % upper sideband 14.41 MHz (for 848)
wl=double((1.0-1.0/fsb_scaler)*w0); % lower sideband 12.71 MHz (for 848)
c0_real=0; % real part of the carrier Fourier coefficient
c0_imag=0; % imag part of the carrier Fourier coefficient
c1_real=0; % real part of the up. sideband Fourier coefficient
c1_imag=0; % imag part of the up. sideband Fourier coefficient
c2_real=0; % real part of the lo. sideband Fourier coefficient
c2_imag=0; % imag part of the lo. sideband Fourier coefficient
center=floor((count+1)/2); % center address

%********* signal selection ****************************
% Number of samples for six subcarrier periods
N_data=floor((0.5+6*fsb_scaler/(vtime(2)-vtime(1))/fc));

% Note: (vtime[2]-vtime[1]) is the scope sample rate
N_data = min(N_data, length(vd));

start = max(0, center - ceil(N_data / 2));

for i=1:N_data
    %- Bartlett window ------------------------------------------------
    if mod(N_data, 2) == 0  % N_data is even
        if i < floor(N_data /2)
```

```
54              Wb=2.0*double(i)/double(N_data - 1);
55          else
56              Wb=2.0*double((N_data-i-1))/double(N_data - 1);
57          end
58      else    % N_data is odd
59          if i < floor(N_data /2)
60              Wb=2.0*double(i)/double(N_data - 1);
61          else
62              Wb=2.0-2.0*double(i)/double(N_data - 1);
63          end
64      end
65
66      %- DFT ------------------------------------------------------------------
67      k=i+start;
68
69      c0_real=c0_real+vd(k)*double(cos(w0*vtime(k))*Wb);
70      c0_imag=c0_imag+vd(k)*double(sin(w0*vtime(k))*Wb);
71      c1_real=c1_real+vd(k)*double(cos(wu*vtime(k))*Wb);
72      c1_imag=c1_imag+vd(k)*double(sin(wu*vtime(k))*Wb);
73      c2_real=c2_real+vd(k)*double(cos(wl*vtime(k))*Wb);
74      c2_imag=c2_imag+vd(k)*double(sin(wl*vtime(k))*Wb);
75  end
76
77  %****************** DFT scale ***************************
78  c0_real=4.0*c0_real/ double(N_data);
79  c0_imag=4.0*c0_imag/ double(N_data);
80  c1_real=4.0*c1_real/ double(N_data);
81  c1_imag=4.0*c1_imag/ double(N_data);
82  c2_real=4.0*c2_real/ double(N_data);
83  c2_imag=4.0*c2_imag/ double(N_data);
84  % Note: 4.0F includes the correction coef. of the Bartlett window
85
86  %*************** absolute Fourier coefficient **********
87  c0_abs=double(sqrt(c0_real*c0_real + c0_imag*c0_imag));
88  c1_abs=double(sqrt(c1_real*c1_real + c1_imag*c1_imag));
89  c2_abs=double(sqrt(c2_real*c2_real + c2_imag*c2_imag));
90
91  %************** Phase of Fourier coefficient **********/
92  c0_phase=double(atan2(c0_imag,c0_real));
93  c1_phase=double(atan2(c1_imag,c1_real));
94  c2_phase=double(atan2(c2_imag,c2_real));
95
96  end
```

Listing A.4: `iso10373_dftexe.m`